THESIS FOR THE DEGREE OF DOCTOR OF PHILOSOPHY

Thermal insulation of the combustion chamber in a light duty diesel engine

JOOP SOMHORST

Division of Energy Conversion and Propulsion Systems
Department of Mechanics and Maritime Sciences
CHALMERS UNIVERSITY OF TECHNOLOGY
Gothenburg, Sweden 2024

Thermal insulation of the combustion chamber in a light duty diesel engine

J O O P S O M H O R S T

ISBN 978-91-7905-991-0

Acknowledgements, dedications, and similar personal statements in this thesis, reflect the author's own views.

Doktorsavhandlingar vid Chalmers tekniska högskola

Ny serie nr 5457

ISSN 0346-718X

Division of Energy Conversion and Propulsion Systems

Department of Mechanics and Maritime Sciences

Chalmers University of Technology

SE-412 96 Gothenburg

Sweden

Telephone +46 (0)31 772 1000

Cover:
Image created with computational fluid dynamics software, showing a piston sector with surface temperatures during combustion for a standard aluminum piston (top) and an insulated piston with thermal properties of yttria stabilized zirconia (bottom)

Chalmers Digitaltryck

Gothenburg, Sweden 2024

Thermal insulation of the combustion chamber in a light duty diesel engine

JOOP SOMHORST

Division of Energy Conversion and Propulsion Systems
Department of Mechanics and Maritime Sciences
CHALMERS UNIVERSITY OF TECHNOLOGY

Abstract

Reduction of heat loss from the combustion chamber in an engine has great potential to decrease fuel consumption and CO_2 emissions. Research on thermal barrier coatings (TBC) has been performed since the early eighties to address this potential. However, reported results for engine efficiency improvements with insulation show a large spread and there is no consensus on the actual benefits of TBCs. The purpose of this PhD project was to make an accurate assessment of state-of-the-art TBCs and establish what coating properties are required to improve indicated engine efficiency.

Cylinder pressure data and measured heat losses to the piston cooling oil in a light duty single cylinder engine formed the basis for the experimental research. A robust and automated measurement method was developed and combined with statistical modeling of the data.

Plasma sprayed yttria stabilized zirconia and anodized alumina were selected to establish the effectiveness of state-of-the-art TBCs. These coatings, applied on the piston top, did not improve indicated efficiency. The high surface roughness of the coatings was an important contributor to the poor performance.

Experiments with a novel coating technology: suspension plasma spraying and a new material gadolinium-zirconate, led to a slightly improved indicated efficiency. Details in the heat release analysis indicated that the high open porosity in this coating might lead to increased heat losses and fuel entrainment.

An investigation of possible charge entrainment effects in a standard plasma sprayed zirconia thermal barrier coating was performed, using a combination of engine experiments, CFD simulations and a 0D crevice model. The crevice model predicted the observed deviations of the apparent rate of heat release surprisingly well, which is strong evidence for the existance and significance of this crevice effect.

To significantly increase engine efficiency with thermal insulation, materials with further reduced thermal conductivity and volumetric heat capacity are needed, while negative effects such as high surface roughness and crevice effects from permeable porosity should be minimized.

Keywords: diesel engine, efficiency, heat transfer, temperature swing, thermal barrier coating, surface roughness, surface sealing, porosity, crevice effect.

To my family

List of publications

This thesis is based on the work contained in the following publications:

Paper I Somhorst, J., Oevermann, M., Bovo, M., and Denbratt, I., "A Method to Evaluate the Compression Ratio in IC Engines with Porous Thermal Barrier Coatings," *SAE Technical Paper 2018-01-1778*, 2018, doi:10.4271/2018-01-1778.

Presented at the SAE International Conference on Powertrains, Fuels & Lubricants, 17-19 September 2018, Heidelberg, Germany.

Paper II Somhorst, J., Oevermann, M., Bovo, M., and Denbratt, I., "Evaluation of thermal barrier coatings and surface roughness in a single cylinder light duty diesel engine", *International Journal of Engine Research*, 2019, doi: 10.1177/1468087419875837.

Paper III Somhorst, J., Uczak de Goes, W., Oevermann, M., Bovo, M., "Experimental Evaluation of Novel Thermal Barrier Coatings in a Single Cylinder Light Duty Diesel Engine", *SAE Technical Paper 2019-24-0062*, 2019, doi: 10.4271/2019-24-0062.

Presented at the SAE ICE2019 14th International Conference on Engines & Vehicles, 15-19 September, Capri, Italy.

Paper IV Somhorst, J. Oevermann, M., "Effects of thermal barrier coating porosity on combustion and heat losses in a Light Duty Diesel engine", *International Journal of Engine Research*, 2024, doi: 10.1177/14680874231215526.

Acknowledgements

I would like to start with the acknowledgement of the Volvo Cars Industrial PhD Program, started in 1999, facilitating the education of about 30 to 40 PhD students each year. It is great to get the chance to work in both worlds, industry and academia.

From Volvo Cars I would also like to give special thanks to some of my colleagues: Lucien Koopmans who gave me the opportunity to embark on the same voyage he made 14 years ago. Carolin Wang-Hansen, my manager, really helped me to keep up the motivation and made sure I could focus on my PhD project within the dynamic world at Volvo Cars. Mirko Bovo, thank you for your supervision, your positive humor and the spot-on metaphors. I will never forget the one with the Ferrari and the clutch.

I could not have done the engine experiments at Volvo Cars without the help of Janne and Christer, the legendary single cylinder engine mechanics. We were changing pistons and running tests every day, for three weeks in a row. The test cell was not unlike a formula-one pit stop. Tools driven by compressed air, making loud whizzing noises when the engine was disassembled and reassembled in an amazing speed.

From Chalmers, I would like to start with thanking Ingemar Denbratt for making it possible to do my PhD within the CERC program and his positive attitude towards my project. Michael Oevermann, my main supervisor, you have given me good advice and valuable feedback on my work, even though we come from very different backgrounds and fields of experience. I also need to mention Jon-Anders, with whom I shared the 'Volvo room' at Chalmers. I really appreciated all of the shared lunches and the interesting discussions about anything, including combustion engines. I will remember your optimism, your contagious smile and your love for Radio Paradise.

In the cooperation with University West I really appreciated the discussions about this - for me - new field of technology and the positive approach to new developments. Thanks, Wellington Uczak de Goes, for supporting with cutting of pistons and coating analysis and keeping order in the big matrix of materials and spraying processes. Nicolaie Markocsan, for leading the FFI project, Stefan Björklund for spraying all the pistons and samples, Mohit Gupta for the insightful comments in our meetings.

The last part of the PhD project was performed parallel to working full time at Volvo Technology AB and I am very grateful for the support from Loffe, my group manager and Henrik Lindeberg who made sure the financing was in place to continue.

Funding from the Swedish Energy Agency through the CERC program and for the FFI project "Novel Thermal Spray Coatings for Increased Thermal Efficiency of Diesel Engines" is also gratefully acknowledged.

Finally, I am truly grateful to my wife Ann-Charlotte and my daughter Louise for the support and the understanding of my physical and mental absence during the intense periods of measuring and writing. You are the best!

Joop Somhorst,

Gothenburg, January 2024.

Table of contents

1 Introduction

1.1 Motivation

Volvo Car Corporation has been producing its own diesel engines since 2000, starting with the 5-cylinder 'new engine diesel' (NED5). At that time, with a common rail fuel injection system capable of delivering 1600 bar injection pressure and a specific performance of 50 kW/L, it was a very modern and powerful engine. Since then, the performance of the company's engines has steadily increased, and with downsizing to reduce fuel consumption, the specific power has increased even faster. The specific performance of the current 4-cylinder VED4 is 87 kW/L, an increase of over 70%. The power density has reached a point where the heat load from the combustion on the cylinder head and piston is becoming critical. It is difficult to increase cooling performance further, and advanced (expensive) materials are required.

As awareness of global warming problems has increased, increasingly strict legislation has been introduced regarding both use of renewable fuels and CO_2 emission limits. The fleet average limits for CO_2 emissions from passenger cars (produced by each manufacturer supplying the EU market) in the NEDC (New European Driving Cycle) are 130 g/km by the end of 2015, 95 g/km by 2021, and an expected target for 2025 is 75 g/km. Similar legislation has been passed in Japan, China, the USA, Canada, India, Mexico, Brazil and South Korea, with more countries to follow.

A way to reduce (local) CO_2 emissions and meet the legislation requirements is to introduce electrification of the powertrain, but this is still very costly. Hence, there will be a limited range of affordable hybrid and fully electrical vehicles in the near future and combustion engines will be needed for at least a few more decades. Thus, the car industry is still making efforts to reduce the fuel consumption of both gasoline and diesel engines in order to meet the future CO_2 emission reduction targets at affordable costs.

One of the energy conversion losses in the internal combustion engine is heat transfer from the hot cylinder charge and exhaust gas to the surrounding walls. Figure 1 shows the typical heat flow distribution in a combustion engine. If this heat loss to the coolant can be reduced, more heat can be converted to work and the heat load on the exposed engine components would be reduced. Both fuel economy and engine durability would improve, and it would be possible to increase specific power. Moreover, the increased temperature of the exhaust gases can give more energy to the exhaust turbine and enable faster catalyst light of for improved emission conversion. Additionally, when less heat is transferred to the coolant, the cooling system dimensions and weight can be reduced.

Note from the author: the world has changed rapidly since the motivation for this PhD thesis was formulated. The importance of efficient light-duty diesel engines, at least for the European market, has declined in the wake of diesel-gate and the fast electrification of passenger cars pioneered by Tesla. Nevertheless, the results of this research can still be applied on heavy duty and marine engines, where electrification remains a challenge and fuel efficiency has high priority.

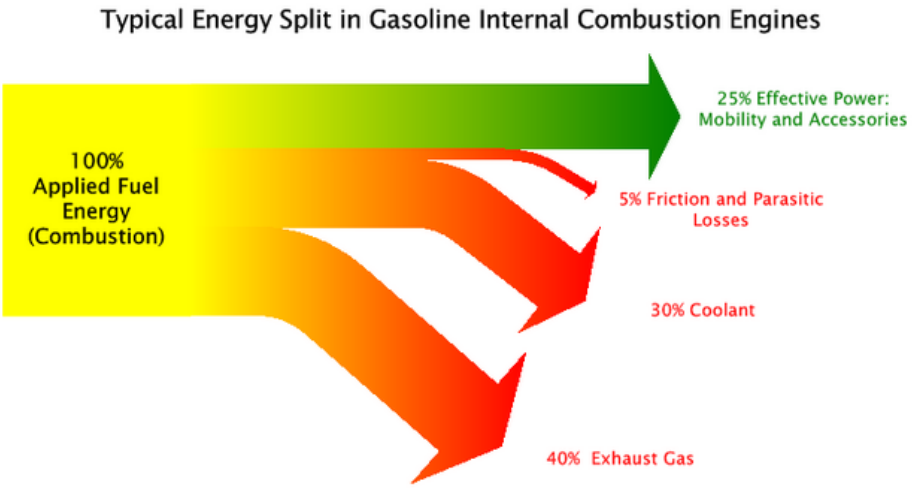

Figure 1. Engine energy flow distribution; typical coolant losses are between 20 to 35% of the total fuel energy.

1.2 Objectives

The main objectives at the start of this PhD project were:

1. Reduction of fuel consumption and CO_2 emissions by 2% through increasing the indicated efficiency from heat loss reduction.
2. Improved engine durability at high power output, with respect to components with high thermal loading. This might be achieved with very local measures in the combustion chamber.

The means to be researched and developed were thermal barrier coatings and surface structures that reduce the heat flow from hot gas to the walls.

2 Background

2.1 Principles of heat transfer

There are three ways to transfer heat - thermal energy - between different objects: conduction, convection and radiation. Figure 2 illustrates this with an example for a solid wall between two fluids where the temperature in the fluid on the left is higher than the temperature in the fluid on the right. The incident radiation can come from the fluid, but more often it will come from a radiant source at high temperature, not shown in this picture. Each mode of heat transfer is explained in more detail in the following subsections.

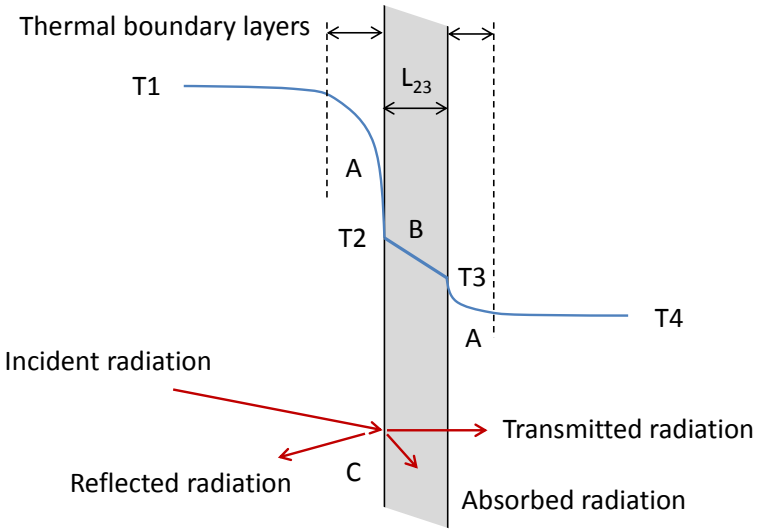

Figure 2. An example of heat transfer between two fluids separated by a solid wall showing A: convection, B: conduction and C: radiation.

2.1.1 Conduction

Heat conduction takes place where the transport of thermal energy is done by direct exchange of kinetic energy between molecules. Although this type of heat transfer also takes place in fluids it is most used to describe heat transfer in solids, where it is the only way to transport heat, apart from radiation in transparent solids. In one-dimensional form, for a distance L_{23}, a thermal conductivity k and a surface area A, the equation for the rate of heat transfer (steady state) from location 2 to 3 is:

$$\dot{Q}_{cond} = \frac{k}{L_{23}} A(T_2 - T_3) \quad (1)$$

For the transient heat transfer in solids, two more properties are of significance: thermal diffusivity a and thermal effusivity e. Thermal diffusivity is a measure of the time it takes for heat to travel through a material, or the time it takes to reach thermal equilibrium. The expression below shows that a material with high thermal diffusivity has a high ratio between conductivity and volumetric heat capacity.

$$a = \frac{k}{\rho\, c_m} \tag{2}$$

The thermal effusivity e defines the capability of a material surface to exchange heat, for example between to solid bodies in contact. When both thermal conductivity and volumetric heat capacity are high, heat can be exchanged fast, while the surface temperature remains relatively unchanged. A material at room temperature with high effusivity feels cold, like for example aluminum, as it removes heat quickly from the skin while maintaining a low surface temperature. Low effusivity is important for low dynamic heat exchange. An example is the use of wood as material for floors and furniture.

$$e = \sqrt{k\, \rho\, c_m} \tag{3}$$

Table 1 gives the thermal properties related to thermal conduction for some well-known materials. There is a big variation in conductivity, the differences in volumetric heat capacity for the solids are small in comparison.

From the table, aluminum is a very suitable material for cooling fins on electronic components, glass is an excellent material for hot drinks and wood can be used as a 'warm' material in our house interiors. And still air of course is a perfect insulator in for example clothing.

Table 1. Thermal properties for pure aluminum, iron, glass, wood and air at 1 atm. and 25 °C. Source: [1]

	k	$\rho \times c_m$	$a \times 10^5$	e
	[W/m.K]	[kJ/m^3.K]	[m^2/s]	[W.s$^{0.5}$/m^2.K]
Al (pure)	237	2440	9.71	24047
Fe (pure)	80	3518	2.27	16776
Glass	1.4	1875	0.08	1620
Wood (average)	0.13	1125	0.01	382
Air	0.026	1.2	2.14	5.6

2.1.2 Convection

In fluids, heat is transported by conduction (diffusion) and advection, grouped together under the term convection. Convection transfers heat from one region to another, or to a solid surface in Figure 2 shown in the regions labeled A. In the introduction here, only forced convection in turbulent flows will be discussed, as this is the case for the internal flows in a combustion engine.

In most flow cases a boundary layer develops between the bulk flow and the wall. The fluid velocity at the wall is equal to zero and heat transport perpendicular to the surface will be reduced as the fluid moves more and more parallel closer to the

surface. In case of a turbulent flow, three regions can be defined in the boundary layer. The near-wall viscous laminar sublayer, the transitional buffer layer and the turbulent layer, with increasingly larger flow structures away from the wall.

In the boundary layer heat is transferred by advection and conduction. Heat transfer by diffusion can mostly be neglected. Equation (4) shows the general relation for the convective heat transfer. As for conduction, heat transfer increases linear with surface area and temperature difference.

$$\dot{Q}_{conv} = h_c\, A(T_1 - T_2) \tag{4}$$

The heat transfer coefficient h_c for forced, turbulent convective flow is a function of a number of parameters shown in Equation (5), representing bulk flow velocity U, a typical length scale L, thermal conductivity k, dynamic viscosity μ, specific heat capacity c_p, density ρ and surface roughness ϵ.

$$h_c = f\big(U, L, k, \mu, c_p, \rho, \epsilon, \dots\big) \tag{5}$$

The rather complex expression for the heat transfer can be simplified by using dimensionless numbers, a common approach in the field of fluid dynamics. The Nusselt number is defined in Equation (6), and can be expressed in the Reynolds number and Prandtl number, Equations (7) to (9).

$$Nu = \frac{\text{total convective heat transfer}}{\text{conductive heat transfer}} = \frac{h_c L}{\mu} \tag{6}$$

$$Nu = f(Re, Pr, \dots) \tag{7}$$

$$Re = \frac{\text{inertial forces}}{\text{viscous forces}} = \frac{\rho\, U\, L}{\mu} \tag{8}$$

$$Pr = \frac{\text{momentum diffusion rate}}{\text{heat diffusion rate}} = \frac{c_p\, \mu}{k} \tag{9}$$

In combustion engines, the in-cylinder charge flow is highly turbulent. Often a comparison is made with turbulent pipe flow where correlations have been derived to calculate the convective heat transfer coefficient.

$$Nu = 0.023\, Re^{0.8} Pr^{0.33} \tag{10}$$

Combining all equations gives an expression for the heat transfer coefficient for pipe flow:

$$h_c = 0.023\, \frac{\mu}{L} \left(\frac{\rho\, U\, L}{\mu}\right)^{0.8} \left(\frac{c_p\, \mu}{k}\right)^{0.33} \tag{11}$$

The Reynolds number is a measure of turbulence level of the flow and depends on bulk flow velocity, a characteristic length and kinematic viscosity μ/ρ. The Prandtl number is defined by fluid properties only. For most gases, Pr is fairly constant for a large range of pressures and temperatures. Equation (10) is often used as the basis for engine heat transfer correlations.

Surface roughness plays an important role in convective heat transfer. It can increase heat transfer significantly by increasing the effective contact surface area between fluid and solid and by increasing turbulence in the boundary layer. To affect the turbulence, the surface roughness should protrude through the laminar, viscous sublayer into the transitional buffer region where the turbulence increases. If the aim is to increase heat transfer, the typical surface roughness height should be at least 2-3 times the thickness of the laminar sublayer [1].

The aim of this research however, is the opposite: the target is to minimize heat transfer. For a wall to be considered smooth, the surface roughness profile should be contained within the viscous laminar sublayer. The laminar sublayer thickness itself depends on flow conditions and fluid properties. The main factor is the turbulence level; reduction of the Reynolds number will increase laminar boundary layer thickness. Consequently, low surface roughness is important in flow cases with high Reynolds numbers if low heat transfer is desired.

Often the roughness height is divided by the typical length scale of the flow to get the dimensionless roughness parameter: ϵ/L.

2.1.3 Radiation

Heat transfer by radiation does not require direct contact between the objects and occurs instantly. Every object with a temperature higher than 0 Kelvin emits radiation, the quantity increasing exponentially with temperature. Equation (12) shows the Boltzmann relation for the net heat transport between two infinite parallel plates with temperature T_1 and T_2. The variable σ is the Boltzman constant. In this simple form the plates are assumed to behave as black bodies. The expression shows that radiation becomes exponentially more significant at high temperatures.

$$\dot{Q}_{rad} = \sigma\, A(T_1^4 - T_2^4) \tag{12}$$

Real objects do not emit as much radiation as a black body and do reflect and transmit radiation as well. To account for real world properties there are a number of efficiency factors related to radiation namely: emissivity ε, absorbtivity α, reflectivity ρ and transmissivity t. The effect of finite surfaces exchanging radiation energy is described by a form factor ξ.

The calculation of heat transfer by radiation is rather complex and often neglected in engine modeling, although it can be of importance for engine operating conditions with high load and high radiation from soot oxidation in the cylinder.

2.1.4 Heat transfer correlation models

Based on the correlation for turbulent pipe flow (10), Hohenberg and Woschni among others have developed empirical correlations for engine heat transfer. These models have been tuned with a large range of engines and have proven very useful for engine design. The correlation for the heat transfer coefficient in equation (13) by Woschni [2] shows the dependency on the cylinder bore B, charge pressure p and charge temperature T. The variable w represents the turbulence level and is a function of mean piston speed and accounts for combustion generated turbulence.

$$h_c = 3.26 \frac{p^{0.8} w^{0.8}}{B^{0.2} T^{0.55}} \tag{13}$$

From the general heat transfer theory and with this validated experimental correlation for the heat transfer coefficient, the general measures for heat transfer reduction can be listed:

- reduction of wall surface area
- decrease of charge temperature
- increase of wall temperature
- reduction of near wall turbulence
- low surface roughness
- high reflectivity of the wall surface

2.1.5 Impinging jet

Heat transfer in direct injected diesel engines is highly inhomogeneous. This aspect is not captured by the zero-dimensional correlations like the expression from Woschni. Heat transfer is particularly high in the region of fuel jet impingement on the combustion chamber wall. Jet velocity and temperature are very high and the boundary layer at this location is typically very thin. This aspect is important when considering where to apply thermal insulation. The jet impingement region is also challenging for CFD simulations. The standard low resolution wall models tend to overpredict heat transfer for impinging jets in diesel engines.

2.1.6 Combustion chamber deposits

This section about combustion chamber deposits originates from a separate literature study and is not published. However, it is highly relevant in the context of thermal insulation because i) soot deposits effectively insulate the combustion chamber and improve indicated efficiency and ii) soot deposit formation depends on the surface temperature and interacts with the presence of thermal barrier coatings and iii) soot deposits might show a way forward to create more effective TBCs.

Combustion chamber deposits (CCD) are a normal occurrence in internal combustion engines. These deposits originate from incomplete combustion products like soot and hydrocarbons. In compression ignition engines, the main source for deposits is soot from fuel burned under local rich conditions. In spark ignition engines, where the fuel

burns stoichiometric, lubrication oil and fuel wall condensates are the main sources of deposits. The importance of deposits for heat transfer is that they can possess a low thermal conductivity. Already in early experiments by Hohenberg [3] and Woschni [4], measuring and quantifying heat losses from the combustion chamber, the insulating properties of soot deposits were recognized.

Soot deposits might cover surface roughness, or they might follow or even enhance the underlying roughness (indication from my own pictures, where the burning jet hits the wall). The process that enhances the surface roughness could be similar to the process for suspension plasma spraying, building feather like structures, depositing particles on the sides of the 'bumps'.

The smallest elements in soot are spherules with an internal structure of carbon platelets, similar to graphite. The typical size of these spherules is 10-50 nm. Soot particles consist of agglomerated spherules and have a typical size range of 10-200 nm. Unburned hydrocarbons condensate on the particulates, resulting in a range of dry to sticky/wet soot particles, depending on the amount and kind of hydrocarbons absorbed. The final soot particles themselves have low porosity and the density is close to that of graphite. However, when the soot is deposited on the combustion chamber surface, the porosity of the deposit can adopt quite high values [5].

In Table 2, typical physical properties of soot are listed, as well as the properties of carbon, graphite and diamond. The heat capacity is very similar for the different forms of carbon, increasing somewhat for the more complex molecules as expected. But the conductivity of carbon and soot is much lower than that of graphite and diamond, which are actually very good heat conductors. As soot is formed into a deposit, the heat conductivity can become even lower, which is related to the level of porosity. As a result, the range of thermal conductivity of soot varies from modern thermal barrier coatings, around 1.5 W/m.K, down to very low values of 0.07 W/m.K. Although soot can be a thermal insulator, it absorbs radiation very well. It is not known how this affects total heat transfer. The soot layer might get very hot from the radiation, but not effectively transmit the heat to the metal surface below due to the low thermal conductivity.

Table 2. Physical properties for soot deposits, in comparison with carbon, graphite and diamond. Sources: [6–9].

	c_m [J/kg.K]	k [W/m.K]	Porosity [%]	ρ [kg/m^3]
Soot deposits	840-1260	0.07-1.6	5-95	170-2180
Carbon	600-1000	1.7	-	1800-2100
Graphite	708-717	119-168	-	1900-2300
Diamond	427-516	900-3320	-	3500

The mechanisms for deposition have been studied by a number of researchers in experiments and simulations [7,9,10] The main process for deposition is found to be thermophoresis. The relatively large soot particles experience a force from the surrounding gas molecules due to the temperature gradient in the near-wall charge.

The hotter and faster moving gas molecules furter away from the wall transfer a higher impulse to the particles compared to the colder and slower gas molecules near the wall. The net force pushes the soot particles towards the wall surface. The other important process involved in deposit formation is oxidation. Combustion chamber deposits are oxidized when high temperature and excess oxygen are available. The resulting deposit layer growth is thus a balance between the deposition by thermophoresis and deposit removal by oxidation. A cold wall will give a thicker deposit layer compared to a hot wall: the soot deposition rate from thermophoresis is high, the oxidation rate is low. Experimental results with thermal barriers confirm this effect: a hot TBC wall showed less soot deposits [4]. The deposit layer thickness is also changing with engine operating conditions. For example, high sooting conditions will create more deposits, high engine loads and combustion temperature will enhance soot oxidation.

As deposit formation is governed by local near wall conditions, the deposit thickness and properties will differ depending on the location in the combustion chamber. Typically, most deposits are formed in the piston top land and on the surfaces that come in contact with burning sprays. Outside of these regions, the deposits are relatively thin. The typical deposit layer thickness is between 30 and 150 µm [8,9,11,12], where a thinner layer in general has higher porosity and the thicker layer is more solid. Deposit formation times also greatly vary. It appears that the thicker, more solid deposits can take many hours to stabilize, while the thin, porous soot layers can be stable in a timescale of minutes [3,7,8].

Pure soot is likely to give a deposit with a loose, porous structure, while soot with a high amount of unburned hydrocarbons is likely to stick together, for example where the fuel spray interacts with the piston bowl as shown in Figure 3. Even chemical reactions can occur between hydrocarbons and especially oil additives that bind the unburned products to a solid layer. The latter is typically seen in the piston top land area where lubrication oil is present.

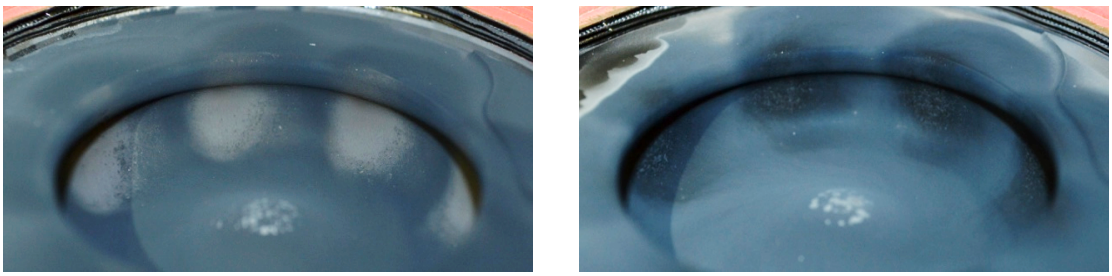

Figure 3. Soot deposits in the piston bowl. The left piston has been run at 5 bar IMEP, 1500 rpm with high EGR, the right piston at 20 bar IMEP, 3000 rpm without EGR.

When doing engine experiments involving heat transfer, the effect of deposits cannot be ignored. If possible, the amount of deposits should be controlled when comparing different engine hardware. This can be done by setting fixed initial conditions (ex. cleaned surfaces) and applying well-controlled engine operating conditions with a well-defined running duration in each operating point. However, different hardware might affect the composition and layer thickness of the deposits. Being aware of and

accounting for deposit effects is a necessary part of the experimental work on heat transfer in combustion engines.

2.1.7 Adiabatic engines

The pioneering work within the field of combustion chamber insulation was performed in the early 80's by Kamo and Bryzik [13–16]. The subject of their work was actually not to increase indicated efficiency. Their goal was to create an adiabatic engine that would not include a cooling system and that had a turbo compound system to make use of the heat redirected to the exhaust. Insulation was achieved by the use of ceramic monoliths or steel with low thermal conductivity like Inconel, in combination with air gap insulation.

There were similar research projects with adiabatic engines at that time with focus on increasing indicated efficiency. Both big improvements and deteriorations of indicated efficiency were reported. In general there was a large spread in published research results as will be shown later in this chapter.

One of the major issues with this concept was the permanently elevated temperature of the combustion chamber walls. This resulted in poor volumetric efficiency, deteriorated combustion and increased NO_x emissions. Other problems were durability of the ceramic engine parts and lubrication of the piston-liner contact.

2.1.8 Thermal barrier coatings

The alternative to the adiabatic engine was to develop relatively thin thermal barrier coatings. Wallace et al. [17] and Morel et al. [18] studied the cyclic wall temperature behavior and formulated expressions for the penetration depth of the temperature variations and the so-called temperature swing of the surface, shown in Equations (14) and (15). The thermal penetration depth for a certain attenuation is proportial to the root of the material diffusivity, the temperature swing is inversely proportional to root of the material effusivity. A thermal barrier coating that is can follow the charge temperature does not have to be thicker than the penetration depth. A TBC thickness higher than the penetration depth would only increase the average surface temperature. As a reference: a typical penetration depth with 95% attenuation for aluminum is in the range of 1 mm.

$$\text{penetration depth:} \quad \delta_p \propto \sqrt{a\,t} \qquad or \qquad \delta_p \propto \sqrt{\frac{k}{\rho\, c_m}\, t} \tag{14}$$

$$\text{temperature swing:} \quad \Delta T \propto \frac{1}{\sqrt{\rho\, c_m\, k}} \tag{15}$$

The temperature swing concept required materials with low thermal conductivity and low heat capacity. Most of the used materials were ceramics, metal oxides, applied by plasma spraying, thermosetting slurry coatings or hard anodizing of aluminum.

Thermal insulation of the combustion chamber with TBCs has been investigated by many researchers, with experiments as well as thermodynamic process simulations. Most of the experiments show an increase in exhaust temperature and a reduction in heat losses to the coolant, as expected and predicted by simulations. However, the

experimental results for the indicated engine efficiency show a large variation and there is no general agreement on the benefit of TBCs for indicated efficiency [19–21]. Moreover, it seems that, on average, the effect of insulation with TBCs on indicated efficiency is limited.

The variation in the reported benefits from TBCs is partly related to the large range of tested engine hardware, the variation in engine operating conditions and the engine technology level used in the experiments. Another cause for the varying results from experiments is the increased wall temperature that follows with insulation. This temperature increase results in a higher charge temperature and lower charge density. For compression ignition (CI) engines this can lead to a lower air-fuel ratio and differences in ignition delay, fuel-air mixing, emission formation and oxidation. Especially combustion phasing and the rate of heat release have a significant effect on the indicated efficiency. How these secondary effects change the efficiency is engine specific and depending on engine load. Kobori [22] published a detailed overview of these secondary effects for an insulated CI engine.

Several theories have been proposed to explain the limited benefits from TBCs on indicated efficiency: (i) The increased wall temperature caused by TBCs would increase the heat transfer coefficient [19], especially in the presence of near wall combustion, so called convection vive [23]. (ii) Most TBCs would absorb more radiation than an uncoated metal surface does [24]. (iii) A TBC could reduce soot deposits which are a 'natural' thermal insulator, due to the higher surface temperature [4,25]. (iv) A high surface roughness and open porosity, typical for plasma sprayed coatings, can increase heat transfer [26] and slow down combustion in CI engines [27]. Finally, (v) the thermal conductivity and heat capacity of the investigated coatings might not meet the requirements for an effective insulation [28,29]. (vi) A higher charge temperature can slow down combustion due the increase in charge viscosity. Surface roughness can slow down combustion in a number of ways: reduction of large-scale charge motion and turbulence from swirl and tumble [27], increased friction between spray and wall might slow down the penetration and mixing rate.

Negative effects from high surface roughness have been reported in several publications on spark ignition [30,31] as well as compression ignition engines [32,33]. To mitigate the negative impact of surface roughness in a CI engine, Kawaguchi et al. [29] limited the application of their new TBC to the piston top surface, excluding the bowl as shown in Figure 4. However, the reported efficiency improvement of this coating was for a low engine load, while the authors used high load conditions to prove the negative effect of surface roughness in the bowl. The typical reported difference in engine efficiency is about 1-3% between a smooth and rough surface finish. However, in some cases no effect was shown, or efficiency deteriorated as much as 6%. Also for experiments with surface roughness the results varied, for similar reasons as described in the previous paragraph.

The published experimental results, particularly for CI engines, do not show a clear consensus with respect to the effectiveness of thermal barrier coatings.

Figure 4. Piston from Toyota with a TBC of anodized aluminum [29].

2.1.9 History of reported efficiency improvements

The purpose of the following analysis was to get an impression and overview of the development of thermal insulation of the combustion chamber in internal combustion engines, spark-ignited and compression ignited. Reported efficiency data has been gathered from engine experiments and simulations in Figure 5 for a period from 1978 to 2018. The efficiency definition ranges from indicated efficiency to full engine efficiency. Also engine sizes and types vary. The references are listed in Table 3, in order of year of publication.

In the early development years of thermal insulation, 1-D engine cycle simulations showed very promising results. This was typically for adiabatic engines where the increase exhaust enthalpy was used for turbo compounding. Some experimental results were very positive. But there were similar numbers of experiments that showed a significant increase in fuel consumption. Over the years, the spread becomes less, especially for the predicted efficiency gains. This is probably caused by better simulation tools and better engine models.

Some of the variation can be explained by the variety of engines. Another cause for variations are changing conditions when a thermal barrier is applied in the combustion chamber. For example, ignition delay is shortened when the cylinder charge temperature is increased, resulting in changed combustion phasing. A second example is that the compression ratio is changed, sometimes no compensation is made for the extra insulation layer, sometimes the presence of an extra layer was overcompensated. Different types of thermal barrier coatings will give different results.

However, towards the end of the time period considered, the measured and predicted ficiency gains are converging to more modest improvements. Although not shown in the figure here, this trend continued after 2018. It is likely that developments of the simulation tools and experimental tools, combined with better knowledge about thermal barrier coatings give more accurate results over time.

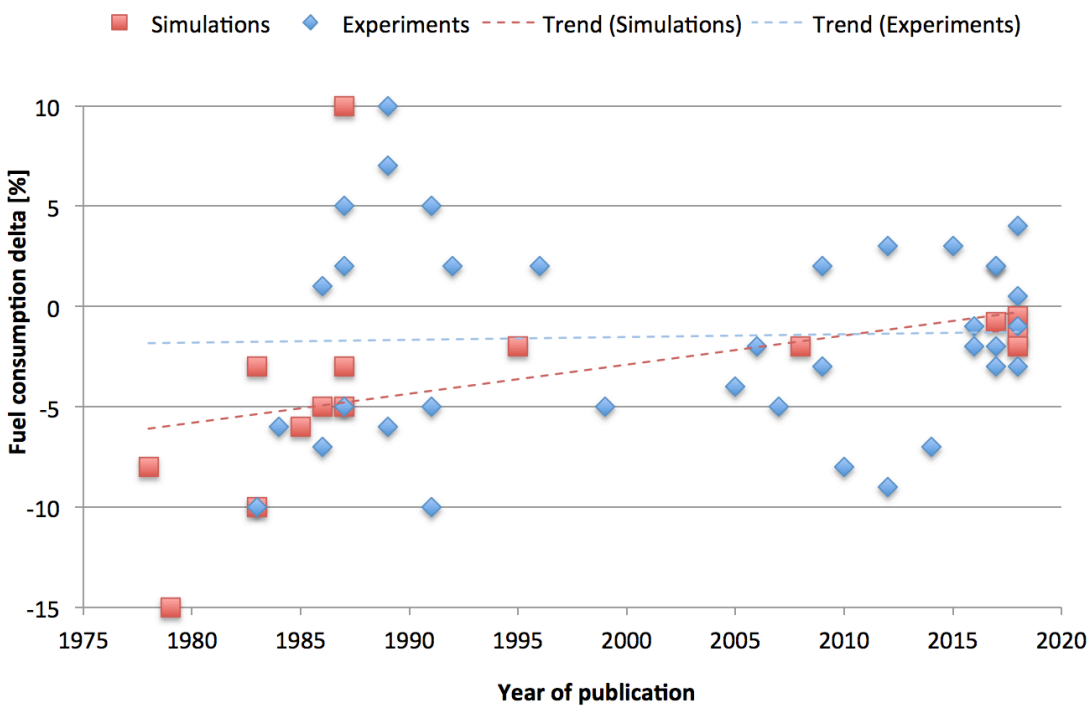

Figure 5. Selection of reported efficiency improvements from experiments and simulations with thermal insulation of the combustion chamber.

Some of the references in Table 3 are used multiple times for different load points or when experiments and simulations were compared in the same publication. For some publications, values were averaged to get a single value.

Table 3. References for the fuel consumption (ΔFC) data in Figure 5.

Year	ΔFC%		Main author	Ref	Year	ΔFC%		Main author	Ref
1978	-8	Sim	R. Kamo	[13]	2005	-4	Exp	C. Hergart	[34]
1979	-15	Sim	F. Wallace	[17]	2006	-2	Exp	I. Taymaz	[35]
1983	-3	Sim	F. Wallace	[36]	2007	-5	Exp	D. Saad	[37]
1983	-10	Sim	F. Wallace	[36]	2008	-2	Sim	C. Rakopoulos	[38]
1983	-10	Exp	W. Bryzik	[14]	2009	-3	Exp	P. Ramu	[39]
1984	-6	Exp	W. Wade	[40]	2009	2	Exp	A. Tricoire	[41]
1985	-6	Sim	T. Morel	[42]	2010	-8	Exp	T. Arment	[43]
1986	-5	Sim	T. Morel	[44]	2012	3	Exp	A. Modi	[45]
1986	1	Exp	C. Moore	[46]	2012	-9	Exp	A. Modi	[45]
1986	-7	Exp	P. Havstad	[47]	2014	-7	Exp	D. Das	[48]
1987	2	Exp	S. Henningsen	[49]	2015	3	Exp	J. Serrano	[50]
1987	-5	Exp	S. Henningsen	[49]	2016	-1	Exp	Y. Wakisaka	[51]
1987	10	Sim	G. Woschni	[19]	2016	-2	Exp	T. Powell	[52]
1987	-3	Sim	G. Woschni	[19]	2017	-2	Exp	A. Kawaguchi	[53]
1987	5	Exp	G. Woschni	[19]	2017	2	Exp	H. Osada	[33]
1987	-5	Sim	D. Assanis	[54]	2017	-0.8	Sim	S. Caputo	[55]
1989	-6	Exp	A. Alkidas	[56]	2017	2	Exp	S. Jerome	[57]
1989	7	Exp	D. Dickey	[58]	2017	-3	Exp	S. Jerome	[57]
1989	10	Exp	W. Cheng	[59]	2018	-1	Exp	K. Uchihara	[60]
1991	-5	Exp	K. Osawa	[61]	2018	-3	Exp	V. Merzlikin	[62]
1991	-10	Exp	D. Assanis	[63]	2018	-1.5	Sim	P. Andruskiewicz	[64]
1991	5	Exp	D. Assanis	[63]	2018	0.5	Exp	T. Kaudewitz	[65]
1992	2	Exp	S. Kimura	[66]	2018	-0.5	Sim	D. Gatti	[67]
1995	-2	Sim	V. Wong	[68]	2018	4	Exp	P. Andruskiewicz	[69]
1996	2	Exp	D. Tree	[32]	2018	-2	Sim	A. Poubeau	[70]
1999	-5	Exp	L. Kamo	[71]					

3 Research questions

Reduction of heat losses in internal combustion engines, especially diesel engines, has been subject of investigation for a long time. In the early days, the target was to create an adiabatic engine with high efficiency and without a need for cooling. Stainless steel and air gap insulated pistons and cylinderheads were tested, as well as ceramic thermal barrier coatings. The results from these investigations were not as positive as expected; the thermal efficiency was even reduced in many cases. Since then, numerous configurations have been tested and simulated with a large range of varying outcomes. No means for reduction of heat transfer with insulation has made its way to the market today, apart from one engine from Toyota (2016) on a limited market.

With this background and the objectives for the project in mind, the following research questions were formulated:

1) What is the actual benefit and potential of today's state of the art thermal barrier coatings in internal combustion engines?
2) What are the requirements for a thermal barrier coating to increase indicated efficiency by at least 2%?

4 Method

The approach in this PhD project has been mainly experimental, using a single cylinder light duty diesel engine. The first experiments were performed to establish the performance of two state-of-the-art thermal barrier coatings. In the second campaign potential improvements with novel thermal barrier coatings were evaluated. The final experimental campaign focused on the investigation on the effect of permeable porosity on heat loss and combustion.

The experiments were completed with simulations. A wall temperature swing model was created to estimate the potential of current thermal barrier coating materials and define requirements for increased efficiency gains. For the investigation of the crevice effect, a zero-dimensional crevice model was combined with a CFD model to predict the efficiency gain with an ideal coating and estimate the magnitude of additional heat loss and fuel penetration with a porous coating material.

4.1 Experiments

The purpose of the experimental method was to measure, with high accuracy, the effect of thermal barrier coatings on fuel consumption and heat losses.

The chosen method was to test the thermal barrier coatings in a single cylinder engine. The analysis was mainly based on cylinder pressure measurements. From these measurements the indicated work and apparent rate of heat release were calculated. With the measurement of the fuel consumption and exhaust emissions an energy

balance for the high-pressure cycle could be made. This energy balance shows the indicated efficiency, wall heat losses, exhaust enthalpy losses and losses from unburned emissions. As a complement to the calculated heat losses, the heat losses to the piston cooling oil were measured as well.

The compression ratio is an important parameter for the cylinder pressure analysis. To calculate the compression ratio the clearance volume must be known. Normally this volume is determined by measurement of the piston and cylinderhead volumes. In the case of the coated pistons, this method did not give accurate results due to the porosity of the thermal barrier coatings. Therefore, an alternative method to determine the compression ratio was developed, described in section 4.1.3.

The measured data was modeled using multiple linear regression to increase the precision of the indicated efficiency estimation. The model could also be used to isolate different factors that influence efficiency, heat losses and emissions.

In the method section a short summary is presented for each topic. More details can be found in the attached publications.

4.1.1 Cylinder pressure analysis and energy balance

The basis for calculation of the indicated efficiency, heat losses and exhaust enthalpy is the measured cylinder pressure. From the cylinder pressure the apparent rate of heat release (aRoHR) or Q_n can be calculated according to equation (16). The derivation of this equation can be found in Heywood [5], page 510. The ratio of specific heats κ is a function of gas composition and temperature, implemented according to a publication by Hohenberg and Killman [72].

$$\frac{dQ_n}{d\theta} = \frac{\kappa}{\kappa - 1} p \frac{dV}{d\theta} + \frac{1}{\kappa - 1} V \frac{dp}{d\theta} \tag{16}$$

The law for the conservation of energy gives equation (17), the energy input from the fuel is equal to the indicated work, the wall heat losses and the exhaust enthalpy.

$$Q_f = W_{i,g} + Q_w + H_{exh} \tag{17}$$

The energy in the fuel is not completely converted to heat, some energy is lost in incompletely burned emissions in the exhaust (Equation (18)).

$$Q_f = m_f Q_{LHV} - m_{CO} Q_{LHV_{CO}} - m_{THC} Q_{LHV_{THC}} \tag{18}$$

The indicated work, wall heat loss and exhaust enthalpy can now be calculated with equations (19), (20) and (21).

$$W_{i,g} = \int_{-180}^{180} p \frac{dV}{d\theta} d\theta \tag{19}$$

$$Q_w = Q_f - Q_n \tag{20}$$

$$H_{exh} = Q_n - W_{i,g} \tag{21}$$

The cumulative net apparent heat release Q_n is calculated for the part of the cycle where the intake and exhaust valves are closed. It is assumed that heat losses before intake valve closing and after exhaust valve opening are small compared to the rest of the high-pressure cycle.

$$Q_n = \int_{-145}^{145} \frac{dQ_n}{d\theta} d\theta \tag{22}$$

4.1.2 Single cylinder research engine

The single cylinder research engine is based on a medium duty base engine from AVL and combined with the combustion system of a Volvo light duty diesel engine, with specifications according to Table 4. Details of the measurement system are listed in Table 5, and a picture of the engine is shown in Figure 6.

Table 4. Single cylinder engine specifications.

Test engine type	**AVL 5812**
Displaced volume	492 cc
Stroke	93.2 mm
Bore	82.0 mm
Compression ratio (nominal)	15.5
Bowl type	re-entrant
Number of Valves	4
Swirl Number (Honeycomb)	2.0 to 3.2
Nozzle hole number x diameter	8 x 0.125 mm
Included spray angle	155 degrees
Fuel injection system	Common Rail, 2500 bar
Injector actuator type	Solenoid

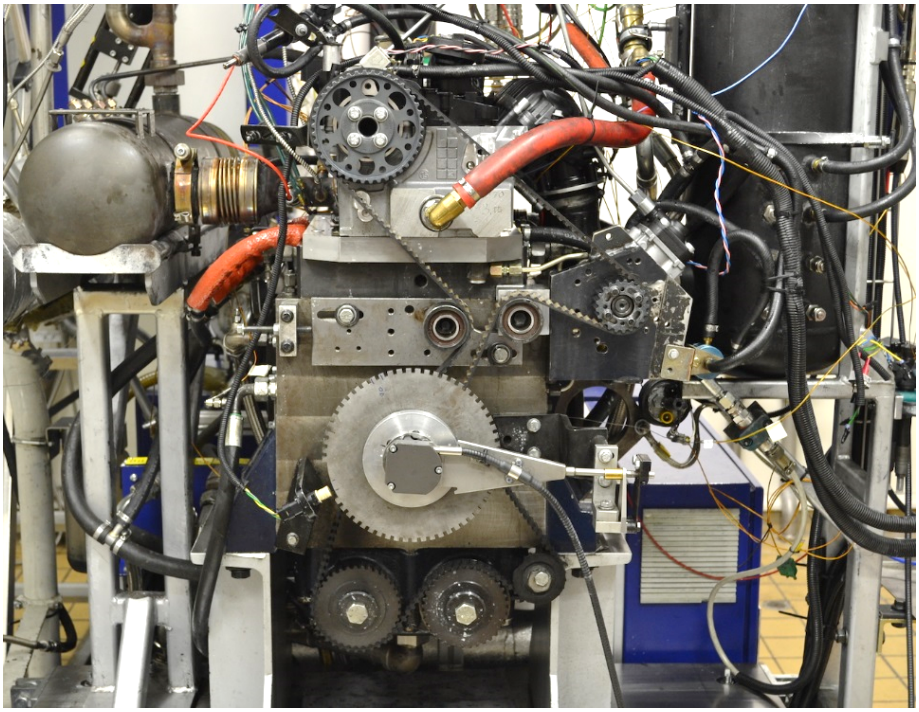

Figure 6. Single cylinder diesel research engine at Volvo Cars.

Table 5. Specification of the measurement system.

Variable	**Sensor / instrument**
Cylinder pressure	AVL GH14P
Crank angle position	AVL 365C
Intake temperature	Pentronic PT100
Intake pressure	GEMS 4000 0-6 bar abs
Exhaust pressure	GEMS 4000 0-10 bar abs
Fuel mass flow	AVL 733 fuel balance
Emissions, EGR	Horiba MEXA-7100DEGR
Intake air flow	Aerzen Zf 038.06

4.1.3 Compression ratio determination

An alternative method to determine the compression ratio was needed because the volume of the coated pistons could not be measured correctly with the standard measurement using a liquid. This was due to the porosity of the thermal barrier coatings which was not or only partly filled by the liquid. The compression ratio estimation uses cylinder pressure traces from a motored engine and is based on a master's thesis by Krieg [73]. The method is described in detail in Paper I.

Figure 7 illustrates the effect of porosity of a thermal barrier coating on the compression ratio, provided that the coated piston has the same surface contour as an uncoated piston. The volume in the pores adds extra volume to the clearance volume which reduces the compression ratio.

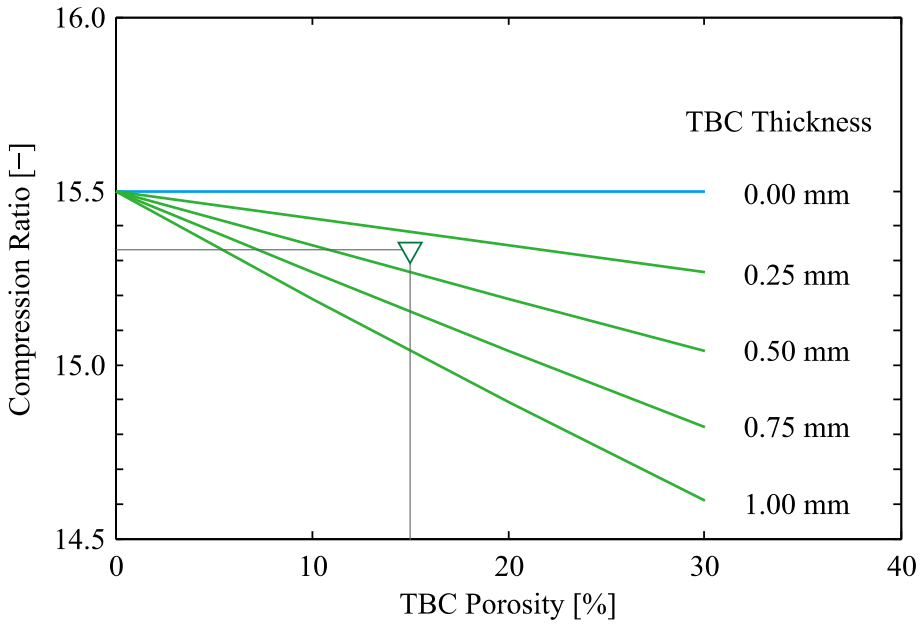

Figure 7. Compression ratio reduction as a function of TBC thickness and porosity. The green triangle indicates typical values for a plasma sprayed zirconia TBC.

Calculation of the apparent rate of heat release is sensitive for the value of the compression ratio. In Figure 8 the aRoHR is plotted for the reference piston and a coated piston. The yellow curve for the coated piston with the measured compression ratio shows an unfeasible heat loss before start of combustion. It can also be seen that the error in the compression ratio gives similar effects as the presence of a thermal barrier coating on the apparent rate of heat release.

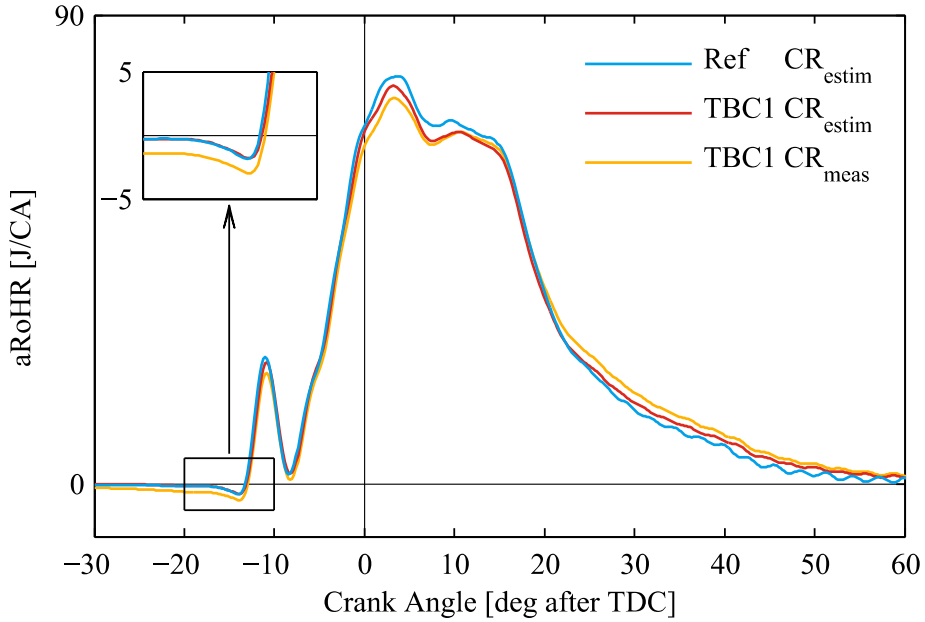

Figure 8. Apparent rate of heat release for the reference piston (Ref) and a piston coated with alumina (TBC1), calculated with measured and estimated values for the compression ratio.

4.1.4 Piston cooling oil heat flux measurement

To complement the calculated heat loss from the thermodynamical assessment, the heat flow to the piston cooling oil was calculated from the temperature increase of the oil in the cooling gallery and the piston cooling oil flow, according to Equation (23). The typical heat flux to the piston cooling oil is 60 to 70% of the total heat flux to a piston with a cooled ring carrier [74].

$$\dot{Q}_{oil} = \rho_{oil}\, c_{p,oil}\, \dot{V}_{oiljet}\, (T_{oilexit} - T_{oiljet}) \tag{23}$$

The amount of heat transferred to the piston cooling oil is a measure of the thermal resistance between the piston surface and the cooling oil in the gallery. Adding a TBC or modification of the piston surface roughness for example, will change the thermal resistance, which can be measured by a change of the heat loss to the piston cooling oil. There will be differences in the thermal resistance between uncoated pistons as well, due to tolerances in geometry and contact resistance between the stainless-steel cooling gallery and the aluminum of the piston. However, these differences are expected to be small in comparison to the effect of the TBCs. If there is a significant influence, this will be seen in the confidence level of the MLR model for the piston cooling heat flux.

The oil jet in this setup is likely to be laminar (Re = 2900) with very little dispersion within the short distance to the inlet of the cooling gallery. Most of the oil from the nozzle is expected to enter the cooling oil gallery. The main influence on the capturing efficiency would be increased backflow with higher engine speed [75].

To improve the accuracy of the exit oil temperature measurement, a short pipe was added to the cooling oil gallery exit, directing the oil flow to the temperature sensor, shown in Figure 9. The sensor itself was mounted in a funnel that collected the oil,

thereby minimizing the cooling effect from the surrounding crankcase gas. The principle for the measurement was adopted from Dahlström et al. [76].

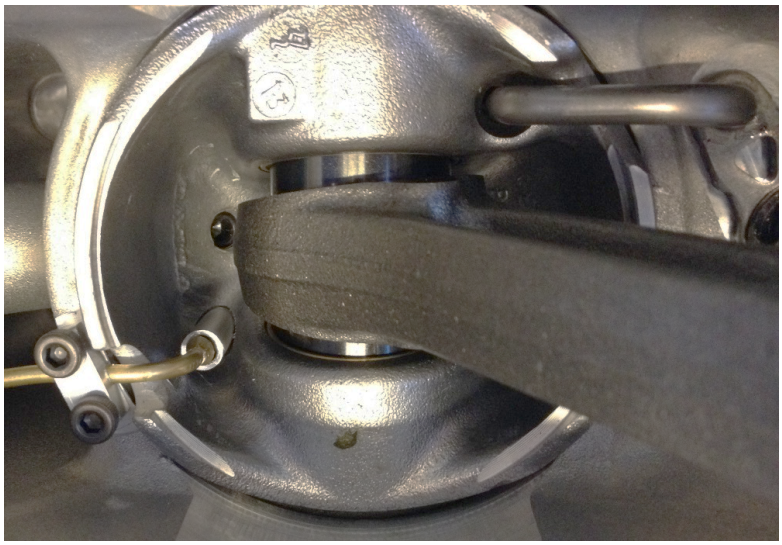

Figure 9. Bottom view of piston and cylinder with the oil cooling jet pipe on the top right and the temperature sensor mount on the left bottom [76].

4.1.5 Engine operating points and test sequence

Four engine operation points (EOP) were chosen to represent low, medium and high load at medium speed and high power conditions at high engine speed. Table 6 lists the engine speed, fuel mass, fuel pressure and injection pressure as well as intake and exhaust pressure. All load points were run with one pilot fuel injection of 2 mg. In paper II, EOP A, B and C were used, in paper III all EOP were run, and in paper IV only load points at 1500 rpm were measured. With fixed fuel mass for each point, IMEPg varies depending on indicated efficiency. Engine operating point B is an important load point to optimize for fuel economy and has been selected when a more detailed analysis was made.

Table 6. Engine operating points for the experiments.

Operating point	Speed [rpm]	Fuel [mg/str]	P_intake [bar]	P_Exhaust [bar]	P_fuel [bar]	IMEPg [bar]
C/D*	3000	60	2.6	2.8	1500, 2000	~23
C*	1500	45	2.2	2.4	1200	~17
B	1500	30	1.7	1.9	1000	~12
A	1500	15	1.3	1.5	500	~6

In each of the engine load points a few more parameter variations were included. These parameters were start of injection, and fuel injection pressure at high load. EGR was varied to create an increasing amount of soot deposits on the combustion chamber walls during the test runs in the first experimental campaign. These soot deposits have an insulating effect, and this will be compared with the insulating effect of the thermal barrier coatings.

Each hardware setup was measured in a predefined sequence of engine operation points. The test runs started with motoring conditions for each EOP. Thereafter each load point was run in fired operation including motoring before and after. The purpose of the motored operating points was to calculate the compression ratio and to evaluate the motored heat losses with TBCs and different soot deposit levels. The test run was automated with fixed times for the stabilizing of boundary conditions and the recording of measurements.

4.1.6 Statistical data modeling with MLR

Multiple linear regression (MLR) is a statistical method that fits a linear equation to a result (response) from multiple inputs (factors). The input factors can be continuous or categorical with multiple levels. The factors are scaled by their range and centered by their median, to be able to compare the relative contribution of each factor. It is possible to include factor interactions as well as squared factors, but this was not needed to create good models in the presented work.

Several benefits come from modeling of the measured data:

- Combining data from multiple measurements in each engine operating point makes the estimation of the results more precise.
- Fitting a model to the data creates correlation coefficients for the different input factors. With these coefficients, the contribution of each input factor can be studied separately.
- With the model it is possible to make predictions and study new combinations of the input factors.
- The model provides 95% confidence intervals for the calculated results and for the model coefficients.

In investigations described in Paper II, III and IV, MLR models were created for the measurement results from the fired and motored energy balance, the combustion delay and the exhaust emissions. The input factors for the models were piston surface coating, surface roughness, compression ratio and factors that represent the experimental conditions. The software used for the statistical analysis was MODDE 11 from Umetrics.

4.2 Simulations

In this chapter three simulation models are described. The first "temperature swing" model is used to make an estimate the fuel efficiency gain with ideal thermal barrier coatings based on calculation of the wall surface temperature swing with a fluctuating heat flux. The results provide an upper limit of what can be expected and show what coating material properties are needed for a certain level improvement.

The second model, a CFD model, is used to simulate the medium load case EOP B from experimental investigations. It provides detailed in-cylinder data for charge composition and temperature, which gives input to the crevice model. And with the thin wall module, a coating on the piston was simulated, to evaluate the temperature swing and heat losses for a coating with thermal conductivity and heat capacity of the experimental coating, but without increased surface roughness, permeable porosity, effect of changing soot deposits or radiation absorption.

The third model, the crevice model, is a relatively simple model of effect of a porous volume in the coating. This type of model has been used in engine research for prediction of heat losses and trapping fuel in, for example, the piston top land. Boundary conditions like wall near charge temperature and composition were taken from the CFD simulation.

4.2.1 Temperature swing model

F. Wallace was among the first to acknowledge the benefit of a fast following, fluctuating wall temperature to reduce heat transfer and formulated the expression "temperature swing" as early as 1979 [17].

The temperature swing model presented here serves to create an understanding of the expected benefits with a thermal barrier coating. When the potential is not realized in experiments, counteracting effects must be present. The model will also show in what range the thermal properties of a thermal barrier must be to achieve a certain efficiency gain.

The temperature swing model is based on the derivation and equations from literature: Wallace [17], Morel [18], Ferguson [77] and Incropera [78]. With the assumption that the cylinder charge temperature oscillates harmonically, Equation (24), a simple set of equations follow that allows for calculation of the wall temperature at the surface and in the solid.

$$T_{charge} = \overline{T}_{charge} + \Delta T_{charge} \cos(\omega t) \tag{24}$$

The dominant heat flux oscillation frequency is higher than the engine rotational frequency by at least a factor two. Using a factor of two is on the conservative side, thereby slightly overpredicting the amplitude of the wall temperature swing. The wall surface temperature lags the charge temperature with up to π/4 radians depending on material properties.

$$\omega = 2.0 \times 2\pi \frac{n_{engine}}{60} \tag{25}$$

The fluctuation of the wall surface temperature is governed by the charge temperature fluctuation, heat transfer coefficient, oscillation frequency and effusivity, defined in Equation (3).

$$\Delta T_{wall} = \Delta T_{charge} \left(1 + \frac{\sqrt{2}}{\mathrm{N}} + \frac{1}{\mathrm{N}^2}\right)^{-0.5} \quad ; \qquad \mathrm{N} = h_c \frac{1}{\sqrt{\omega\, k\, c_v}} \tag{26}$$

For the optimal thickness of the coating, it is of interest how deep the temperature wave penetrates in the wall. The penetration depth depends on the defined attenuation level ΔT_x, the diffusivity, defined in Equation (2), and the frequency of the temperature oscillation.

$$\delta_{p,x} = -ln\left(\frac{\Delta T_x}{\Delta T_{wall}}\right)\sqrt{\frac{2k}{\omega\, c_v}} \tag{27}$$

This set of equations, relates the temperature swing and thermal penetration depth to the thermal properties of a thermal barrier coating. The next section explains the equations that link the temperature swing to engine efficiency and exhaust temperature increase.

The following assumptions were applied:

1. The fuel conversion efficiency is 100%, all fuel is oxidized completely.
2. Heat loss to the combustion chamber wall is proportional to the temperature difference between wall and charge. The phase shift between wall and charge temperature is not considered, which will overestimate the temperature difference.
3. The heat transfer coefficient and charge temperature are assumed constant near combustion top dead center (averaged over -10 to 30 CA aTDC), when the majority of the heat transfer takes place. Values for the heat transfer coefficient and charge temperature are derived from measurement data and from the heat transfer model by Hohenberg [3].
4. The lowest temperature of the wall temperature swing is equal to the wall temperature without coating.
5. A reduction of heat loss with insulation leaves additional heat for conversion to work. The assumption is made that this additional heat will be converted to work with the same efficiency as for the combustion chamber without coating.
6. Exhaust enthalpy is the energy that remains in the cylinder at the end of the expansion stroke. In the case of a thermal barrier coating, the extra retained heat is partly converted to work, partly going to the exhaust heat. The assumption is that exhaust manifold gas temperature is proportional with the exhaust enthalpy at the end of expansion.
7. The model covers the high-pressure cycle only.

With these assumptions, the model is expected to over-predict the reduction in heat losses, efficiency gain and exhaust temperature, thereby giving an upper limit of the potential of a thermal barrier coating material. Below follow the equations that are used to calculate the results.

The indicated work, wall heat transfer and exhaust enthalpy are scaled with the fuel energy content in Equation (28). The sum of these scaled terms should be unity, which allows for the calculation of the exhaust enthalpy at the end of the expansion stroke, Equation (29). The indicated work and heat transfer can be derived from experimental engine data.

$$ratWork = \frac{W_{i,g}}{Q_{fuel}}; \qquad ratHT = \frac{Q_{wall}}{Q_{fuel}}; \qquad ratExh = \frac{H_{Exh}}{Q_{fuel}} \tag{28}$$

$$ratExh = 1 - ratWork - ratHT \tag{29}$$

The theoretical efficiency for conversion of heat to work is defined by dividing the indicated efficiency or $ratWork$ with the fraction of the heat from combustion that is not transferred to the wall in Equation (30). This theoretical efficiency is used in Equation (32) to estimate the extra work that can be extracted when wall heat transfer is reduced.

$$ThdEff = \frac{ratWork}{1 - ratHT} \tag{30}$$

The relative wall heat loss reduction in Equation (31) is proportional to the original heat loss fraction and the reduction in temperature difference between the wall surface and cylinder charge.

$$\Delta ratHT = -ratHT \frac{\Delta T_{wall}}{\Delta T_{charge}} \tag{31}$$

The efficieny increase can now be calculated according to Equation (32):

$$\Delta ratWork = -\Delta ratHT \times ThdEff \tag{32}$$

The change in relative exhaust enthalpy, Equation (33), must be equal to the sum of the relative change of the heat transfer and the change in indicated work, as the sum of these energy terms remains constant.

$$\Delta ratExh = -\Delta ratHT - \Delta ratWork \tag{33}$$

Finally, the exhaust temperature increase is estimated by assuming it is proportional to the exhaust enthalpy increase and the exhaust temperature level for a combustion chamber without insulation.

$$\Delta Texh = Texh \times \frac{\Delta ratExh}{ratExh} \tag{34}$$

The temperature swing model was validated with data from literature, covering results from 1D engine simulations, CFD simulations and engine measurements, and found to be in reasonably good agreement for the temperature swing amplitude and efficiency gains.

References used for the validation, also shown in the result section:

- Kawaguchi [79], with a hard anodized alumina SirPA coating from Toyota,
- Andrie [80], with a low capacitance coating with silica hollow spheres,
- Broatch [81], evaluating a zirconia-based coating from IFP,
- Hegab [82], investigating Keronite, a hard anodized alumina coating,
- Babu [83], evaluating a proprietary coating comparing with standard YSZ,
- Schaedler [84], with a low capacitance coating with nickel hollow spheres.

4.2.2 CFD model setup and thin wall module

The purpose of the CFD simulations was threefold: i) to identify when and where the burning spray interacts with the piston wall, ii) to calculate temperature and chemical composition of the charge near the piston wall to provide boundary conditions to the crevice model, iii) to calculate the heat losses and rate of heat release without and with a thermal barrier coating having the thermal properties of YSZ.

The software used for the CFD calculations was AVL Fire v2018. A sector of 45 degrees for a single spray was modeled (see Figure 10), using the RANS formulation. Traditionally, combustion CFD is performed with fixed wall temperatures. The average surface temperature in a combustion engine with metal walls does not fluctuate more than 10-20 degrees during a cycle. However, the surface temperature fluctuations become quite significant in the presence of an insulating material such as zirconia, especially at the locations were the burning sprays interact with the piston wall [5,29,85].

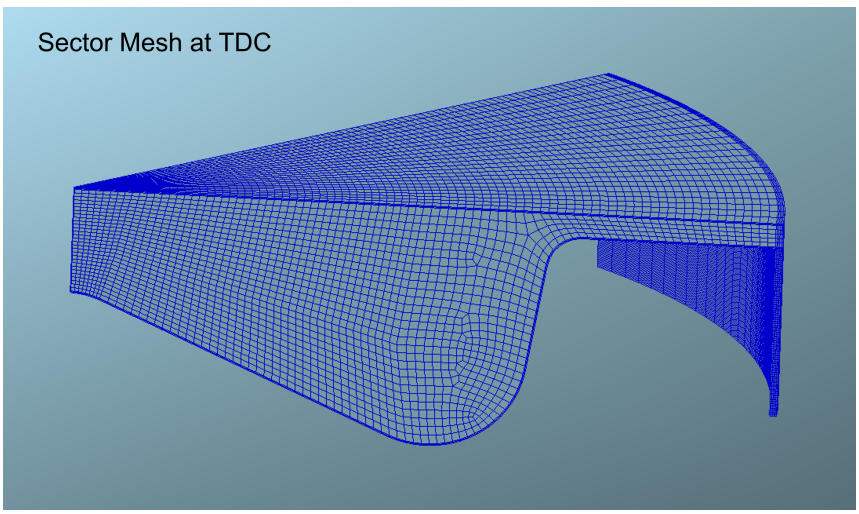

Figure 10. Sector mesh of the combustion chamber for CFD simulations.

The AVL CFD software includes a module to simulate conjugate heat transfer (CHT) for a thin layer of the combustion chamber surfaces. This module solves the heat flux and temperature equations for a thin layer at the wall surface, lateral and normal to the surface, with the same time step as for the fluid domain. Typically, the active part of the surface extends just a few millimeters into the solid, and the solid below the thin wall model domain is assumed to be constant in temperature during a combustion cycle.

The solid domain for the thin wall is created by extrusion of the fluid elements at the solid surface into the solid. A general layout for the mesh is shown in Figure 10. The thin wall can consist of different materials and for each material the number of layers can be defined. A compression factor is available to increase the resolution close to the interface between fluid and solid. The boundary conditions on the fluid side are set by the fluid temperature and heat transfer coefficient from the adjacent fluid element. On the solid side of the thin wall, the environment, the substrate temperature is fixed. These boundary conditions are of the same type when no thin wall module is used. The thin wall model is accurate when the thin wall thickness is small compared to the curvature of the solid surface.

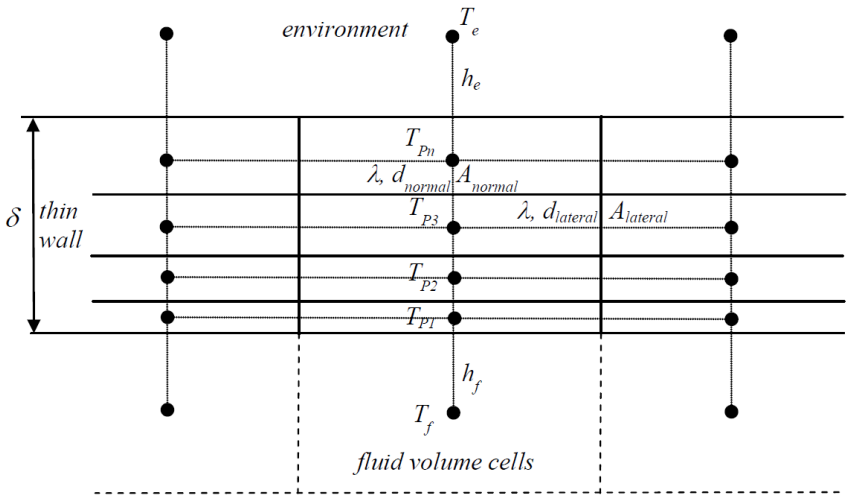

Figure 11. Principal design for thin wall mesh (from AVL Fire manual).

The selection of the sub-models and mesh refinement for the CFD model setup was partly based on the work by Fridriksson and Šarić [86,87]. Standard parameter values were used for all models apart from the auto-ignition model parameters, where adjustments were made to make the predicted pilot fuel combustion similar to the experimental data. Details of the sub models used are described in Table 7.

Table 7. CFD model description.

Property	**Description**
CFD Software	AVL Fire v2018
Average cell size	0.5 mm
Near wall boundary layers	2x 0.1 mm
Turbulence model	RANS, k-ζ-f
Wall treatment	Hybrid, Han-Reitz
Surface roughness	Not activated = default: • Roughness height 0 mm • Roughness constant 0.5
Spray model • Break up model • Turbulent dispersion • Particle interaction • Drag law • Evaporation	Langrangian particle tracking • Wave standard • Enabled • Schmidt • Shiller Nauman • Dukowicz
Combustion model	ECFM-3Z, includes auto-ignition model and chemical kinetics model
Thin wall at piston surface	3D CHT, multiple layers
Fuel properties	Diesel EN590 B7

4.2.3 Crevice model for open porosity in thermal barrier coatings

The heat loss and fuel entrainment in the pore volume of the thermal barrier coating is modeled with a crevice model. This type of model has been developed already in the early 80-ies by Gatowski [88] to describe heat losses and fuel trapping in crevice volumes in the combustion chamber of SI engines. Examples of crevice volumes are the piston top land and volumes in and around the spark plug and fuel injector. Due to the large surface to volume ratio of such a volume, the charge in these volumes quickly cools down to the temperature of the walls and can contain a relatively large portion of the cylinder charge around TDC, including fuel in case of a premixed charge. The surface to volume ratio for pores in plasma sprayed TBCs is at least one order of magnitude higher than for example the piston top land. Thus, it is assumed that the crevice model is valid for this type of coating as well.

The main assumptions for the crevice model are that incoming gas will immediately assume the crevice wall temperatures, and the pressure in the crevice is equal to the average combustion chamber pressure, i.e., no flow losses. With these assumptions, using the ideal gas law, a simple set of equations can be derived, as shown by Heinle [89]. Equation (35) describes the mass flow into the crevice which is directly proportional with the pressure change in the combustion chamber. Equations (36) and (37) describe the heat flux to the crevice walls, which is different for inflow and outflow conditions. During inflow, heat flux to the crevice wall originates from energy entering the crevice as well as energy from compressing and heating the charge in the crevice. During outflow, the expanding charge will absorb some heat from the walls, as the temperature of the charge in the crevice is assumed to be constant. The line with Equations (38) shows the relations for specific enthalpy and internal energy, related to the specific heats for constant volume and constant pressure. The gas properties are calculated using the NASA tables for the appropriate local gas composition and temperature.

$$\frac{dm_{cr}}{d\theta} = \frac{V_{cr}}{T_{cr}R}\frac{dp}{d\theta} \tag{35}$$

$$\frac{dQ_{cr}}{d\theta} = -\frac{dm_{cr}}{d\theta}\left(h_{cyl} - u_{cr}\right), \quad \frac{dm_{cr}}{d\theta} > 0 \tag{36}$$

$$\frac{dQ_{cr}}{d\theta} = -V_{cr}\frac{dp}{d\theta}, \quad \frac{dm_{cr}}{d\theta} < 0 \tag{37}$$

$$h_{cyl} = c_p T_{cyl}; \quad u_{cr} = c_v T_{cr}; \quad T_{cr} = T_{wall} \tag{38}$$

The crevice volume in the equations above is determined by the surface area, the average thickness and the average porosity of the coating:

$$V_{cr} = A_{tbc} \times h_{tbc} \times \Phi \tag{39}$$

The extra heat loss simulated with the crevice model can be directly related to the apparent rate of heat release, but the effect of fuel entrainment is not so straight forward.

What happens, step by step, when a burning jet approaches, reaches and covers the piston bowl surface?

1. While the burning jet travels towards the piston bowl wall, cylinder charge pressure increases due to combustion and charge (air) is pushed into the porous coating. Heat loss in the crevice will reduce the apparent rate of heat release compared to the case without a porous coating.
2. When the jet reaches the wall, part of the reacting mixture at the head of the jet will be pushed into the coating. The combustion reactions in this entrained reactive mixture will extinguish due to the reduction in temperature. In the presence of a porous coating, less fuel will burn, there will be a deficit of rate of heat release.
3. After the initial contact the jet will become a wall jet and continue traveling parallel with the bowl surface, quickly covering the whole piston. While the reaction zone is traveling along the wall, charge pressure is still rising, and part of the reaction zone will be pushed into the coating and combustion reactions will get extinguished. Again, this will be a deficit compared to combustion without a porosity at the surface. After passing of the reaction zone, rich mixture from the core of the jet will continue to penetrate the open porosity.
4. In contrast to entrainment of the reaction zone, there is no direct effect on heat release of fuel entrainment from the rich core into the coating, as the reactivity/heat release in the rich zone is small in comparison.

In Figure 12, images from a burning jet illustrate the reaction zone at the front of the free jet, just before impinging the wall, and the moment after impingement when the flame front is at the head of the wall jet.

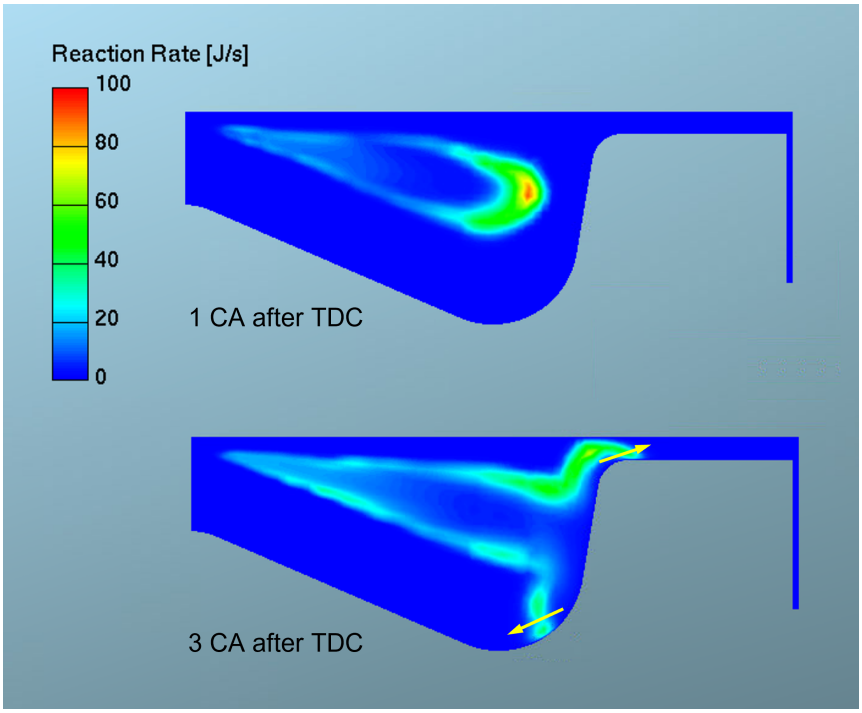

Figure 12. Rate of heat release distribution in the vertical cross section through the center of a burning jet, calculated with the CFD model for EOP B. The yellow arrows indicate the direction of the flame front traveling across the surface.

The fuel entrainment process is illustrated in Figure 13. Partly burned fuel enters the crevice volume when the jet comes into contact with the thermal barrier coating while the cylinder pressure is rising. Typically, the core of the jet is rich and consists of hydrocarbons, carbon monoxide, water, carbon dioxide and nitrogen.

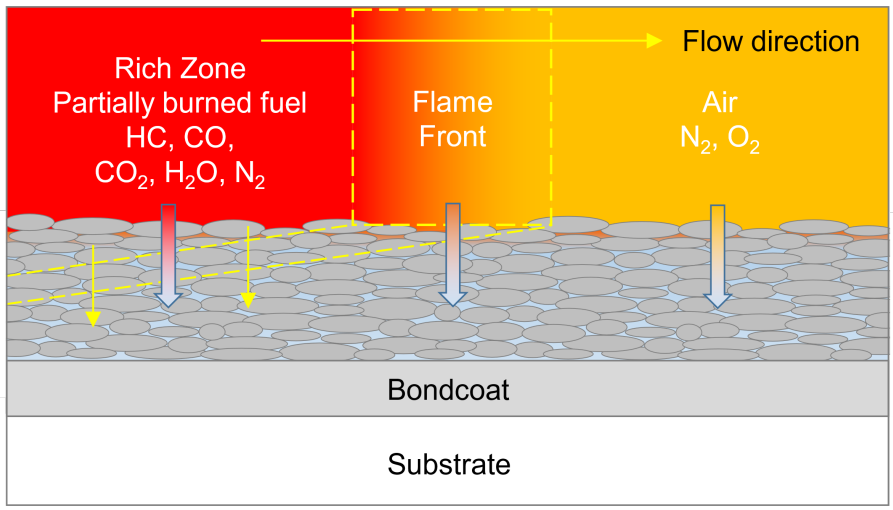

Figure 13. Entrainment of partially burned fuel from the core of the jet and flame front into the porous TBC during compression and combustion.

With Equation (40) a simple relation is proposed to calculate the energy deficit due to partial entrainment of the reactive flame front. The ratio between the contact surface A_{comb} of the reaction zone in the flame front and the total coating surface A_{tot} is estimated from CFD simulation results as a function of crank angle.

$$\frac{dE_{comb}}{d\theta} = \frac{A_{comb}}{A_{tot}} \frac{dm_{cr}}{d\theta} \left(LHV_{CO}[\mathrm{CO}] + LHV_{HC}[\mathrm{HC}]\right) \tag{40}$$

Later in the cycle, when the cylinder pressure drops, fuel is released from the coating as illustrated in Figure 14. The burning rate of this released fuel depends on the local availability of oxygen and the temperature level, but in the crevice model the fuel is assumed to oxidize immediately when leaving the porous coating.

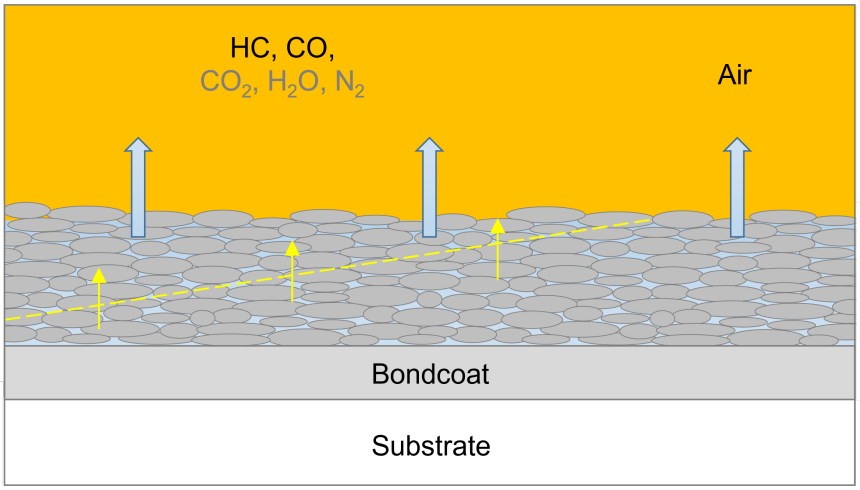

Figure 14. Release of HC and CO from the porous TBC during pressure drop in the expansion stroke.

The objective of this simple model with rather rough assumptions is to estimate the magnitude of the heat loss and fuel entrainment effects on the apparent rate of heat release and compare it with experimental data.

4.3 Tested thermal barrier coatings

Three sets of pistons were procured with coatings for engine testing. The first engine test campaign aimed to evaluate two state-of-the-art (2016) thermal barrier coatings. The second test campaign was dedicated to novel thermal barrier coatings with a new spraying process, material, and surface sealing. The third experimental campaign focused on crevice effects in a standard YSZ coating, including effects of surface sealing on the crevice effect.

4.3.1 State of the art thermal barrier coatings

Two thermal barrier coatings were of particular interest for understanding the performance of TBCs. The first one was plasma sprayed Yttria Stabilized Zirconia (8wt%) or 8YSZ. This TBC is well established and has been used in gas turbines for many years but results from application in internal combustion engines have been varying. The second TBC of interest was developed by Toyota, produced by hard anodizing aluminum of the piston surface. This coating was named SiRPA, or Silica Reinforced Porous Anodized aluminum. Toyota presented this coating in 2015, after investigating the requirements to achieve an improved temperature swing of the coating surface, in a newly developed 2.2L LD diesel engine.

The purpose of testing these two state-of-the-art thermal barrier coatings was to assess their performance with an accurate and complete set of data in relevant operating conditions applied on the Volvo LD Diesel combustion system. A complete set of data includes fuel consumption, emissions, heat losses and combustion process details derived from cylinder pressure such as apparent rate of heat release.

Yttria Stabilized Zirconia

Yttria Stabilized Zirconia is probably the most researched and well-known thermal barrier coating material for engineering. This coating material originates from the gas turbine industry and the most used formulation with 6 to 8% yttria was published by NASA in 1978 [90]. It is used to protect turbine blades and combustion chambers from hot combustion gases and allows for high process temperatures which benefits turbine efficiency. This ceramic material is relatively ductile, it is stable up to high temperatures and has low thermal conductivity. Therefore, it is not surprising that it was selected early for insulation of the combustion chamber in automotive applications.

The chemical formula for the most used variant of YSZ is ZrO_2-$8Y_2O_3$. Adding 8wt% yttria to the zirconia improves fracture toughness and increases high temperature stability allowing for a service temperature from 1200 °C up to 1350 °C. The thermal conductivity of the bulk material is 2 to 2.5 W/m.K. When used in a thermal barrier coating, applied with air plasma spraying, thermal conductivity is reduced due to porosity and the many interfaces and micro cracks between the splats. Typical values, provided by suppliers, are 0.8 to 1.8 W/m.K. Coating porosity ranges from 8 to 20%, depending on the process parameters used for spraying. The thermal expansion coefficient is $10x10^{-6}$ m/m.K, close to that of steel. Zirconia is transparent for oxygen which can lead to oxide formation at temperatures above 700 °C between coating and substrate. This is one of the reasons that in gas turbine applications with YSZ, a bond coat is required. This metallic bond coat is designed to create a thin alumina oxygen barrier - "thermally grown oxide" or tgo - layer at the interface between bond coat and

top coat (YSZ). The bond coat also improves adhesion of the TBC to the substrate and compensates for differences in thermal expansion ratios.

Before application of the bond coat, the surface of the substrate is grit blasted to improve adhesion between bond coat and substrate. Typically, the bond coat is applied with air plasma spraying (APS) or high velocity oxyfuel spraying (HVOF). The latter gives higher density and better adhesion to the surface. The top coat of YSZ is typically applied with air plasma spraying. The YSZ spray solidifies at the surface and is stacked in the form of pancakes or 'splats'. Cracks or spaces parallel to the aluminum surface reduce thermal conduction but can also initiate mechanical failure of the coating. Typical bond coat thickness is in the range of 50 to 100 µm, typical YSZ top coat thickness ranges from 100 to 1000 µm. However, the risk for mechanical failure increases with higher thickness.

Application of the zirconia coating and bond coat for our experiments was done at University West in Trollhättan. This University has a close cooperation with the gas turbine industry and is specialized in thermal spraying processes. For spraying, the piston was mounted in a rotating fixture, while the spray gun followed a programmed track to coat the piston surface with an even thickness. Figure 15 shows the coated piston. The nature of the application process creates a relatively rough coating surface, typical Ra values are in the range of 7 to 12 µm.

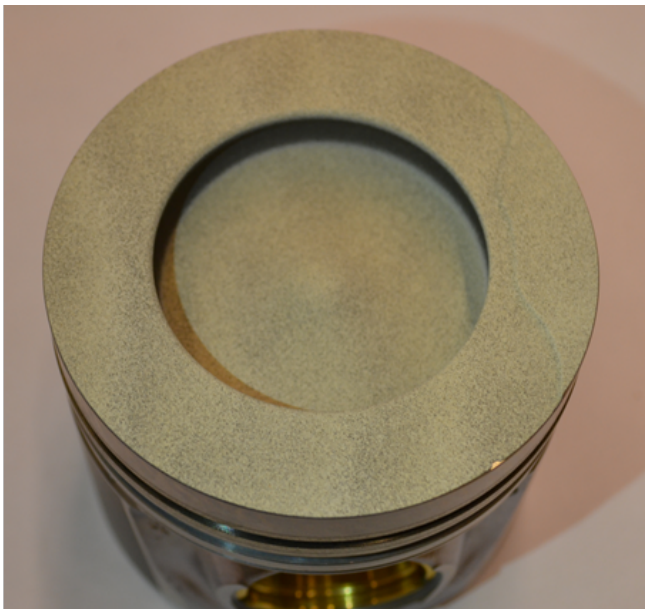

Figure 15. Coated piston surface with plasma sprayed zirconia.

Because the coating adds material to the surface, a thin layer from the piston top was machined off to target the same compression ratio as for the uncoated piston.

The coating was also applied on 1 inch coupons with the same spraying parameters to evaluate the coating thickness, structure and thermal properties. Figure 16 shows a cross section of such a coupon with bond coat and top coat of YSZ.

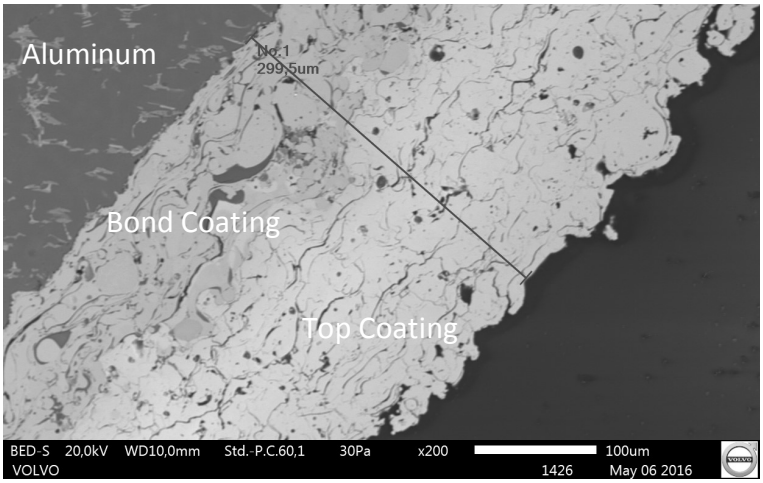

Figure 16. Electron microscope image of cross section of plasma sprayed zirconia on an aluminum coupon.

The specification for the used spraying powders from Oerlikon:

- Top coat: Oerlikon Metco 204b-ns, chemical composition: ZrO_2-$8Y_2O_3$.
- Bond coat: Amdry 365-2, chemical composition: Ni 23Co 17Cr 12Al 0.5Y

SiRPA - Silica Reinforced Porous Anodized Aluminum

Anodizing of aluminum products is a surface treatment to improve oxidation and wear resistance and is used for many aluminum products like laptop casings, light weight climbing gear, bicycle parts, wheel rims, cookware as well as aircraft components.

To anodize the surface of an aluminum object, the object is placed in an acidic bath and subjected to a current or voltage difference. The result is a chemical reaction where alumina, aluminum oxide, is formed at the surface (Al_2O_3). As the oxide layer gets thicker, channels are formed perpendicular to the surface to transport ions, creating a structure similar to a honeycomb (see Figure 17). The number and size of the channels or pores in the oxide layer can be controlled with process parameters like voltage, current and composition of the acidic solution. There are three categories of anodizing aluminum, where hard anodizing (type III) is used to create the thickest range of coatings that can be applied with this process, typically 20 to 100 µm.

The SiRPA coating was developed by Toyota and introduced in 2015 in a 2.2L LD Diesel engine [91]. Two years earlier, in 2013, Toyota presented a concept called "temperature swing coating". The idea is that the surface of this type of coating would follow the charge temperature during the combustion cycle. This concept is not new, it was formulated as early as 1979 by F. Wallace [17], but the work by Toyota created new awareness and increased focus on this type of coating. The target was to create a coating with very low effusivity, which requires low thermal conductivity and low volumetric heat capacity.

Toyota measured the thermal conductivity of SiRPA to be 0.65 W/m.K. This is at the low end for hard anodized oxides, reported by Lee [92]. Volumetric heat capacity is reported to be as low as 1.3 J/cm3.K. To reach low effusivity, high porosity is required as the name of the coating indicates. And to reinforce and seal the coating

against penetration of hot charge and fuel, the surface was impregnated with silica (SiO_2), which was applied as a liquid inorganic perhydropolysilazane and cured in an oven. The surface roughness of SiRPA is around 7 µm, which had a negative effect on combustion when applied in the piston bowl. For that reason, Toyota chose to apply the SiRPA coating only on the piston top outside of the bowl (see Figure 4).

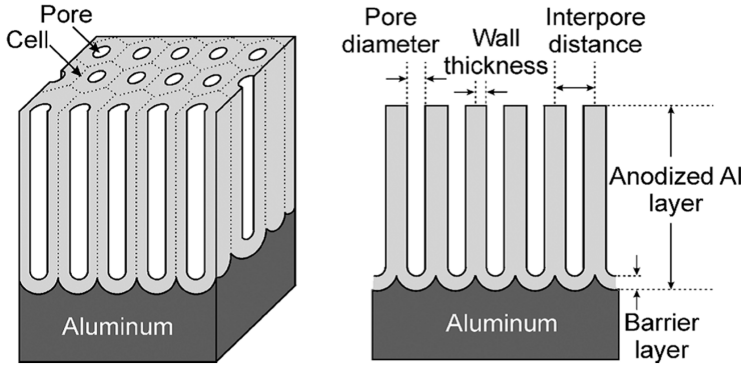

Figure 17. General structure of anodized aluminum.

Mahle, Volvo's piston supplier for the LD diesel engines, prepared the pistons for this experiment with a hard anodized layer. Before coating application, half of the target coating thickness was machined off from the piston top. When the coating grows from the surface, the volume doubles. In this way, the compression ratio of the piston would be unchanged. Figure 18 shows a piston with a hard anodized surface for the whole piston crown. To mimic the Toyota application, pistons with coating only at the squish surface were procured and tested as well.

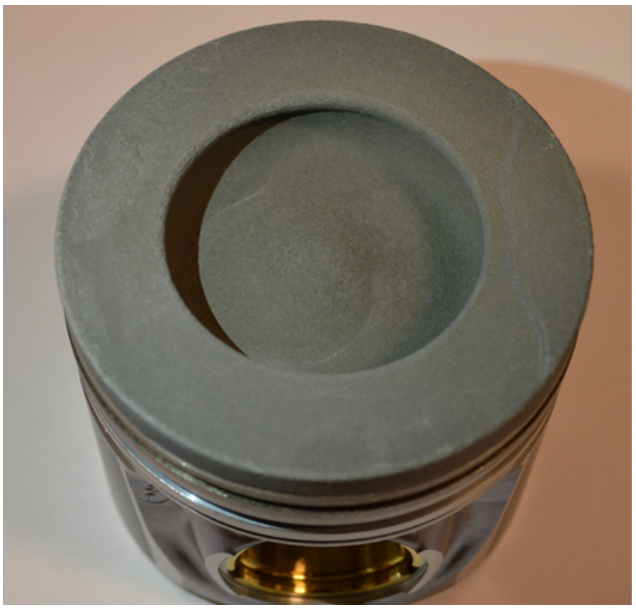

Figure 18. Piston with hard anodized aluminium oxide surface.

In Figure 19 a cross section is shown of the oxide layer and the aluminum piston substrate. This part was cut out of a coated piston to verify the coating thickness and analyze the coating structure. In this image it is hard to identify an organized honeycomb structure of channels, the aluminum layer might have been damaged by cutting the sample from the piston. However, a similar cross section taken from SiRPA published by Kawaguchi et. al. looks very similar [29]. Surface roughness measurements showed a comparable surface roughness for the zirconia and alumina coatings.

Unfortunately, Mahle did not share details of the coating process nor expected coating properties. At the time of these experiments, it was not possible to measure the coating properties at Volvo.

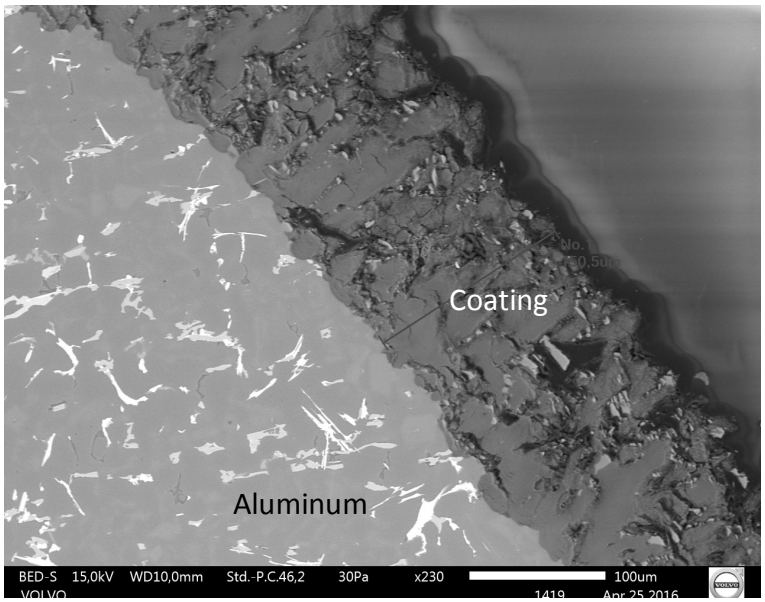

Figure 19. Electron microscope image of a cross section of the piston surface showing the aluminum substrate and the layer of alumina coating.

4.3.2 Novel thermal barrier coatings

In 2017, a project called "Novel Thermal Spray Coatings for Increased Thermal Efficiency of Diesel Engines" was started, initiated by the author of this thesis. The project partners were University West, Volvo Cars, AB Volvo and Scania AB. The project was partly financed by Swedish Vinnova FFI. University West has a research department specialized in thermal spray and additive manufacturing and a tight cooperation with GKN, manufacturer of gas turbine for aircraft industry. This project made it possible to explore new developments in the field of thermal sprayed thermal barrier coatings and aim for lower effusivity values.

One of the new developments was suspension plasma spraying (SPS) which allows for the use of very small particles and creation of completely different coating structures. The particles are suspended in a solvent such as water or ethanol which prevents the small particles from evaporation as well as early melting and coalescing with other particles forming bigger particles. A featherlike structure can be created as

shown in Figure 20 with vertical gaps. This structure allows for larger differences in thermal expansion between substrate and coating and improves coating durability. Moreover, the small grain size creates many interfaces which reduces thermal conductivity [93].

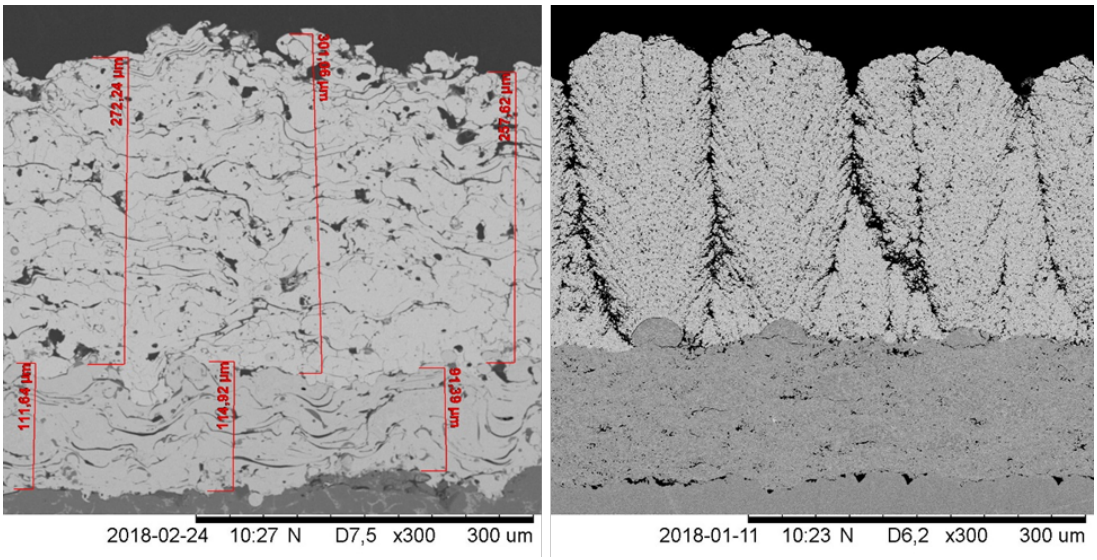

Figure 20. Air plasma sprayed (left) and a suspension plasma sprayed (right) thermal barrier coatings of YSZ with bond coat. Images taken from cross-cuts with a scanning electron microscope.

A new material, with ~30% lower thermal conductivity and better high temperature stability compared to 8YSZ, is gadolinium-zirconate (GdZr). The chemical formula is $Gd_2Zr_2O_7$. A disadvantage with this material is that it is less ductile and has a lower coefficient of thermal expansion. For that reason, SPS is a very suitable spraying method for GdZr as it makes the coating more robust for thermal expansion.

From the first experiments and literature research it became apparent that it might be beneficial to seal the coating surface, to prevent hot gas and unburned fuel to enter the porous coatings. One way to apply a thin sealing layer is the use of a polysilazane. This is a liquid polymer-based pre-ceramic precursor, that cures to a ceramic at elevated temperatures. Typically, silicon-nitrides Si_3N_4 and silicon-oxides SiO_2 can be produced with this method. For this project, Durazane 1800 from Merck was selected, forming silicon-nitride, based on research results from Barroso [94] and on the direct availability of this material. Typical thermal properties for amorphous silicon-nitride are: k = 3-5 W/m.K, cv = 2.1 J/cm3.K [95]. In Figure 21 a cross-section is shown of a polished suspension plasma sprayed coating, sealed with Durazane, cured at 225 °C in an oven. The sealing will cure further at higher temperatures in the engine, but the bronze piston bushing limited the use of higher oven temperatures. The sealing layer itself is very thin and hardly visible in the image.

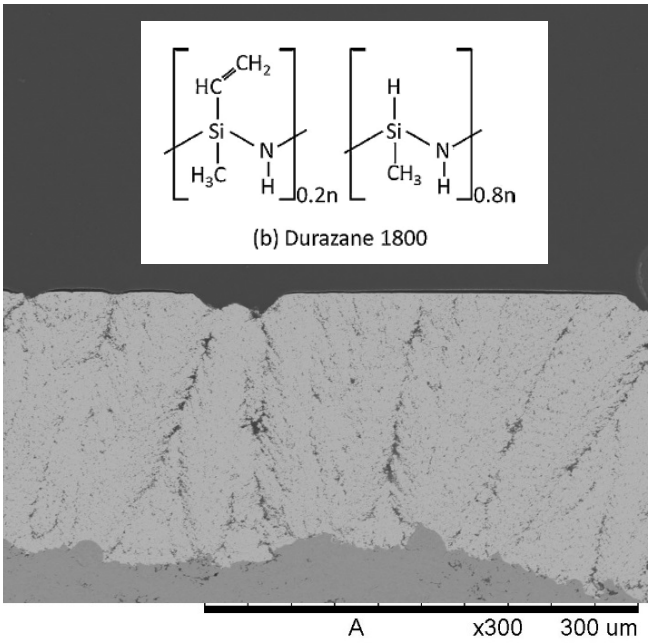

Figure 21. Cross-section of suspension plasma sprayed YSZ, sealed with Durazane after polishing of the coating surface. Image taken with a scanning electron microscope.

For the experimental campaign with the novel thermal barrier coatings a design of experiments was used to identify the effects of coating material, the spraying method and surface sealing. This resulted in six different piston coatings, listed in Table 8 and displayed in Figure 22.

In the corresponding paper III, more details of the coating application and thermal properties can be found. A further analysis of the coating structure and the effect of spraying angle for these pistons was performed at University West by Uczak de Goes [96].

Table 8. Piston coating specification for the novel thermal barrier coatings.

Piston ID	Material top coat	Spraying method	Sealed surface	Polished surface
ZAC	8YSZ	APS	yes	yes
ZAO	8YSZ	APS	no	yes
ZSC	8YSZ	SPS	yes	yes
ZSO	8YSZ	SPS	no	yes
GSC	GdZr	SPS	yes	yes
GSO	GdZr	SPS	no	yes

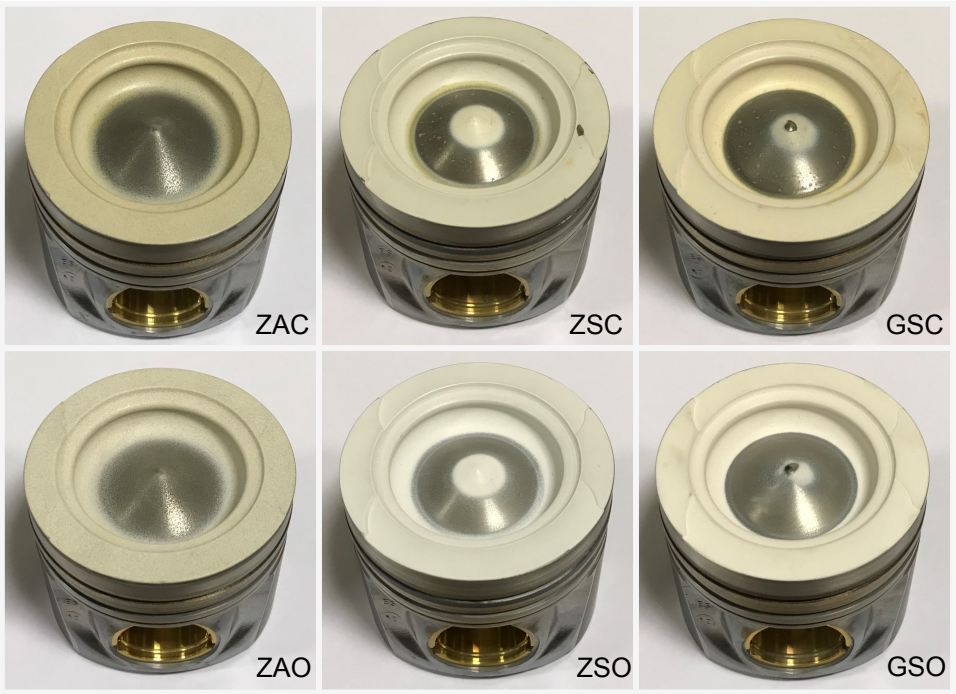

Figure 22. Pistons with novel thermal barrier coatings, see Table 8 for coating details.

To conclude and illustrate that thermal spraying is a process that requires many iterations of fine tuning and optimizing spray parameters, Figure 23 is included with two pistons from the spraying trials. These trials were performed to create the desired bond coating thickness and to adjust the thermal load on the piston during for suspension plasma spraying. On the left piston, the oil cooling gallery is exposed after a test where the piston top melted due to the high heat flux from the plasma spray.

Figure 23. Spray trials with bond coat (right piston) and suspension plasma sprayed YSZ (left piston).

4.3.3 Coatings for crevice effect investigation

This section is about coatings for the crevice effect investigation. The crevice effect can be described as energy loss due to entrainment of hot charge and unburned fuel in the permeable porosity of a thermal barrier coating. From experiments with coatings described in the previous section there were indications that this crevice effect affected the measured apparent rate of heat release in a negative manner.

The same type of YSZ coating was used as in the previous campaigns. This time the coating was sprayed with a target thickness of about 300 µm instead of 200 µm to have a significant crevice volume in the coating.

One part of testing the hypothesis of the crevice effect was sealing of the coating surface to prevent penetration of the hot charge and unburned fuel. The sealing with Durazane 1800, used for the previous coatings, did not seem very effective; the apparent rate of heat release was not affected to a big extend. Therefore two other types of sealing layers were selected that could be applied with thermal spraying and that create very dense coatings: the metal alloy Ni95Al5 and ceramic aluminum oxide Al_2O_3 applied with SPS. In Figure 24 SEM images show a cross section of the YSZ coating with both types of sealing layers. For these samples, the top coat was not polished before application of the sealing layer.

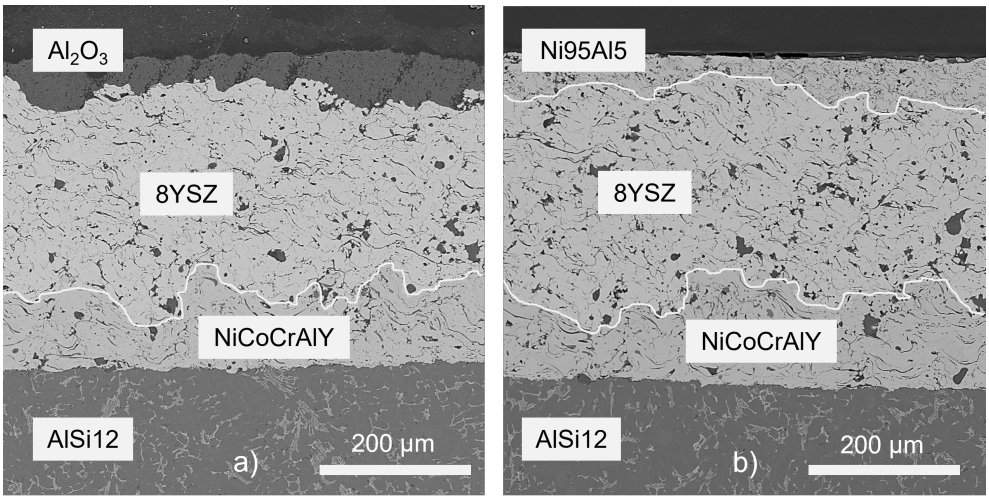

Figure 24. Electron microscope images of the TBC with a) alumina and b) nickel alloy sealing layers. The white lines at the interfaces are added for clarity.

The selected metal alloy Höganas Amperit 281 is normally used to create dense bond coatings for use below 800 °C and for restoration of worn or mismachined components. The chosen Treibacher Aurercoat Al_2O_3 water suspension is designed for the production of dense, wear resistant coatings by suspension plasma spray (SPS).

The thermal and physical properties of the two sealing materials are quite different: the metal sealing layer has a higher thermal conductivity and volumetric heat capacity, but it can be polished to a very low surface roughness and has higher radiation reflectivity. The metal is also more ductile compared to the ceramic layer and the coefficient of thermal expansion is higher. Especially the difference in surface roughness adds an extra dimension to the investigation.

The YSZ coating on the pistons was polished before application of the sealing layers. An average thickness of the sealing layer of 50 µm was required to ensure complete coverage of the rough coating surface.

The three coated pistons and reference piston used for the crevice effect investigation can be seen in Figure 25. The metal sealing layer is polished to the same surface roughness as the uncoated piston. The ceramic surfaces for the other two pistons are much harder, only the roughness peaks were removed with polishing. More details can be found in Paper IV.

Figure 25. Uncoated reference piston and pistons coated with YSZ. The surface of the two pistons at the bottom is sealed with a nickel alloy (left) and alumina (right) layer.

5 Results

The results from the experiments and a major part of the simulations are described and discussed in detail in the attached publications. In this chapter a red line is sketched through the results to create an overview and show coherence of the work. The results from the surface temperature swing model were not published separately and will be presented and discussed in detail in paragraph 5.2.

Here the highlights are listed in short:

- The state-of-the-art coatings of air plasma sprayed yttria stabilized zirconia and hard anodized aluminum did not improve indicated efficiency. The main causes were the high surface roughness and the reduced compression ratio from open porosity in the coating. According to predictions with a multiple linear regression model based on the measured data, indicated efficiency would be similar to the uncoated piston if the coated pistons would have had the same surface roughness and compression ratio.
- Soot deposits reduced indicated losses when motoring with 0.2 bar, a soot burn-off sequence increased indicated efficiency with 0.7%. This indicates the significance of the insulating effect of soot deposits.
- The temperature swing model predicts that effusivity values below 900 $W.s^{0.5}/m^2.K$ are required if an indicated efficiency increase of more than 2% is to be realized with a TBC on the piston crown. In theory, the tested state-of-the-art coating of YSZ on the piston top should give an efficiency increase of about 1%. This indicates that there are processes that counteract this potential efficiency increase.
- Among the investigated novel thermal barrier coatings, the suspension plasma sprayed gadolinium-zirconate without sealing layer performed the best. An efficiency improvement of 0.6% was predicted with the model based on the measurement data when surface roughness and compression ratio were at the same level as for the reference piston. This result was not obvious from the measured thermal properties, but the high porosity of this coating stands out. The sealing layer of Durazane 1800 reduced the combustion duration and increased heat losses. No benefit for fuel efficiency was seen compared to non-sealed coatings.
- The investigation of charge and fuel entrainment in a porous YSZ coating showed that a zero-dimensional crevice model can predict the magnitude and principal shape of deviations in the measured rate of heat release relative to an uncoated piston. The contribution from increased heat losses and fuel entrainment were equally significant. Heat losses for the coated piston increased also when motoring. The level of these extra losses was predicted by the crevice model as well. The surface sealing layers of nickel alloy and alumina were damaged by the challenging conditions in the combustion chamber and could not prevent charge penetration in the coating.

5.1 Evaluation of state-of-the-art thermal barrier coatings

Two state of the art thermal barrier coatings (from 2016) were evaluated in single cylinder engine experiments, 8YSZ (ZrO) and a hard anodized aluminum inspired by Toyota's SiRPA coating (AlO). The pistons coatings were applied in four variants: two covering the whole piston crown, polished (Pol) and unpolished (Rgh), plus two only covering the squish surface, polished and unpolished. Also, a variant with a rough surface was created for the uncoated piston as part of the investigation of the effect from surface roughness on efficiency. Figure 26 shows the measured gross indicated efficiency for the uncoated pistons and the coated pistons with coating of the whole piston crown. It is obvious that high surface roughness reduces indicated efficiency significantly. And the coated pistons have lower indicated efficiency, even when polished compared to the uncoated piston. The YSZ coated piston shows the lowest efficiency at the lower load points.

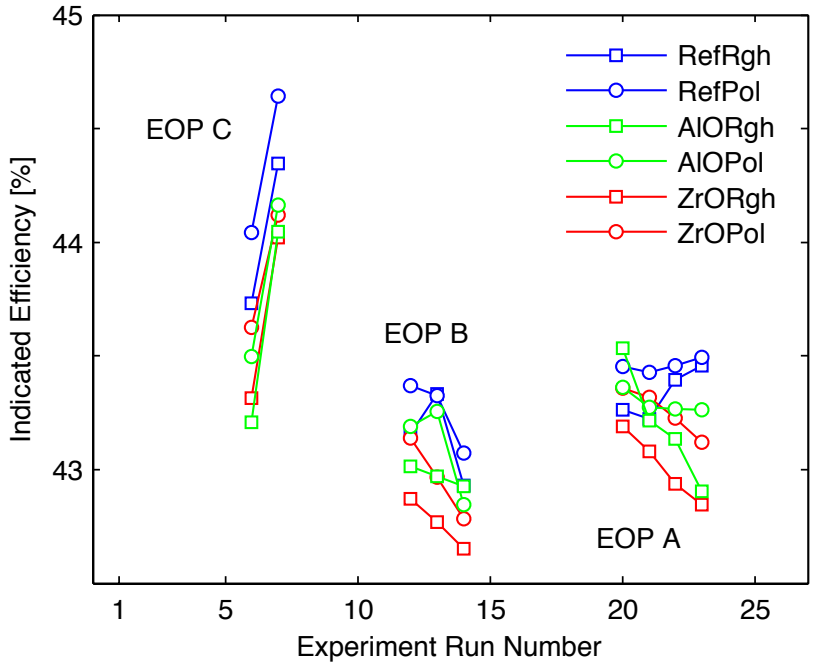

Figure 26. Gross indicated efficiency versus run number. For EOP C (high load) two different fuel pressures are shown, curves for EOP A and B (medium and low load) show increasing levels of EGR.

Modeling the measured data with a multiple linear regression model is a way to improve the accuracy of the estimation for the different responses, and it allows for separation of effects from compression ratio, surface roughness and coating specification. The measured gross indicated efficiency taken from the MLR model for three pistons with the ZrO and AlO coating is compared to the standard reference in Figure 27. Also here the rough coating performs worst, the polished coating is slightly better and the piston with polished coating on the squish surface only is almost on par with the reference. The AlO coating seems to perform slightly better than the ZrO, but the difference is hardly significant

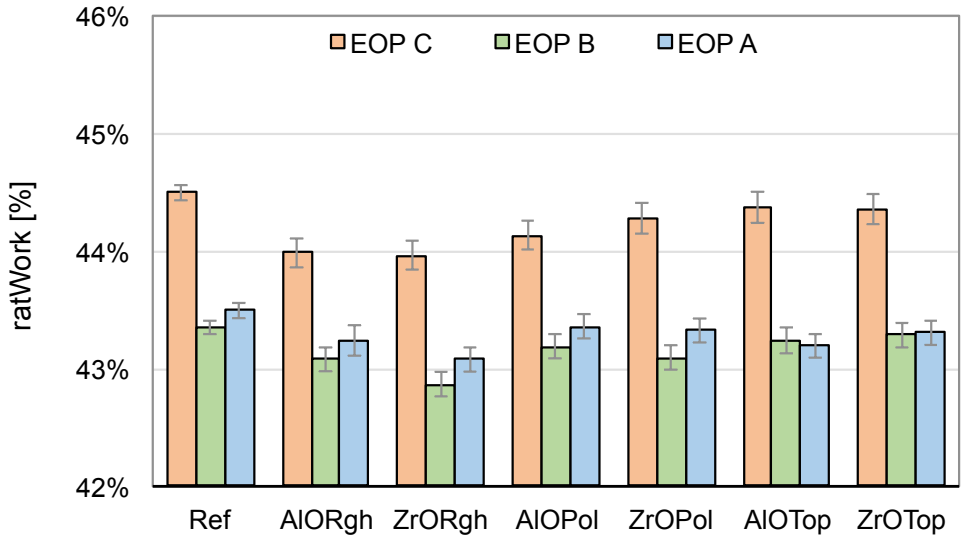

Figure 27. Estimation of the indicated efficiency from the modeled data. No EGR for EOP A and B, high rail pressure level for EOP C. Error bars show the 95% CI.

When the MRL model is used to predict the gross indicated efficiency, assuming the same compression ratio and surface roughness for all pistons, there is no significant difference from coating application. If there is a benefit from insulation (the heat load on the piston cooling oil is actually reduced), it is probably counteracted by phenomena such as crevice effect, convection vive or oxidation of insulating soot layer due to increased surface temperatures, discussed in the background section.

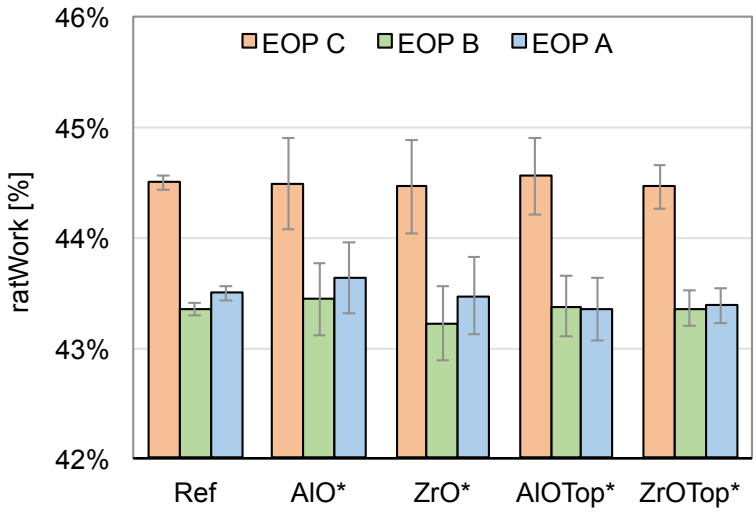

Figure 28. Predicted indicated efficiency (ratWork) with Ra = 1.3 µm, CR = 15.5 for all pistons. The error bars show 95% CI. The stars on the labels mark that these are predictions for coatings with modeled properties.

The significance of soot deposits for heat loss and indicated efficiency was investigated as well. In Figure 29, the in-cylinder motoring losses are shown, without soot layer (S0), measured with new or cleaned parts before combustion started, and after running with combustion for each engine load (S1, S2, S3). Lower heat losses

caused by soot deposits reduce motoring losses with about 0.2 bar. Comparing the impact of soot deposits to typical engine friction values (FMEP) shows the significance for engine efficiency. Normally FMEP is a positive value, here the sign is changed for easier comparison. An increase in IMEPH with 0.2 bar for EOP B would improve indicated efficiency by 1.8%.

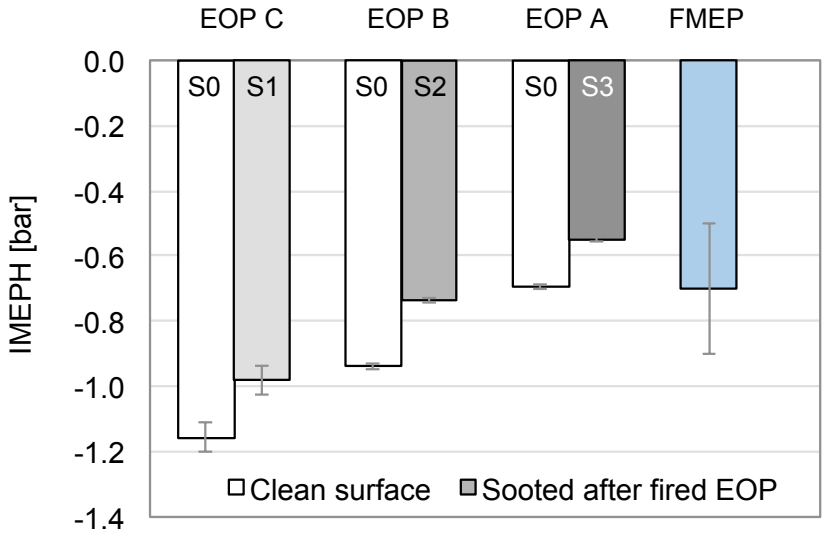

Figure 29. Effect of soot deposits on IMEPH, shown for the reference piston. Typical friction losses (FMEP) are included for comparison. The error bars represent the 95% confidence intervals. The low and high level for FMEP corresponds to friction at 1500 and 3000 rpm.

Another way to investigate the effect of soot deposits is to perform a "soot burn-off" sequence. Typically, especially when using EGR, the soot deposits are formed at low engine loads and partly oxidized at higher engine loads. Figure 30 shows such a sequence. First the engine is run at lowest load, EOP A at 1500 rpm with 15 mg of fuel per stroke until stable fuel consumption is reached. Then the load is increased to EOP B conditions, 30 mg fuel per stroke, and EOP C with increased engine speed to 3000 rpm and 60 mg fuel per stroke. After burn-off, the lower load points are measured again. Three measurements are taken in each load point to increase confidence for the data. After soot burn-off, the indicated specific fuel consumption is increased with 0.7%.

These two evaluations show the significance of the soot deposits for heat transfer and engine efficiency. The magnitude is in the same order as the expected improvements from thermal barrier coatings. Oxidation of soot deposits due to the increased surface temperature of a thermal barrier coating can be a negative side-effect of significance.

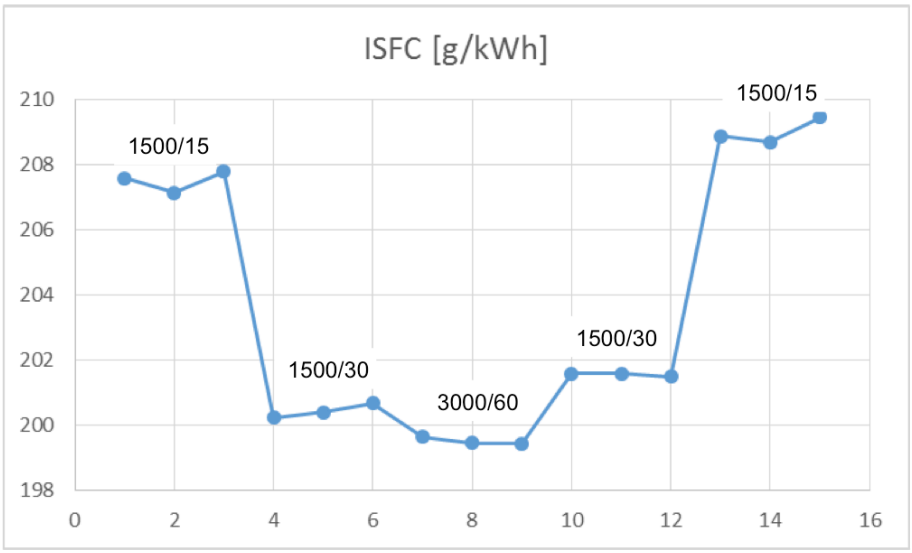

Figure 30. Indicated specific fuel consumption for EOP A, B and C (see-Table 6) in a soot burn-off test sequence. Each load point was measured 3 times. The numbers in the figure are engine speed / fuel mass.

5.2 Temperature swing evaluation

With the surface temperature swing model, described in 4.2.1, predictions were made for the cyclic coating surface temperature variation and thermal penetration depth. The modeled load case here is part load operation EOP B, assuming a coating on the piston crown only, representing 60% of the total surface area of the combustion chamber. The data in Table 9 was used as input for the calculations. The gross indicated efficiency and heat losses were derived from experimental data. The average charge temperature and heat transfer coefficient were calculated from the cylinder pressure trace with the ideal gas law and heat transfer model by Hohenberg [3].

Table 9. Input data for the temperature swing model simulating EOP B.

Parameter	Value	Unit	Description
ratWork	0.44	-	Gross indicated work relative to fuel energy w/o coating
ratHT	0.23	-	Heat transfer relative to fuel energy w/o coating
ratPist	0.60	-	Relative piston top surface area
Twall	473	K	Wall substrate temperature below coating (fixed)
Tcharge	1800	K	Average charge temperature (-10 to 30 CA aTDC)
h_c	1900	W/m^2K	Average heat transfer coefficient (-10 to 30 CA aTDC)

From the modeled temperature swing, further predictions were made for the increase in indicated efficiency and exhaust temperature. The figures in this section will present the results as a function of thermal conductivity and volumetric heat capacity.

Equation (30) and (31) can be used to predict the performance of an engine where the surface temperature of the piston top would assume the charge temperature instantly. This would require a coating with an effusivity of zero. Using the values for efficiency and heat loss in Table 9, the gross indicated efficiency would increase from 44% to 52%, or a reduction of fuel consumption with 18%. In case the whole combustion chamber has adiabatic walls, the predicted fuel consumption reduction is even higher: 30%. This result is in line with an energy loss breakdown by Weberhauer et. al. [97]. The theoretical energy saving potential of heat loss reduction is huge. However, as will be shown, realization of this potential is exceptionally challenging with respect to coating material requirements.

To put the simulation results in context, published data from a number of representative TBC materials are added in the figures. These materials, with their thermal properties and citations listed in Table 10. Typical data for combustion chamber deposits (CDD) and air are included as well. The publications were selected to match engine size and engine operating conditions with light duty diesel and medium speed and load.

The first three coating materials in the table are based on plasma sprayed YSZ, with variants in base material and spraying parameters. The next two coatings consist

mainly of alumina and silica formed by anodizing aluminum; SiRPA is hard-anodized, the Keronite coating is created with plasma electrolytic oxidation. The surface of the SiRPA coating is reinforced and sealed with a thin silica layer. The last two coating materials contain hollow spheres (HOSP) made of nickel and alumino-silicate respectively. The nickel spheres are sintered to form a coating, while the silicate spheres are embedded in a phosphate metal binder matrix. The sintered nickel coating contains a significant porous volume between the spheres. Sealing the surface of this coating to prevent charge and fuel penetration was not successful, this is reflected in the performance.

Table 10. Properties and references for the coatings included in the figures.

	k [W/m.K]	$c_v \times 10^6$ [J/m^3.K]	$a \times 10^6$ [m^2/s]	e [W.s$^{0.5}$/m^2.K]	reference
YSZ Classic	1.7	2.46	0.69	2045	[83]
YSZ HOSP	0.80	2.34	0.34	1368	[98]
Zr-based IFP	0.85	2.60	0.33	1487	[81]
HA SiRPA	0.67	1.30	0.52	933	[29,79]
PEO Keronite	0.65	1.52	0.43	994	[82,99]
HOSP Nickel	0.20	0.30	0.67	245	[84]
HOSP Silicate	0.35	0.46	0.76	401	[80,83]
CCD Solid	1.6	2.75	0.58	2096	[6–9]
CCD Porous	0.10	0.20	0.50	141	[6–9]
Air (100 bar 1500 K)	0.10	0.03	3.3	55	[100]

The predicted surface temperature swing is plotted with iso-lines against thermal conductivity and volumetric heat capacity in Figure 31. Not shown, because out of scale; the temperature swing for an aluminum surface in this engine operating point is about 10°C. Low values for effusivity i.e. thermal conductivity and volumetric heat capacity are required to create a significant temperature swing. For some of the coating materials in the figure, surface temperature swing values were published. Most of them simulated with 1-D engine models, but the value for the SiRPA coating is actually measured. The reported values for the temperature swing compare well with the simulation model, providing validated input for the calculation of the rest of the parameters.

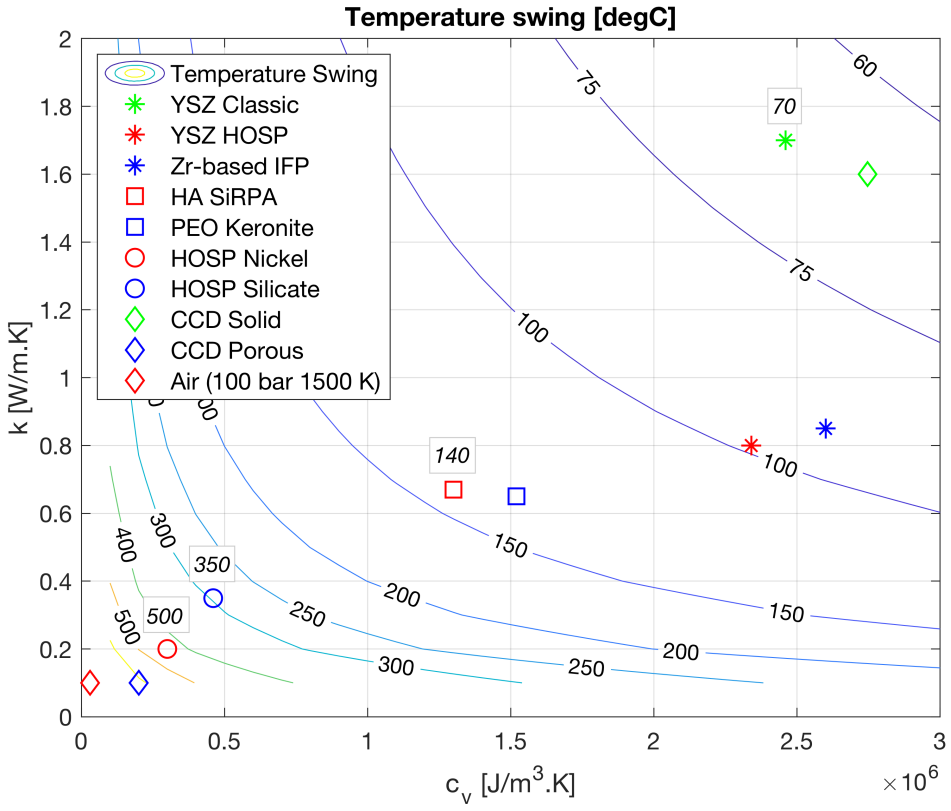

Figure 31. Temperature Swing for LD Diesel, EOP B, engine speed 1500 rpm, 30 mg/str fueling, engine load 11.2 bar IMEP. The italic labels show simulated/measured surface temperature swing values from some of the references.

The temperature swing is attenuated in the coating. The thermal penetration depth of the heat wave in a thermal barrier coating is of interest to understand how thin a coating can be. A coating with too high thickness will create a steady state temperature gradient and the average surface temperature will rise which is detrimental for volumetric efficiency.

Looking at Figure 32, the maximum thermal penetration depth with 95% attenuation of relevant coatings is about 200 µm, which is surprisingly thin. Research indicates that the optimal coating thickness is even lower than the thermal penetration depth [70,79]. A coating thickness below the thermal penetration depth will reduce the amplitude of the surface temperature swing, the optimal coating thickness is a compromise.

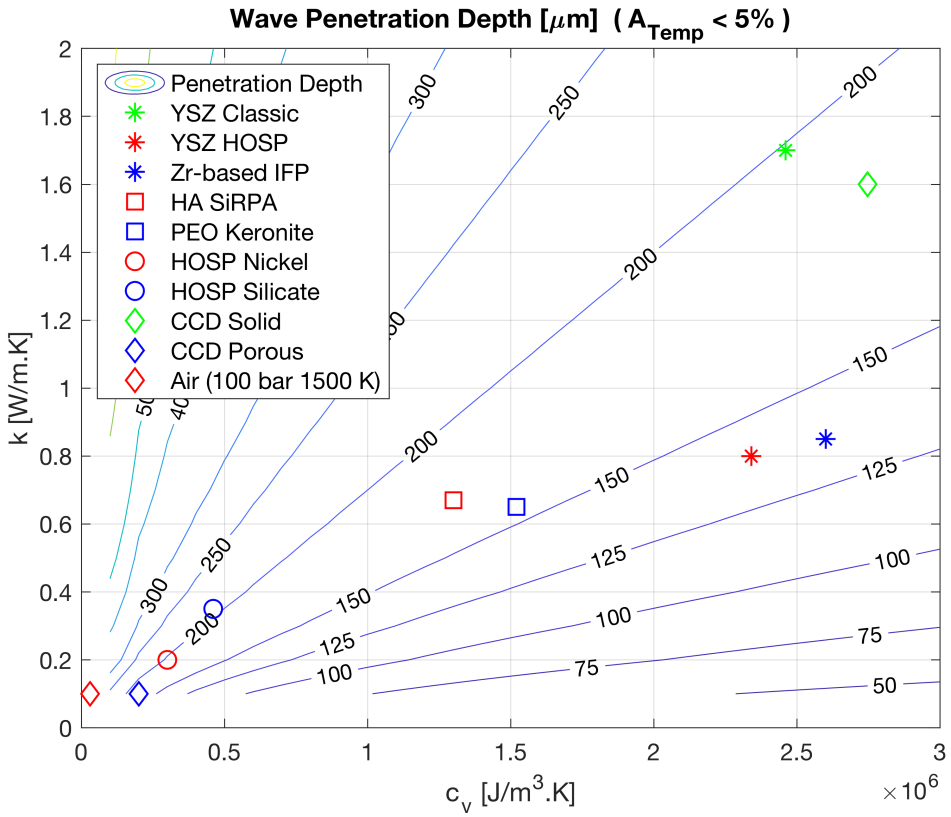

Figure 32. Thermal penetration depth to 5% of the surface temperature amplitude. Operating conditions for EOP B, 1500 rpm, 30 mg/stroke.

The surface temperature swing will elevate the coating surface temperature during combustion which will reduce heat transfer. The retained heat is converted to additional work and exhaust enthalpy according to the engine's thermodynamic efficiency, described in the method section. The iso-lines in Figure 33 depict the predicted relative increase of gross indicated efficiency. This increase is quite modest, low values for effusivity are needed for a substantial efficiency improvement. This is in line with the converging trend over time for the reported fuel efficiency improvements with TBCs in Figure 5 in the introduction.

With the assumptions made, the model is expected to overpredict the efficiency increase from the surface temperature swing. In general, the reported measured efficiencies are lower than the predictions, as expected.

The reported efficiency improvements from the zirconia based coatings diverge. They are low for the coatings with lower effusivity and higher than expected for the classic YSZ. The low improvements are probably caused by counteracting effects like open porosity, crevice effects, surface roughness. The data for the classic YSZ was from a data point that was deviating from most of the measurements in the publication which actually showed an efficiency degradation.

For the alumina based coatings, there is some uncertainty. The Keronite coating has been evaluated in two different papers, one reporting 1.8% efficiency improvement, the second paper reported no improvement. For the SiRPA coating the data is from a piston where the coating application is limited to the squish surface. The efficiency

improvement seems too high for this small surface, and it was only shown for one specific low load engine operating point.

The coating with the embedded silicate spheres performs rather well. The high surface roughness might be one reason for not showing an even a higher efficiency gain. Efficiency predictions for the sintered nickel hollow sphere based coating, presented in the referenced article, were 4 to 8% improvement, which would be in line with the model results. The measured efficiency was very poor. The main reasons were open porosity between the nickel spheres that could not be sealed leading to lower compression ratio, charge and fuel entrainment and high surface roughness. All in all, the efficiency prediction with the proposed model seems in line with measurement data.

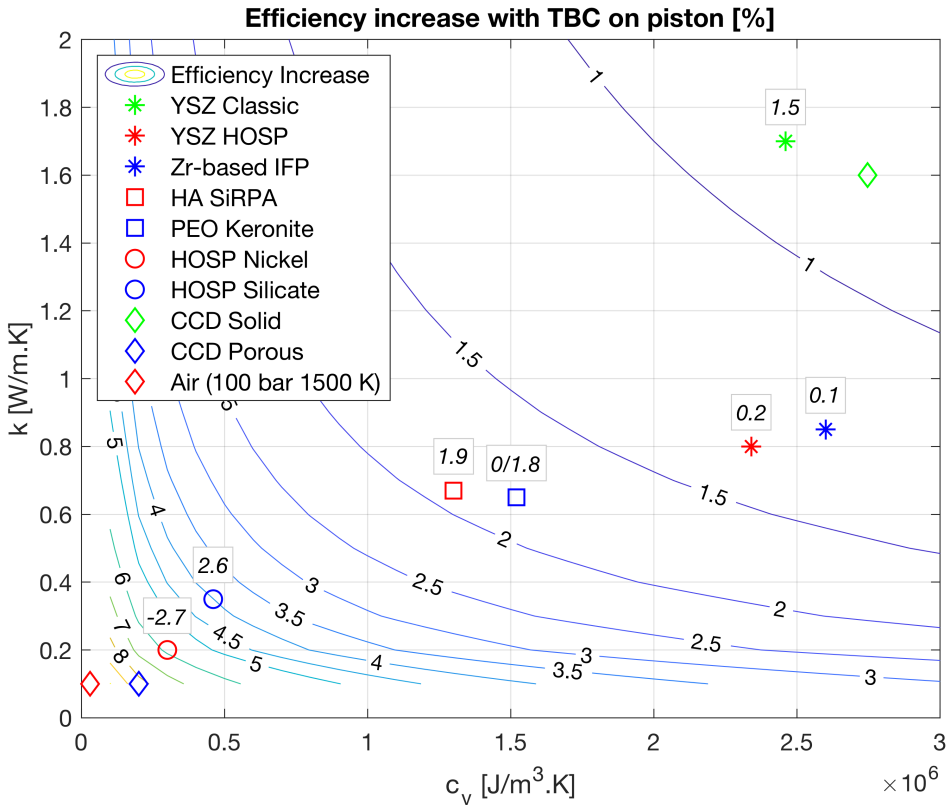

Figure 33. Relative efficiency increase with wall temperature swing of coated piston. Calculated for EOP B conditions, 1500 rpm, 30 mg/str fueling. The italic labels show the measured efficiency increase from some of the references.

The exhaust temperature increase in Figure 34, calculated with the model, is quite modest. A rather low effusivity is required for a significant increase in exhaust temperature and enthalpy. For a turbo charged engine, this would lead to an additional engine efficiency improvement. The included measured values from the publications spread somewhat but are generally small and in line with the model, signifying the model validity.

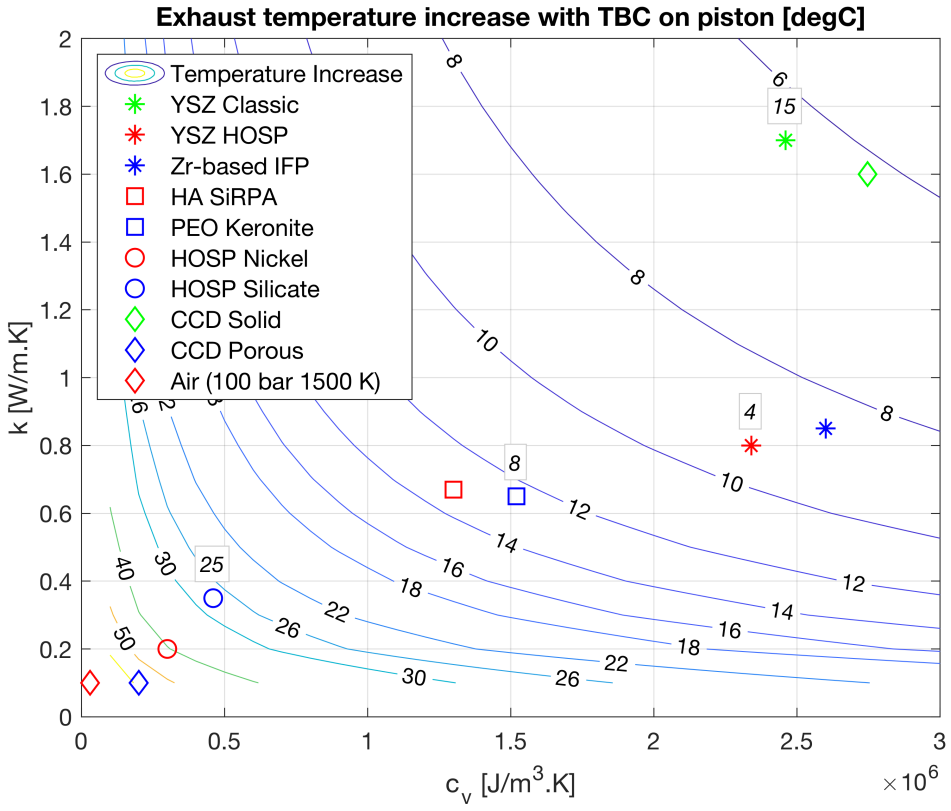

Figure 34. Temperature increase in exhaust manifold for EOP B, 1500 rpm, 30 mg/str fueling, 11.2 bar IMEP as a function of thermal conductivity k and volumetric heat capacity c_v. The italic labels show the measured exhaust temperature increase from some of the references.

The presented model of the surface temperature swing and engine efficiency increase with thermal barrier coatings predicts the outcome well. The model requires little input data and can be easily applied on engines with varying efficiency and heat losses, given that the average charge temperature and heat transfer coefficient during combustion are available from measurements or simulations. The model is set up to overpredict the actual efficiency gains hereby providing an upper limit to target for.

To conclude this section about the temperature swing model results: certain types of soot deposits (CCD), shown in the figures, have a high porosity and would be effective insulators with sufficient thickness and oxidation stability. It would be interesting to design and test a soot-like coating, with high porosity, that is stable and can be procured with a proper thickness.

5.3 Novel thermal barrier coatings

The results presented here are from experiments with novel thermal barrier coatings, described in section 4.3.2. Six pistons were prepared with different types of material, spraying method, with and without a surface sealing layer. In addition, four uncoated pistons were tested to investigate the effect of compression ratio and surface roughness in a small DOE. Two pistons were machined to give 0.2 units lower compression ratio and two pistons (one standard, one low compression ratio) were grit blasted with alumina and polished to create the same type of surface roughness as for a polished plasma sprayed piston.

In Figure 35 the fuel energy distribution is presented for EOP B, 1500 rpm and 30 mg fuel per stroke. The explanation for the labels can be found in Table 8. The blue bars show the uncoated pistons. The effect of compression ratio and surface roughness variation is as expected: lower compression ratio leads to lower indicated efficiency, similar wall heat losses and higher exhaust enthalpy. The centroid of heat release is somewhat earlier, which might be explained by faster combustion due to the modified piston bowl shape. High surface roughness increases wall heat losses, reduces exhaust enthalpy (due to higher heat losses) and delays combustion.

When looking at measured data for the coated pistons, none of the coatings improves efficiency compared to the uncoated reference piston. Wall heat losses are lower, most for the unsealed coatings and exhaust enthalpy is higher, again most for the unsealed coatings. The combustion is delayed when coatings are applied, most for the unsealed coatings.

To make a better assessment of the effect of coating type and eliminate the effect of differences in compression ratio, surface roughness and combustion phasing, the MLR model was used to predict the energy distribution for the different pistons. The factors for compression ratio, surface roughness and centroid of heat release were set at the levels for the uncoated reference piston. As can be seen in Figure 36, some of the coatings improve indicated efficiency with these new assumptions. The suspension plasma sprayed coating from gadolinia-zirconate without surface sealing performs the best. It has the highest indicated efficiency, lowest wall heat losses and highest exhaust enthalpy. The duration of the apparent rate of heat release is also highest. This could be due to reduced heat losses during the expansion stroke.

For the other coatings it is difficult to draw general conclusions. There is no correlation that shows what material or spraying method is better, it seems to depend on the combination. Surprisingly, the sealed air plasma sprayed YSZ coating is behaving rather like the uncoated piston, apart from the increase in heat release duration and small trends for lower heat loss and higher exhaust enthalpy.

Some interesting observations were made when looking at the apparent heat release for the different pistons, relative to the reference piston in Figure 37. The aHR for the rough uncoated piston differs only slightly, the main differences in aHR occur for the coated pistons. The unsealed pistons show the largest reduction and recovery of the aHR. The coating with the largest deviations in aHR has the highest porosity and shows the best performance in the engine. At the same time, the fast reduction of aHR from the time of jet impact on the piston, and recovery when the cylinder pressure starts to drop indicates the presence of crevice effects. Crevice effects are expected to reduce the coating performance. Further research is needed to understand these

results. Could there be a porosity level where the positive effect from lower effusivity becomes larger than the negative effect from crevice losses?

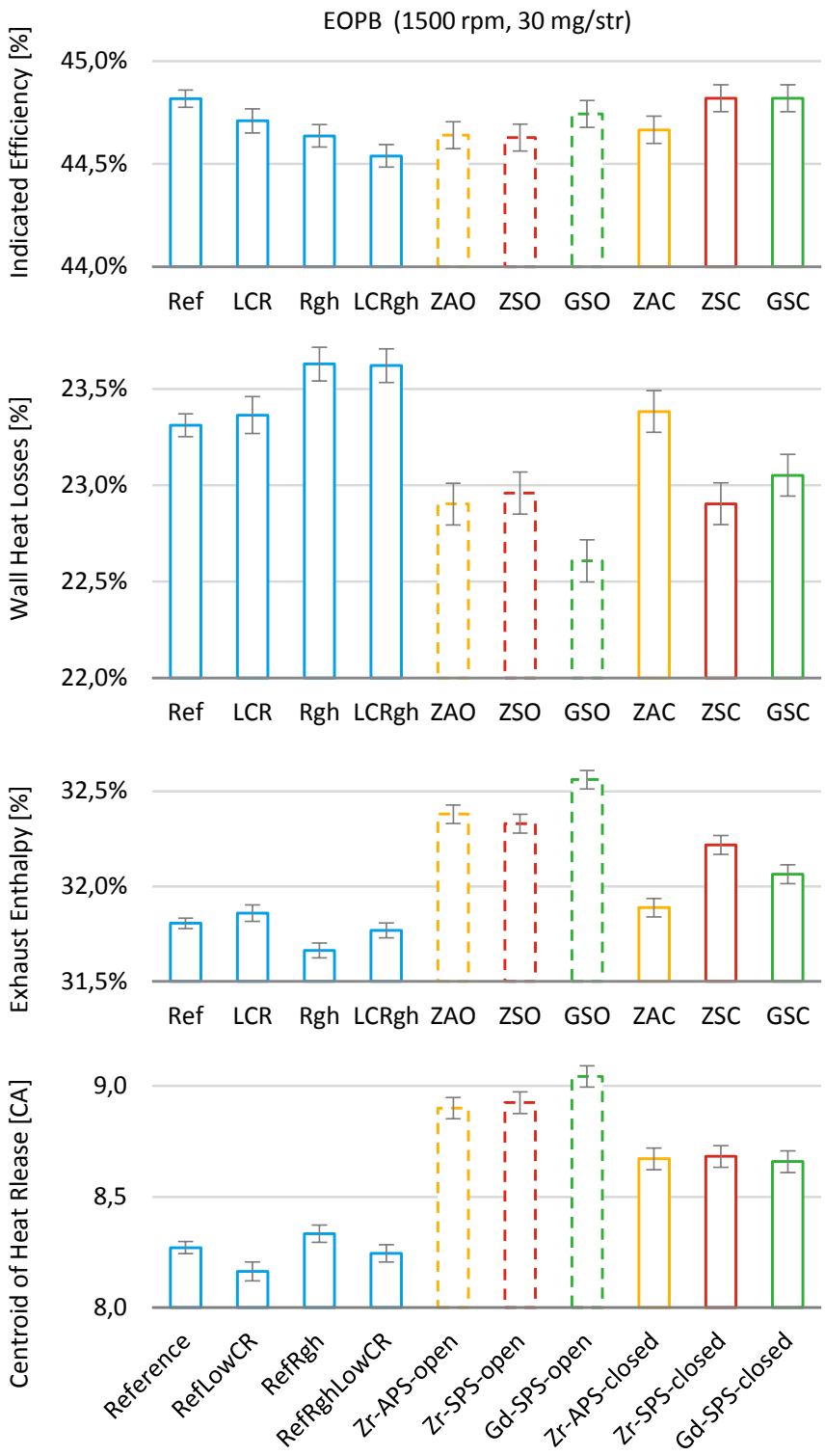

Figure 35. Fuel energy distribution for EOP B as measured. The error bars show the 95% confidence intervals. Explanation for the labels is found in Table 8.

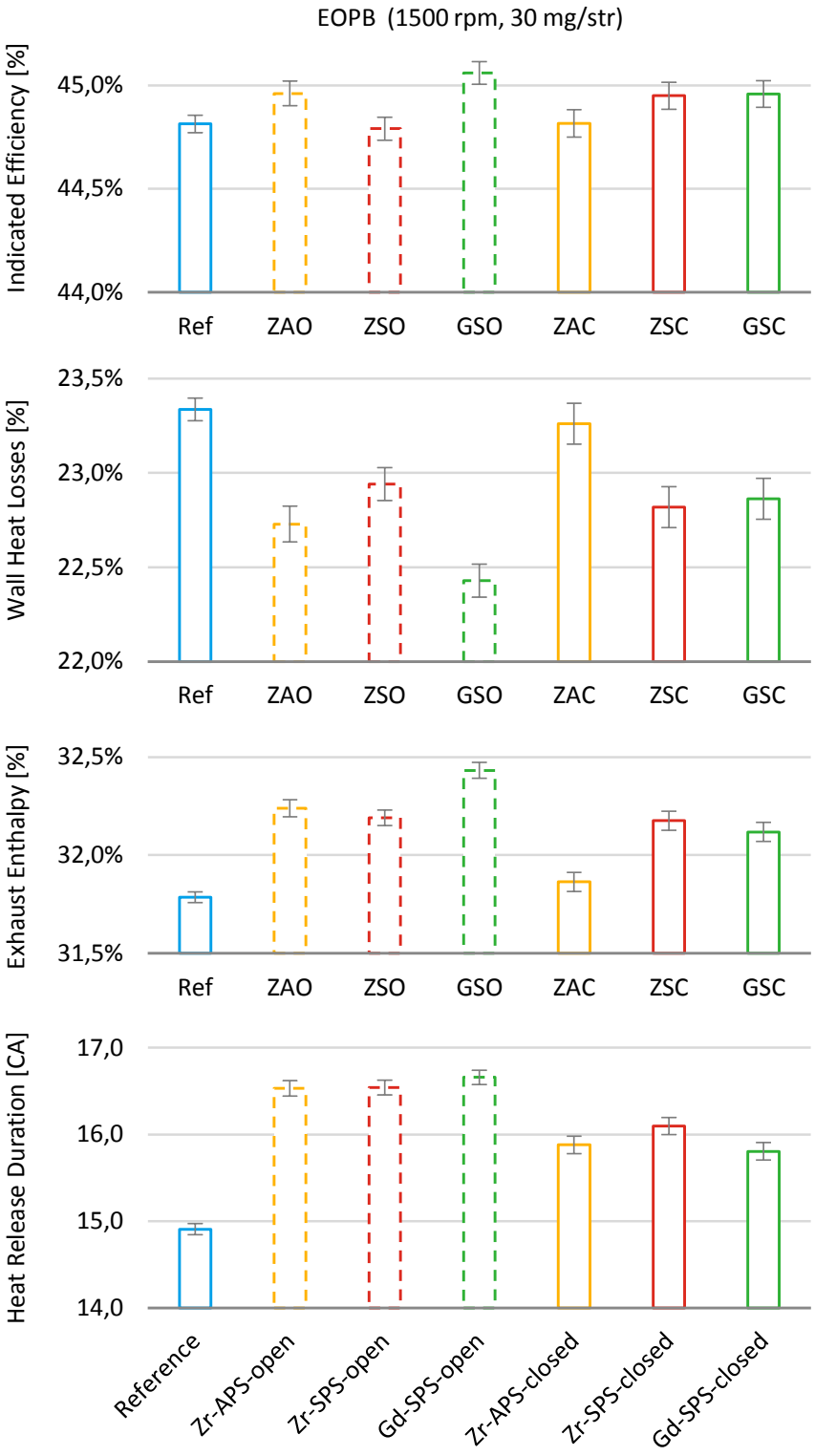

Figure 36. Fuel energy distribution for EOP B, predicted with the model factors CR, Ra (surface roughness) and CHR (centroid of heat release) set as for the reference piston. The error bars show the 95% confidence intervals. The labels are explained in Table 8.

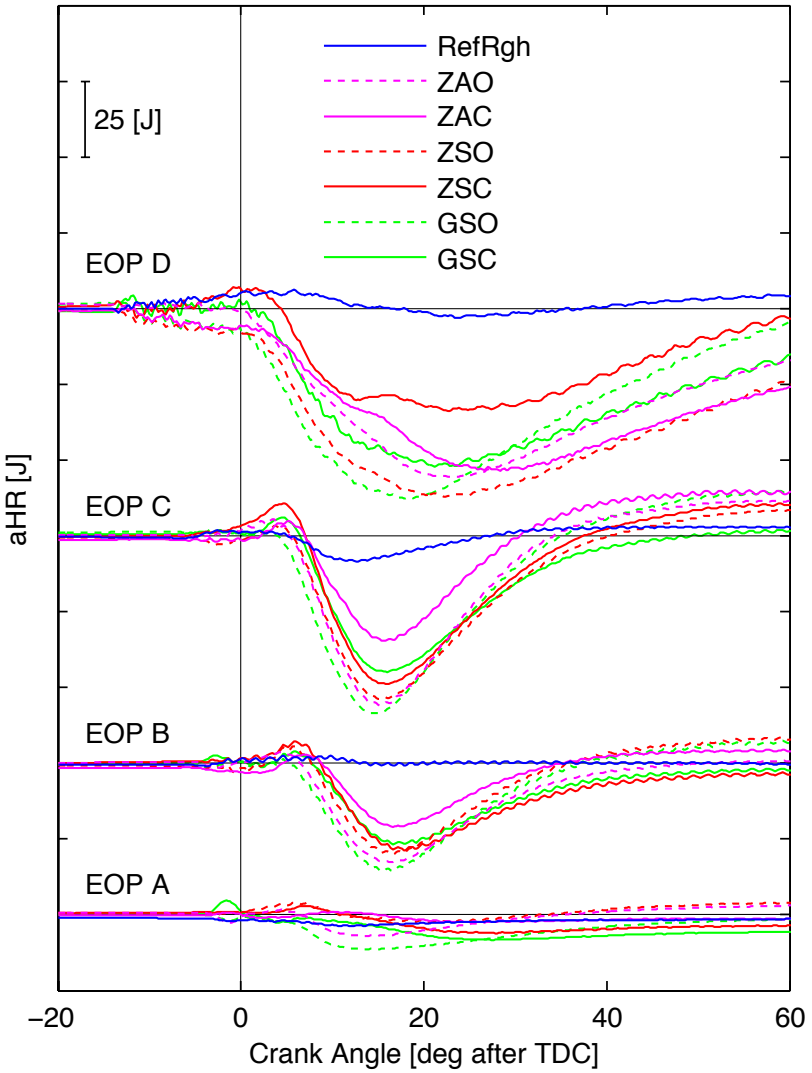

Figure 37. Apparent cumulative heat release for the rough uncoated piston and the coated pistons, relative to the stock reference piston. Explanation for the labels is found in Table 8.

5.4 Permeable porosity and crevice effect

Most plasma sprayed thermal barrier coatings include pores that are interconnected and open to the surface (permeable porosity). For air plasma sprayed YSZ, typical porosity levels are between 8 and 20%. The volume created by coating porosity can be considered as a crevice volume in a combustion chamber, leading to extra heat losses and the risk for trapping fuel. The potential losses involved with charge and fuel entrainment in thermal barrier coatings have been described in literature, but as far as known to the author, no experiments or simulations have been performed to quantify this for diesel engines.

To quantify the crevice effect, experiments and simulations were performed with an air plasma sprayed YSZ thermal barrier coating with a porosity level of about 16%. Additionally, two different sealing materials were evaluated to investigate if the crevice effect could be reduced or completely mitigated.

In Figure 38 results are shown from a zero-dimensional crevice model using the measured cylinder pressure trace for the part load point EOP B. During pressure rise, charge is pushed into the coating. The hot charge cools down and heat is transferred between the gas and solid. After cylinder pressure has reached its peak, charge flows back into the combustion chamber. The crevice effect is magnified when hot gas from the burning jet starts to interact with the coated surface, a few degrees after TDC.

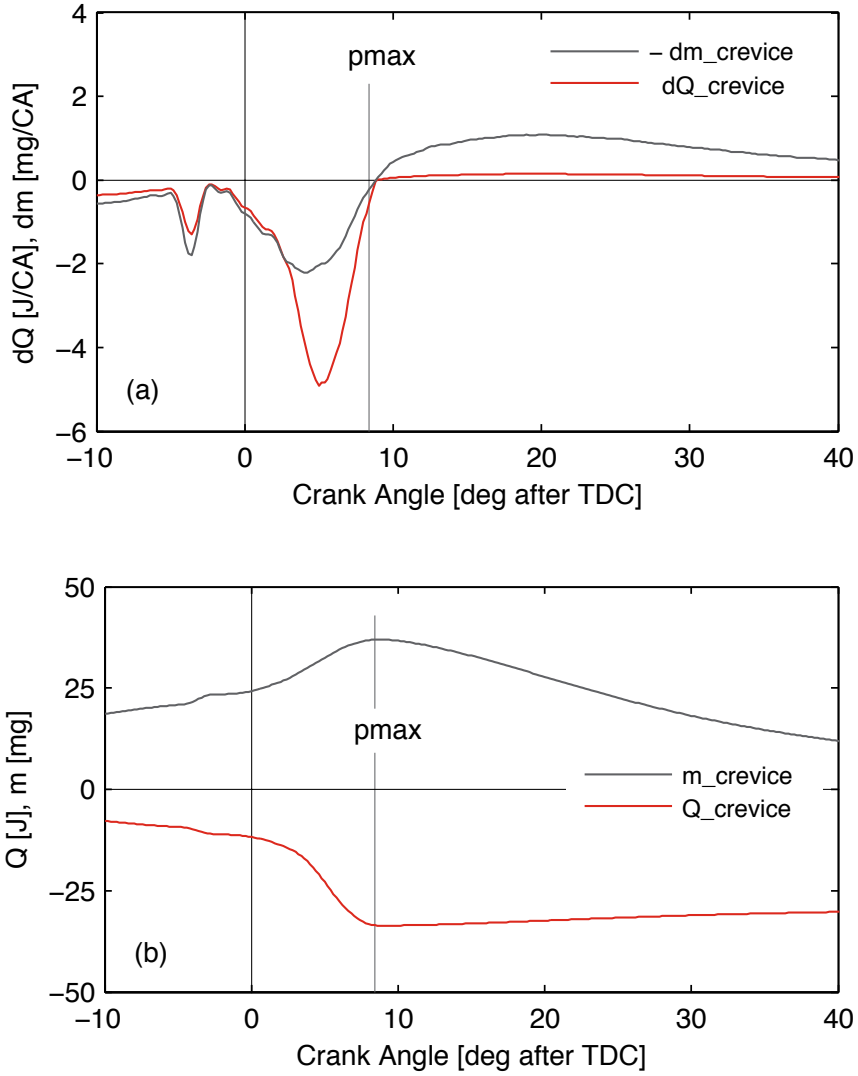

Figure 38. Crevice model results for mass flow and heat flux in and out of the porous coating for EOP B.

In the same fashion as for the novel TBCs, the apparent heat release (aHR) for the coated pistons was compared to the uncoated piston, shown in Figure 39. The initial drop for the aHR coincides with the start of interaction with the burning jet. This drop must be caused by increased heat transfer and/or slower combustion. Both can be caused by the crevice effect (heat transfer and fuel entrainment). After 10-15 degrees, depending on load case, the apparent heat release difference becomes smaller, meaning that heat losses are lower, or combustion is accelerating here. This could be explained by the insulating effect of a coating and/or fuel released from the coating.

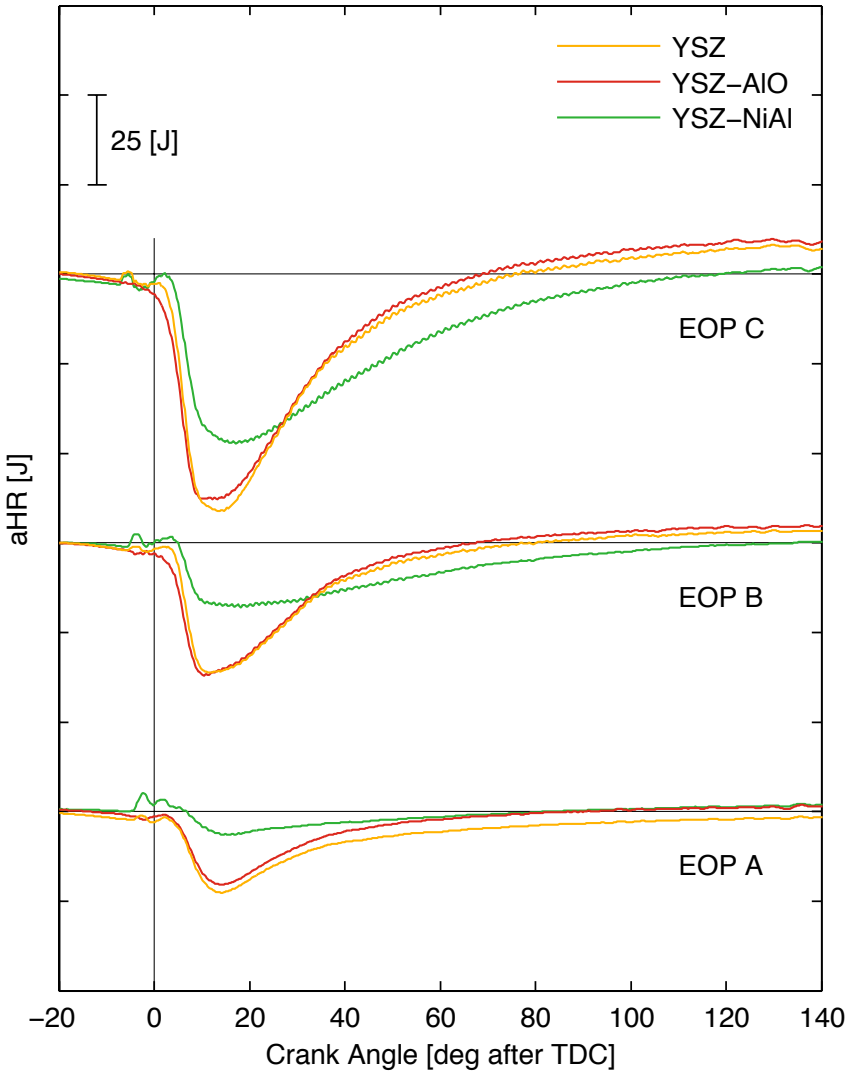

Figure 39. Apparent heat release, relative to the uncoated piston.

The curves for the YSZ coated piston without sealing look very similar to the curves for the YSZ coated piston with the alumina sealing (AlO). The curves for the YSZ coated piston with the metal sealing (NiAl) look different. It appears as if this coating is mitigating the increased heat loss and/or fuel entrainment. The recovery is also less, which could mean that this coating is less insulating.

Pictures of the sealed pistons taken after the experiments (Figure 40) show many small cracks in the ceramic sealing surface, while the metal sealing seems largely intact. This might be part of the explanation for the differences in apparent heat release rate and crevice effect.

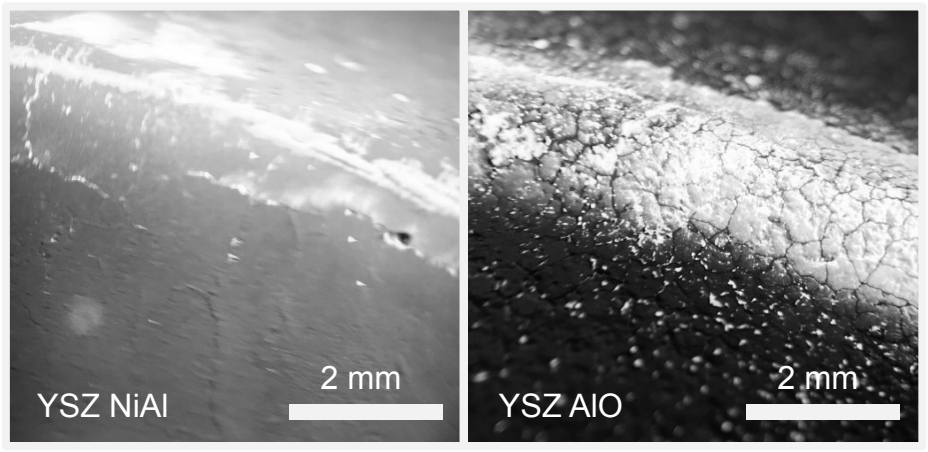

Figure 40. Images of the piston bowl edge after engine testing. On the left, the nickel alloy sealed piston surface, on the right the alumina sealed piston surface.

It would be interesting to know how a "perfect YSZ" coating would perform in theory and how the apparent heat release would be different from the uncoated piston. Simulations in CFD were performed for load case EOP B, with and without a thermal barrier coating. The piston surface was modeled with a so-called thin wall module, resolving the solid below the surface to calculate the dynamic surface temperature during the combustion cycle. With the coating, the surface temperature swing is much higher, and heat flux is lower.

Figure 41 compares the measured and simulated effect on heat release from the presence of the YSZ coating. Where the heat loss is increased in the experiment, the heat loss is reduced in the simulation. The simulation model does not include any negative side effects that could be caused by the coating and shows the potential gain with an ideal TBC.

This information can be used to compare the measured apparent heat release and the theoretical improvement with the thermal barrier coating. The difference must be explained by losses that are not part of the CFD model. The crevice model might be able to explain part of these losses.

In Figure 42 a simulated energy balance is shown that illustrates the impact from an insulation coating with crevice effects, relative to an uncoated piston. The blue curve, Qwall, is the predicted effect of insulation with CFD, more heat is retained in the cylinder. The green curve, Ecomb, shows the fuel bound energy that is transferred into the crevice when burning fuel entrains the coating. The red curve, Qcrev, illustrates the heat losses when hot charge enters the crevice. Summarizing the separate energies gives the yellow curve Esum, showing the total modeled energy balance for a piston with a YSZ coating compared to a non-coated piston.

When comparing the model with the experimental difference for the energy balance (aHR), the features look similar. But in the simulation the energy level of the cylinder charge is higher than in the experiment at 80 degrees after TDC. This difference could be caused by loss mechanisms that are not in the model, for example higher surface roughness for the coated piston. Also, the heat transfer reduction from the CFD simulation could be overpredicted.

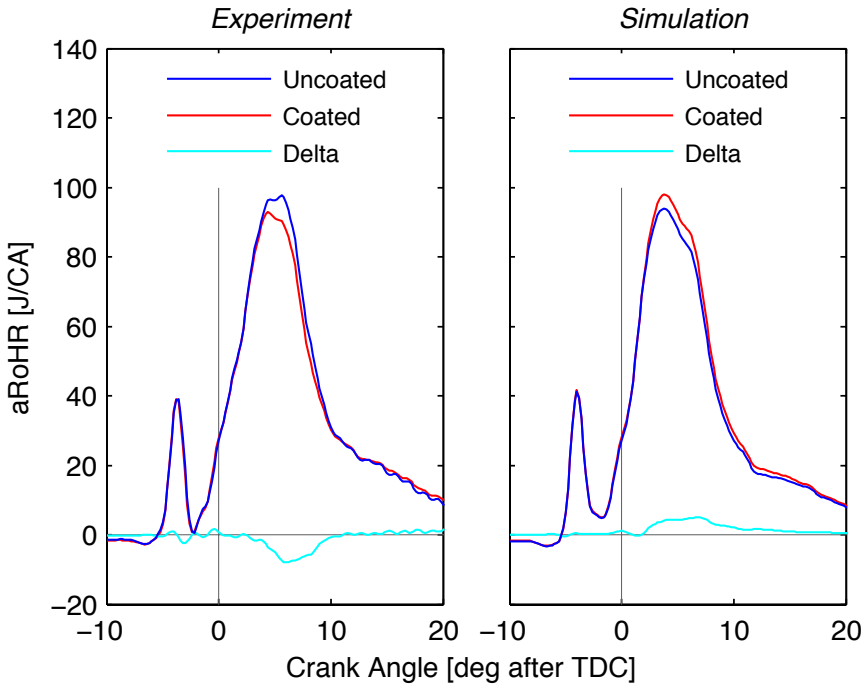

Figure 41. Measured and simulated aRoHR for the piston with YSZ coating without sealing and uncoated piston in EOP B.

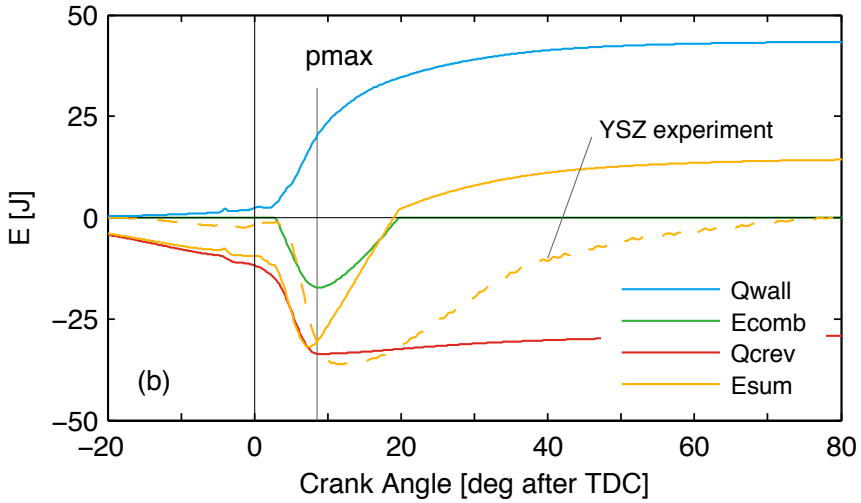

Figure 42. Simulated energy balance including the reduced combustion energy (Ecomb) due to fuel entrainment.

Another strong case to prove the existence of the crevice effect is the result from a motoring experiment. The boundary conditions were as for EOP B, but without fuel injection. The measurement was made directly after assembly, no soot deposits had been formed yet. When motoring, there is no influence from combustion or fuel entrainment. CFD simulation of the motored case predicted reduced heat losses as for the fired case. However, the measured heat loss derived from the apparent heat release was higher for the coated piston. The grey curve Exp-CFD depicts the required loss to

create this difference between CFD and experiment. There is no apparent reason why this would be the case other than the crevice effect. The crevice model predicts a heat loss close to the measured loss. The shape of the curve is different though. One possible explanation could be the presence of flow resistance in the coating, causing a phase shift for the heat loss.

A logical next step is to create a more advanced and detailed crevice model directly coupled to a CFD simulation environment. With such a model, flow resistance, heat transfer and fuel entrainment could be simulated in more detail for better prediction of crevice effects. A way to realize such a model with realistic simulation time is presented in the Outlook section.

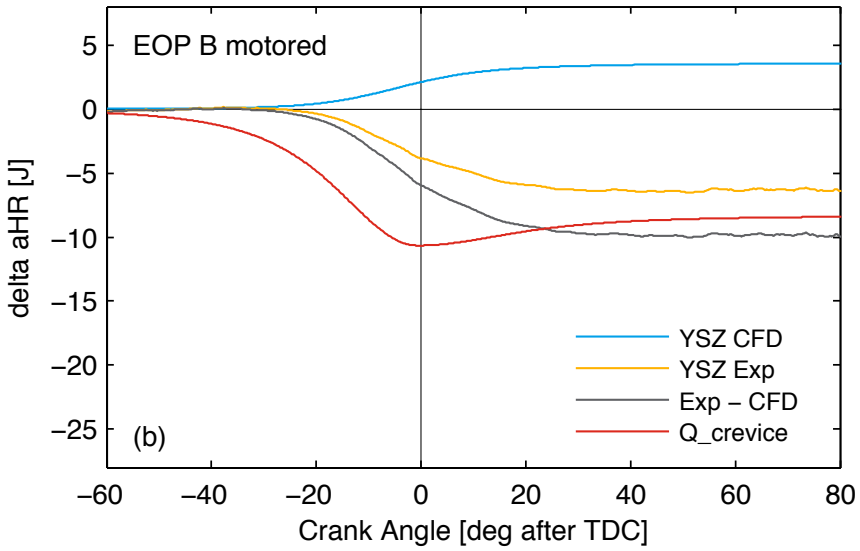

Figure 43. Measured and simulated apparent heat release for motoring conditions, relative to the uncoated piston.

6 Conclusions

The objectives of this PhD investigation were to reduce fuel consumption and reduce engine heat load for a light duty diesel engine by reducing heat losses from the combustion chamber. At the time this investigation started, no industrial thermal insulating solution to reduce heat transfer from the combustion chamber existed, although research in this area has been conducted since the early 80-ies. The research tasks posed for this investigation were to establish the actual performance of state-of-the art thermal barrier coatings, and secondly to define what measures with respect to thermal insulation are required to achieve a fuel consumption reduction of 2%.

The main conclusions of the study, including literature research, experiments and simulations, are as follows:

- In theory, heat loss reduction has high potential to reduce fuel consumption: with adiabatic combustion chamber walls, indicated efficiency would increase by about 30% for a modern light duty diesel engine operating at medium speed and load.
- Elevation of the mean wall temperature using air gap insulation, low thermal conductivity steel and ceramic engine parts proved unsuccessful. The hot walls increased charge temperature during intake, resulting in poor volumetric efficiency. The high charge temperature and reduced air/fuel ratio resulted in high emissions for NOx and Soot and lowered indicated efficiency.
- To avoid heating up of the intake air, the wall temperature must follow the charge temperature during the combustion cycle with a "temperature swing" and be at low temperature during gas-exchange. This can in theory be achieved with a thin thermal barrier coating (TBC) on the combustion chamber walls. The TBC should have low effusivity, i.e. low thermal conductivity and low volumetric heat capacity.
- The limited success, also with the temperature swing coatings, can be attributed to a combination of the following factors:
    - The effusivity of the coating is not low enough.
    - The coating is too thick; the resulting temperature gradient over the coating elevates the surface temperature and charge temperature, resulting in the negative effects described earlier.
    - The application of a thermal barrier coating can lead to a number of negative side effects:
        - Some TBCs have a high surface roughness which increases heat transfer and slows down wall guided combustion. In Paper II, an increase from Ra 0.2 to 7.3 µm increased fuel consumption with 0.91%. In Paper III, an increase from Ra 1.1 to 5.2 µm increased fuel consumption with 0.45%.
        - High surface temperatures can lead to oxidation of an insulating soot layer. Motoring work without soot deposits present was 0.2 bar higher than with soot deposits, described in Paper II. When soot was burned off in a high load point, fuel

consumption increased in a low load point with 0.7% as described in this thesis in section 5.1.

- Some TBCs include permeable porosity that behaves like a crevice volume, increasing heat losses and trapping unburned fuel. From the crevice effect investigation in Paper IV, crevice losses increased fuel consumption by an estimated 1 to 2%.
- Some TBCs might display higher absorptivity for thermal radiation compared to aluminum or steel surfaces.
- High surface temperatures can lead to "convection vive" where oxidation of fuel occurs closer to the wall, effectively increasing the heat transfer coefficient.

Without any negative side effects and a coating surface limited to the piston, a coating with an effusivity lower than 900 $Ws^{½}/m^2.K$ is required for a fuel consumption reduction of 2% for the light duty diesel engine subject in this work. The temperature swing model used in this study is likely to overpredict the fuel savings for a thermal barrier coating. The required effusivity is probably even lower when accounted for the possible negative side effects mentioned above.

7 Outlook

Further decrease of the thermal conductivity and volumetric heat capacity is required if significant gains in efficiency are to be realized with thermal barrier coatings. One way to achieve this is to incorporate more air or another gas in the coating. Recently, two promising coatings have been presented that use hollow spheres. This technology has been investigated before by Kosaka et al. [101], but this path was not pursued further at that time because of poor durability. Andrie et al. used hollow spheres of silicate, containing air, embedded in a matrix, while Babu et al. used hollow spheres of nickel, sintered to form a solid structure [80,83]. For both coating materials the reported effusivity is close to 400 $Ws^{½}/m^2.K$.

Another avenue to include more air is to increase open porosity in a thermal barrier coating. The suspension plasma sprayed gadolinia-zirconate coating described in paper III performed best and had the highest porosity among the tested coatings. The challenge is to increase the porosity level while maintaining the integrity of the coating. Also, sealing of a thermal barrier coating with open porosity has been proven difficult. A sealing layer has to be exceptionally thin in order not to increase the effusivity of the coating surface. And the pressure and temperature fluctuations in a combustion chamber are extremely challenging. Would it be possible to create an unsealed coating with open porosity, where the effusivity is so low that it outweighs the crevice effect, a soot-like coating?

Further development of a detailed model of a coating with open porosity would increase understanding of the actual process of charge entrainment and heat transfer, including the effect on the surface temperature swing. With such understanding, it might be possible to reduce the negative effects of the crevice volume. And moreover, it can be used to explore the impact of very high porosity levels, mimicking soot-like behavior, known to be a good (but unreliable) insulator. To keep computational efforts at a realistic level, a model with local refinement and details could be embedded in a standard CFD model. The local model can have very small dimensions and time steps, including all the details and solving the equations using direct numerical simulation (DNS). Boundary conditions for this detailed model would be exchanged with the standard CFD model at larger time intervals to be able to solve the solution for a whole combustion cycle. To investigate coating behavior for different surface areas in the combustion chamber, the detailed model can be placed in different locations.

The focus in this PhD study has been on thermal barrier coatings in a light duty diesel engine. In the coming decades, the importance of the passenger car diesel engine will become smaller as it is being replaced with electric powertrains to reduce greenhouse gas emissions. However, for heavy duty and marine applications, the internal combustion engine is likely to remain an important prime mover. Here thermal barrier coatings can play an important role in improving thermal efficiency and reducing greenhouse gas emissions until carbon neutral fuels are widely available. A thermal barrier coating might be more effective for fuels that do not form a 'natural' insulating soot layer, such as hydrogen or methane.

How about the application of thermal barrier coatings for other combustion concepts? Historically, research on spark ignited engines has been limited because of the risk for

knock with elevated wall temperatures. However, effective temperature swing coatings can result in cooler walls during gas exchange and compression compared to uncoated walls [102]. This could be particularly interesting for spark ignited hydrogen engines, as hydrogen is very prone to knock. Another combustion concept that has shown to benefit from thermal barrier coatings is homogeneous charge compression ignition (HCCI) [103,104]. The requirement for a low wall temperature during air intake is less stringent, as auto-ignition is promoted by a hotter charge and near wall combustion can be more complete due to a smaller quenching distance.

The quest for effective thermal barrier coatings in internal combustion engines continues.

8 Contributions to the field - paper summaries

8.1 Paper I

"A Method to Evaluate the Compression Ratio in IC Engines with Porous Thermal Barrier Coatings"

The compression ratio is an important engine design parameter. It determines to a large extend engine properties like the achievable efficiency, the heat losses from the combustion chamber and the exhaust losses. The same properties are affected by insulation of the combustion chamber. It is therefore especially important to know the compression ratio when doing experiments with thermal barrier coatings (TBC). Another important reason to know the correct compression ratio is its use in the calculation of the apparent rate of heat release. An error in the value for the compression ratio results in deviations of the calculated heat release that are similar to the effects of TBCs.

With porous TBCs, the standard methods to measure the compression ratio can give wrong results. When measuring the compression ratio by volume, using a liquid, it is uncertain if the liquid fills the total porous volume of the coating. And for a thermodynamic compression ratio estimation, a model for the heat losses is needed, which is not available when doing experiments with insulation.

The subject of this paper is the evaluation and further development of an alternative method to assess the compression ratio. This method was described in a thesis work by Tomas Krieg in 1990 [73]. It is based on motored cylinder pressure data like other thermodynamic methods but does not need a model for the heat losses.

Two important modifications were made to make the estimation work properly. The first one was the addition of elastic engine deformation caused by cylinder pressure and inertial forces. The elasticity constant was determined from CAE models.

The second modification was related to the determination of the crank angle position for the maximum of the motored heat losses. This parameter is central in the method. The assumption in the original paper that the heat loss maximum always occurs between the crank angle position for maximum charge temperature and maximum charge pressure does not hold. The reason for this is the decay of the charge turbulence which is engine specific and has a big influence on the motored heat losses. The turbulence development of the cylinder charge depends on engine design and motoring conditions and cannot be modeled in a simple way. The solution was to measure the crank angle position for the maximum heat losses for an uncoated reference piston with a known compression ratio and assume that it would be the same for the coated pistons. This assumption was verified for differences in surface roughness and heat losses.

The assessment of the compression ratio is very repeatable (within ±0.05 CR units) between engine rebuilds using the same piston.

The author planned and performed the experiments, compiled and analysed the data and wrote the complete paper. Volvo Car's measurement lab supported with compression ratio measurements.

8.2 Paper II

"Evaluation of thermal barrier coatings and surface roughness in a single cylinder light-duty diesel engine"

The effect of two thermal barrier coatings (TBC) and their surface roughness on heat transfer, combustion and emissions was investigated in a single cylinder light duty diesel engine. The evaluated TBC materials were plasma sprayed yttria stabilized zirconia and hard anodized aluminum, which were applied on the piston top surface.

The background for this investigation was the large spread in reported data for the effectiveness of thermal barrier coatings, hence the need for an accurate assessment.

The main tool for the investigation was cylinder pressure analysis of the high-pressure cycle, from which the apparent rate of heat release, indicated efficiency and heat losses were derived. For verification of the calculated wall heat transfer, the heat flow to the piston cooling oil was measured as well. Exhaust emission measurements were also performed.

Application of TBCs can influence engine operating conditions like charge temperature and ignition delay. This is one of the reasons for the large spread in data for efficiency improvements from TBCs found in literature. Therefore, extra attention was paid to choosing stable and repeatable engine operating points and the test run was automated to improve repeatability. The experimental data was modeled using multiple linear regression (MLR) to further improve accuracy. Another advantage of the modeling was that it was possible to isolate the effects of the coatings, surface roughness, compression ratio and soot deposits.

With this method it was possible to determine the indicated efficiency with a 95% confidence interval of ±0.1 percentage point. Efficiency differences as low as 0.2 percentage point could be distinguished between the different pistons.

Both tested thermal barrier coatings showed a reduction of cycle averaged wall heat losses and an increase in exhaust enthalpy, and a decrease in indicated efficiency. Analysis revealed that the high surface roughness of the tested TBCs led to increased wall heat losses and delayed combustion. An increase of surface roughness R_a from 0.2 μm to 7.4 μm resulted in a fuel consumption increase of up to 1%.

The effect of soot deposits on motored heat losses was also derived from the MLR model. The thermal insulation of the soot deposits was significantly better than the thermal insulation of the tested TBCs.

Finally, some results regarding the emissions: surface roughness and the presence of TBCs had a significant impact on the hydrocarbon emissions, especially for low load engine operation, while their effect on the other exhaust emissions was relatively small.

The author planned and performed the experiments, compiled and analysed the data and wrote the whole paper. The YSZ coatings were applied by University West, the anodized pistons were procured by Mahle. Volvo Cars' material lab supported with optical analysis of the coatings, the measurement lab assisted with measurement of compression ratio and surface roughness.

8.3 Paper III

"Experimental Evaluation of Novel Thermal Barrier Coatings in a Single Cylinder Light-Duty Diesel Engine"

This investigation's objective was to improve the thermal properties of plasma sprayed thermal barrier coatings (TBC) for internal combustion engines. There is a need for further reduction of thermal conductivity and volumetric heat capacity and the negative effects on heat loss and combustion phasing of surface roughness and permeable porosity, typical for plasma sprayed coatings, should be minimized.

Four measures for improvement of TBC properties were applied: i) modification of the coating's microstructure by using a novel suspension plasma spraying method, ii) application of gadolinium-zirconate, a novel ceramic material with low thermal conductivity, iii) polishing of the coating to achieve low surface roughness, and iv) sealing of the porous coating surface with a polysilazane. Six coating variants with different combinations of the selected measures were applied on the piston crown and evaluated in a single cylinder light duty diesel engine. Additionally, a two-level design of experiments was performed with four variants of uncoated pistons, to quantify the effect of compression ratio and surface roughness variations.

The experimental data was modeled with multiple linear regression to obtain confidence intervals for the measurement results and to correct the data for variations of surface roughness, combustion phasing and compression ratio for the different pistons. The main tool for evaluation of the coating properties was cylinder pressure analysis, providing the apparent rate of heat release, indicated efficiency, wall heat loss, and exhaust loss. Again, much attention was put into acquiring high-quality data and statistical processing to distinguish the contribution of different factors and get confidence intervals for the measured data.

The new TBC microstructure from suspension plasma spraying in combination with the use of gadolinium-zirconate, without surface sealing, showed the most promising results with respect to indicated efficiency, heat loss reduction and exhaust enthalpy increase. However, this result could not be explained in terms of lower thermal conductivity nor lower effusivity. The differentiating factor for this coating was the high (open) porosity level of 26%. The mechanism of how the high porosity could improve performance, could be subject for future research.

A parallel article was co-authored with Wellington Uczak de Goes [96], where more details can be found concerning the mechanical structure of the applied coatings and their possible impact on thermal properties and insulating performance in the engine. Visual inspection of the thermal barrier coatings after engine testing revealed no signs of failure in any of the coatings.

The author planned and performed the experiments, compiled and analysed the data and wrote the entire paper. University West applied the coatings for the pistons and provided measured thermal properties and optical analysis of the coatings before and after testing. Surface roughness and compression ratio measurements were done at Volvo Cars material lab.

8.4 Paper IV

"Effects of thermal barrier coating porosity on combustion and heat losses in a Light-Duty Diesel engine"

A state-of-the-art thermal barrier coating of plasma sprayed yttria stabilized zirconia and two types of surface sealing were evaluated in a single cylinder light duty diesel engine. The purpose was to investigate the effect of permeable porosity on combustion and heat losses by analyzing the apparent rate of heat release and heat loss to the piston cooling oil. In addition to the engine experiments, simulations were performed to assess the theoretical effect of an insulating coating with CFD and to predict the effect of porosity using a 0-D crevice model. The main conclusions are listed here:

- Permeable porosity of plasma sprayed thermal barrier coatings is a likely cause for increased heat loss and delayed combustion because the volume created by the pores behaves like a crevice volume. The large surface area of the pores in the coating allows for a fast and effective heat transfer between the entrained charge and ceramic insulation material. This might affect the insulation effectiveness of the thermal barrier coating significantly. Secondly, partly oxidized fuel that enters the coating from the near wall flame can become temporarily unavailable for further combustion, delaying the heat release.
- A simple crevice model for permeable coating porosity can explain the observed reduction of the cylinder pressure and delay of the apparent rate of heat release for the tested plasma sprayed coating in this investigation. This crevice effect might be one cause for the poor performance of plasma sprayed YSZ coatings in internal combustion engines.

The following observations support these conclusions:

- Heat loss to the pistons with plasma sprayed coatings increased under motoring conditions. This was shown by two independent methods: analysis of cylinder pressure and measured heat flux to the piston cooling oil. The magnitude of the increased heat loss agreed well with the prediction from the 0-D crevice model for the porous coating.
- Increased levels of CO and HC emissions were observed in the exhaust gas for the experiments with the sealed coatings, especially for the metal sealing layer. Sealing of the coating was not successful, cracks were visible in both the metallic and ceramic sealing layer. The cracks would likely allow for a limited entrainment of partially burned fuel. A restriction of outflow through the small cracks could then lead to a late release of CO and HC from the coating, when circumstances for complete oxidation are less favorable.

The author planned and performed the experiments and simulations, compiled and analyzed the data and wrote the entire paper. University West applied the coatings for the pistons and provided measured thermal properties and optical analysis of the coatings before and after testing.

References

1. Cengel, Y.A. and Ghajar, A.J., “Heat and Mass Transfer, Fundamentals & Applications,” McGraw-Hill, ISBN 978-0-07-339812-9, 2011.
2. Woschni, G., “A Universally Applicable Equation for the Instantaneous Heat Transfer Coefficient in the Internal Combustion Engine,” SAE Technical Paper, 1967, doi:10.4271/670931.
3. Hohenberg, G.F., “Advanced Approaches for Heat Transfer Calculations,” SAE Technical Paper, 1979, doi:10.4271/790825.
4. Woschni, G. and Huber, K., “Influence of soot deposits on combustion chamber walls on heat losses in diesel engines,” SAE Technical Paper 910297, 1991, doi:10.4271/910297.
5. Heywood, J.B., “Internal Combustion Engine Fundamentals,” McGraw-Hill, ISBN 0-07-100499-8, 1988.
6. Dietsche, K.-H. and Klingebiel, M., eds., “Bosch Automotive Handbook,” 7th Editio, Robert Bosch GmbH, ISBN 978-0-470-51936-3, 2007.
7. Wolff, A., Boulouchos, K., and Mueller, R., “A computational investigation of unsteady heat flux through an I.C. engine wall including soot layer dynamics,” SAE Technical Papers, 1997, doi:10.4271/970063.
8. Nishiwaki, K. and Hafnan, M., “The Determination of Thermal Properties of Engine Combustion Chamber Deposits,” SAE Technical Paper Series, 2000, doi:10.4271/2000-01-1215.
9. Wiedenhoefer, J.F. and Reitz, R.D., “Multidimensional Modeling of the Effects of Radiation and Soot Deposition in Heavy-duty Diesel Engines,” SAE Technical Paper, 2003, doi:ISSN 0148-7191.
10. Suhre, B.R. and Foster, D.E., “In-Cylinder Soot Deposition Rates Due to Thermophoresis in a Direct Injection Diesel Engine,” SAE Technical Paper Series, 1992, doi:10.4271/921629.
11. Hopwood, A.B., Chynoweth, S., and Kalghatgi, G.T., “A Technique to Measure Thermal Diffusivity and Thickness of Combustion Chamber Deposits In-Situ,” SAE Technical Paper Series, 1998, doi:10.4271/982590.
12. Kavtaradze, R., Zelentsov, A., Gladyshev, S.P., Kavtaradze, Z., et al., “Heat Insulating Effect of Soot Deposit on Local Transient Heat Transfer in Diesel Engine Combustion Chamber,” SAE Paper 2012-01–12, 2012, doi:10.4271/2012-01-1217.
13. Kamo, R. and Bryzik, W., “Adiabatic Turbocompound Engine Performance Prediction,” SAE Technical Paper 780068, 1978.
14. Bryzik, W. and Kamo, R., “TACOM/Cummins Adiabatic Engine Program,” SAE Technical Papers 830314, 1983, doi:10.4271/830314.
15. Kamo, R., Bryzik, W., and Glance, P., “Adiabatic Engine Trends-Worldwide,” SAE Technical Papers, 1987, doi:10.4271/870018.

16. Kamo, R., Assanis, D., and Bryzik, W., “Thin Thermal Barrier Coatings for Engines,” SAE Technical Paper, 1989.

17. Wallace, F.J., Way, R.J.B., and Vollmert, H., “Effect of Partial Suppression of Heat Loss to Coolant on the High Output Diesel Engine Cycle,” SAE Technical Paper 790823, 1979, doi:10.4271/790823.

18. Morel, T., Keribar, R., and Blumberg, P.N., “Cyclical Thermal Phenomena in Engine Combustion Chamber Surfaces,” SAE Technical Paper 850360, 1985, doi:10.4271/850360.

19. Woschni, G., Spindler, W., and Kolesa, K., “Heat Insulation of Combustion Chamber Walls - A Measure to Decrease the Fuel Consumption of IC Engines?,” SAE Technical Paper 870339, 1987, doi:10.4271/870339.

20. Amann, C.A., “Promises and Challenges of the Low-Heat-Rejection Diesel,” J. Eng. Gas Turbines Power 110(July):475–481, 1988.

21. Jaichandar, S. and Tamilporai, P., “Low Heat Rejection Engines – An Overview,” SAE Technical Paper 2003-01–0405, 2003, doi:10.4271/2003-01-0405.

22. Kobori, S., Kamimoto, T., and Luta, M.T., “Combustion in Low-Heat-Rejection Diesel Engines,” JSME Int. J. 35(1), 1992.

23. Lang, T. and Germerdonk, R., “Einfluss von wandnahen exothermen Reaktionen auf den konvektiven Wärme- fluss (Convection vive),” Chemie Ing. Tech. 61(11):918–919, 1989.

24. Mendera, K.Z., “Effectiveness of Plasma Sprayed Coatings for Engine Combustion Chamber,” SAE Technical Papers, 2000, doi:10.4271/2000-01-2982.

25. Cheng, S.S., “A Physical Mechanism for Deposit Formation in a Combustion Chamber,” SAE Technical Paper, 1994, doi:10.4271/941892.

26. Mruk, A., Jordan, W., Taler, J., Lopata, S., et al., “Heat Transfer Through Ceramic Barrier Coatings Used in Internal Combustion Engines,” SAE Technical Papers, 1994, doi:10.4271/941779.

27. Tree, D.R., Oren, D.C., Yonushonis, T.M., and Wiczynski, P.D., “Experimental Measurements on the Effect of Insulated Pistons on Engine Performance and Heat Transfer,” SAE Technical Papers (412), 1996, doi:10.4271/960317.

28. Wallace, F.J., Kao, T.K., Tarabad, M., Alexander, W.D., et al., “Thermally Insulated Diesel Engines,” Proc. Inst. Mech. Eng. Part A, J. Power Energy 97–105, 1984.

29. Kawaguchi, A., Iguma, H., Yamashita, H., Takada, N., et al., “Thermo-Swing Wall Insulation Technology; - A Novel Heat Loss Reduction Approach on Engine Combustion Chamber,” SAE Technical Paper 2016-01–2333, 2016, doi:10.4271/2016-01-2333.

30. Tsutsumi, Y., Nomura, K., and Nakamura, N., “Effect of Mirror-Finished Combustion Chamber on Heat Loss,” SAE Technical Paper 902141, 1990, doi:10.4271/902141.

31. Memme, S. and Wallace, J.S., “The influence of thermal barrier coating surface roughness on spark-ignition engine performance and emissions,” *Proceedings of the ASME 2012 Internal Combustion Engine Division Fall Technical Conference*, ASME, Vancouver: 893–905, 2012, doi:10.1115/ICEF2012-92078.

32. Tree, D.R., Wiczynski, P.D., and Yonushonis, T.M., “Experimental Results on the Effect of Piston Surface Roughness and Porosity on Diesel Engine Combustion,” SAE Technical Paper 960036, 1996, doi:10.4271/960036.

33. Osada, H., Watanabe, H., Onozawa, Y., Enya, K., et al., “Experimental Analysis of Heat-Loss with Different Piston Wall Surface Conditions in a Heavy-Duty Diesel Engine,” *Comodia 9th International Conference*, JSME, Okayama, Japan: B204, 2017.

34. Hergart, C., Louki, A., and Peters, N., “On the Potential of Low Heat Rejection DI Diesel Engines to Reduce Tail-Pipe Emissions,” SAE Technical Paper 2005-01–09, 2005, doi:10.4271/2005-01-0920.

35. TAYMAZ, I., “An experimental study of energy balance in low heat rejection diesel engine,” Energy 31(2–3):364–371, 2006, doi: 10.1016/j.energy.2005.02.004.

36. Wallace, F.J., Kao, T.K., Alexander, W.D., Cole, A., et al., “Thermal Barrier Pistons and Their Effect on the Performance of Compound Diesel Engine Cycles,” SAE Technical Paper, 1983.

37. Saad, D., Saad, P., Kamo, L., Mekari, M., et al., “Thermal Barrier Coatings for High Output Turbocharged Diesel Engine,” SAE Technical Paper, 2007, doi:10.4271/2007-01-1442.

38. Rakopoulos, C.D., Giakoumis, E.G., and Rakopoulos, D.C., “Study of the short-term cylinder wall temperature oscillations during transient operation of a turbo-charged diesel engine with various insulation schemes,” Int. J. Engine Res. 9(3):177–193, 2008, doi:10.1243/14680874JER00608.

39. Ramu, P. and Saravanan, C.G., “Effect of ZrO2-Al2O3 and SiC Coating on Diesel Engine to Study the Combustion and Emission Characteristics,” SAE Technical Paper, 2009.

40. Wade, W., Havstad, P., Oundsted, E., Trinker, F., et al., “Fuel economy opportunities with an uncooled DI diesel engine,” SAE Technical Paper 841286, 1984, doi:10.4271/841286.

41. Tricoire, A., Kjellman, B., Wigren, J., Vanvolsem, M., et al., “Insulated Piston Heads for Diesel Engines,” J. Therm. Spray Technol. 18(2):217–222, 2009, doi:10.1007/s11666-009-9301-x.

42. Morel, T., Fort, E.F., and Blumberg, P.N., “Effect of Insulation Strategy and Design Parameters on Diesel Engine Heat Rejection and Performance,” SAE Technical Paper 850506, 1985, doi:10.4271/850506.

43. Arment, T., Cowart, J., Caton, P., and Hamilton, L., “The Effect of Ceramic Thermal Barrier Combustion Chamber Coatings on the Performance and Efficiency of a Small Diesel Engine,” SAE Technical Paper, 2010, doi:10.4271/2010-32-0090.

44. Morel, T., Keribar, R., Blumberg, P.N., and Fort, E.F., “Examination of Key Issues in Low Heat Rejection Engines,” SAE Technical Paper, 1986.

45. Modi, A.J., “Experimental Study of Energy Balance in Thermal Barrier Coated Diesel Engine,” SAE Technical Papers 2012-01–03, 2012, doi:10.4271/2012-01-0389.

46. Moore, C.H. and Hoehne, J.L., “Combustion Chamber Insulation Effect on the Performance of a Low Heat Rejection Cummins V-903 Engine,” SAE Technical Paper, 1986.

47. Havstad, P.H., Garwin, I.J., and Wade, W.R., “A Ceramic Insert Uncooled Diesel Engine,” SAE Technical Paper 860447, 1986, doi:10.4271/860447.

48. Das, D., Majumdar, G., Sen, R.S., and Ghosh, B.B., “The Effects of Thermal Barrier Coatings on Diesel Engine Performance and Emission,” J. Inst. Eng. Ser. C 95(1):63–68, 2014, doi:10.1007/s40032-014-0104-6.

49. Henningsen, S., “Evaluation of Emissions and Heat-Release Characteristics from a Simulated Low-Heat-Rejection Diesel Engine,” SAE Technical Paper 871616, 1987, doi:10.4271/871616.

50. Serrano, J.R., Arnau, F.J., Martin, J., Hernandez, M., et al., “Analysis of Engine Walls Thermal Insulation : Performance and Emissions,” SAE Technical Paper, 2015, doi:10.4271/2015-01-1660.

51. Wakisaka, Y., Inayoshi, M., Fukui, K., Kosaka, H., et al., “Reduction of Heat Loss and Improvement of Thermal Efficiency by Application of ‘Temperature Swing’ Insulation to Direct-Injection Diesel Engines,” SAE Int. J. Engines 9(3):2016-01–0661, 2016, doi:10.4271/2016-01-0661.

52. Powell, T., O’Donnell, R., Hoffman, M., and Filipi, Z., “Impact of a Yttria-Stabilized Zirconia Thermal Barrier Coating on HCCI Engine Combustion, Emissions, and Efficiency,” ASME 2016 Intern. Combust. Engine Fall Tech. Conf. 139(November 2017), 2016, doi:10.1115/1.4036577.

53. Kawaguchi, A., Iguma, H., Yamashita, H., Nishikawa, N., et al., “Engine Heat Loss Reduction by Thermo-Swing Wall Insulation Technology (Mechanism Analysis and Effect on Low Temperature Starting),” Comodia 9th Int. Conf., 2017.

54. Assanis, D. and Badillo, E., “Transient Heat Conduction in Low-Heat-Rejection Engine Combustion Chambers,” SAE Technical Paper Series 870156, 1987, doi:10.4271/870156.

55. Caputo, S., Millo, F., Cifali, G., and Pesce, F.C., “Numerical Investigation on the Effects of Different Thermal Insulation Strategies for a Passenger Car Diesel Engine,” SAE Int. J. Engines 10(4):2017-24–0021, 2017, doi:10.4271/2017-24-0021.

56. Alkidas, A., “Performance and emissions achievements with an uncooled heavy-duty, single-cylinder diesel engine,” 1989.

57. Jerome, S.M. and Sundararaj, S., “Experimental Study on the Effect of Thermal Barrier Coating on Cylinder Head of a Semi-Adiabatic Diesel Engine,” SAE Technical Paper, 2017, doi:10.4271/2017-28-1978.Copyright.

58. Dickey, D., “The effect of insulated combustion chamber surfaces on direct-injected diesel engine performance, emissions and combustion,” SAE Int., 1989.

59. Cheng, W.K., Wong, V.W., and Gao, F.., “Heat transfer measurement comparisons in insulated and non-insulated Diesel engines,” SAE Technical Paper, 1989.

60. Uchihara, K., Ishii, M., Nakajima, H., and Motors, H., “A Study on Reducing Cooling loss in a Partially Insulated Piston for Diesel Engine,” SAE Technical Paper 2018-01–12, 2018, doi:10.4271/2018-01-1276.

61. Osawa, K., Kamo, R., and Valdmanis, E., “Performance of Thin Thermal Barrier Coating on Small Aluminum Block Diesel Engine,” SAE Technical Paper, 1991, doi:10.4271/910461.

62. Merzlikin, V.G., Gutierrez, M.O., Makarov, A.R., Bekaev, A.A., et al., “Development of a semitransparent ceramic heat-insulation for an eco-friendly combustion chamber of Low-Heat-Rejection diesel,” *IOP Conference Series: Materials Science and Engineering*, 2018, doi:10.1088/1757-899X/315/1/012017.

63. Assanis, D., Wiese, K., Schwartz, E., and Bryzik, W., “The Effects of Ceramic Coatings on Diesel Engine Performance and Exhaust Emissions,” SAE Technical Papers, 1991.

64. Andruskiewicz, P., Najt, P., Durrett, R., Biesboer, S., et al., “Analysis of the effects of wall temperature swing on reciprocating internal combustion engine processes,” Int. J. Engine Res. 19(4):461–473, 2017, doi: 10.1177/1468087417717903.

65. Kaudewitz, D.T., Lange, D.F., and Rablbauer, R., “Innovative Piston Technologies for Future Efficiency and Emission Targets,” *Aachen Colloquium Automobile and Engine Technology*, Aachen: 1173–1189, 2018.

66. Kimura, S., Matsui, Y., and Itoh, T., “Effects of Combustion Chamber Insulation on the Heat Rejection and Thermal Efficiency of Diesel Engines,” SAE Technical Paper, 1992, doi:10.4271/920543.

67. Gatti, D. and Jansons, M., “One-Dimensional Modelling and Analysis of Thermal Barrier Coatings for Reduction of Cooling Loads in Military Vehicles,” *SAE Technical Paper*, 2018, doi:10.4271/2018-01-1112.

68. Wong, V.W., Bauer, W., Kamo, R., Bryzik, W., et al., “Assessment of Thin Thermal Barrier Coatings for I.C. Engines,” SAE Technical Papers (41 2), 1995, doi:10.4271/950980.

69. Andruskiewicz, P., Najt, P., Durrett, R., and Payri, R., “Assessing the capability of conventional in-cylinder insulation materials in achieving temperature swing engine performance benefits,” Int. J. Engine Res. 19(6):599–612, 2017, doi:10.1177/1468087417729254.

70. Poubeau, A., Vauvy, A., Duffour, F., Zaccardi, J., et al., “Modelling investigation of thermal insulation approaches for Low Heat Rejection Diesel Engines using a Conjugate Heat Transfer Model,” THIESEL 2018 Conf. Thermo- Fluid Dyn. Process. Direct Inject. Engines High-Pressure, 2018.

71. Kamo, R., Mavinahally, N.S., Kamo, L., Bryzik, W., et al., “Injection Characteristics that Improve Performance of Ceramic Coated Diesel Engines,” SAE Technical Paper, 1999, doi:10.4271/1999-01-0972.

72. Hohenberg, G. and Killmann, I., “Basic findings obtained from measurement of the combustion process,” SAE Technical Paper 82126, 1982, doi:10.1081/E-EEE2-120046011.

73. Krieg, K., “Thermodynamische Bestimmung des Verdichtungsverhältnisses mittels eines Indizierverfahrens,” Fachhochschule Aalen, 1990.

74. Kajiwara, H., Fujioka, Y., and Negishi, H., “Prediction of Temperatures on Pistons with Cooling Gallery in Diesel Engines using CFD Tool,” SAE Technical Paper Series, 2003, doi:10.4271/2003-01-0986.

75. Pan, J., Nigro, R., and Matsuo, E., “3-D Modeling of Heat Transfer in Diesel Engine Piston Cooling Galleries,” SAE Technical Paper Series, 2005, doi:10.4271/2005-01-1644.

76. Dahlström, J., Andersson, Ö., Tunér, M., and Persson, H., “Effects of spray-swirl interactions on heat losses in a light duty diesel engine,” ASME 2015, 2015.

77. Ferguson, C.R. and Kirkpatrik, A.T., “Internal Combustion Engines - Applied Thermosciences,” 3rd ed., John Wiley & Sons, ISBN 978-1-118-53331-4, 2016.

78. Incropera, F.P., DeWitt, D.P., Bergman, T.L., and Lavine, A.S., “Fundamentals of Heat and Mass Transfer,” 6th ed., John Wiley & Sons, ISBN 978-0-471-45728-2, 2007.

79. Kawaguchi, A., Wakisaka, Y., Nishikawa, N., Kosaka, H., et al., “Thermo-swing insulation to reduce heat loss from the combustion chamber wall of a diesel engine,” Int. J. Engine Res. (Special Issue):1–12, 2019, doi:10.1177/1468087419852013.

80. Andrie, M., Kokjohn, S., Paliwal, S., Kamo, L.S., et al., “Low Heat Capacitance Thermal Barrier Coatings for Internal Combustion Engines,” SAE Technical Paper 2019-01–02, 2019, doi:10.4271/2019-01-0228.

81. Broatch, A., Olmeda, P., Martin, J., and Dreif, A., “Numerical Study of the Maximum Impact on Engine Efficiency When Insulating the Engine Exhaust Manifold and Ports during Steady and Transient Conditions,” SAE Technical Paper, 2020, doi:10.4271/2020-37-0002.

82. Hegab, A., Dahuwa, K., Islam, R., Cairns, A., et al., “Plasma electrolytic oxidation thermal barrier coating for reduced heat losses in IC engines,” Appl. Therm. Eng. 196(April):117316, 2021, doi:10.1016/j.applthermaleng.2021.117316.

83. Babu, A., Koutsakis, G., Kokjohn, S., and Andrie, M., “Experimental and Analytical Study of Temperature Swing Piston Coatings in a Medium-Duty Diesel Engine,” SAE Technical Paper (2022):235–248, 2022, doi:10.4271/2022-01-0442.

84. Schaedler, T., Andruskiewicz, P., Mashal, A., Najt, P., et al., “Temperature-Following Thermal Barrier Coatings for High Efficiency Engines,” Malibu, California, 2022, doi:10.2172/1875705.

85. Binder, C., Abou Nada, F., Richter, M., Cronhjort, A., et al., “Heat Loss Analysis of a Steel Piston and a YSZ Coated Piston in a Heavy-Duty Diesel Engine Using Phosphor Thermometry Measurements,” SAE Int. J. Engines 10(4), 2017, doi:10.4271/2017-01-1046.

86. Fridriksson, H., Sundén, B., Hajireza, S., and Tunér, M., “CFD Investigation of Heat Transfer in a Diesel Engine with Diesel and PPC Combustion Modes,” SAE Technical Papers, 2011, doi:10.4271/2011-01-1838.

87. Šarić, S., Basara, B., and Žunič, Z., “Advanced near-wall modeling for engine heat transfer,” Int. J. Heat Fluid Flow 63:205–211, 2017, doi:10.1016/j.ijheatfluidflow.2016.06.019.

88. Gatowski, J.A., Balles, E.N., Chun, K.M., Nelson, F.E., et al., “Heat Release Analysis of Engine Pressure Data,” SAE Technical Paper, 1984, doi:10.4271/841359.

89. Heinle, M., Bargende, M., and Berner, H.-J., “Some useful additions to calculate the wall heat losses in real cycle simulations,” SAE Technical Papers, 2012, doi:10.4271/2012-01-0673.

90. Smialek, J. and Miller, R., “Revisiting the Birth of 7YSZ Thermal Barrier Coatings: Steve Stecura,” NASA/TM (March):219452, 2017.

91. Kawaguchi, A., Tateno, M., Yamashita, H., Tomoda, T., et al., “Toyota’s Innovative Thermal Management Appoaches - Thermo Swing Wall Insulation Technology -,” *Aachen Colloquium Automobile and Engine Technology*, 391–414, 2015.

92. Lee, J., Kim, Y., Jung, U., and Chung, W., “Thermal conductivity of anodized aluminum oxide layer: The effect of electrolyte and temperature,” Mater. Chem. Phys. 141(2–3):680–685, 2013, doi:10.1016/j.matchemphys.2013.05.058.

93. Markocsan, N., Gupta, M., Joshi, S., Nylén, P., et al., “Liquid Feedstock Plasma Spraying: An Emerging Process for Advanced Thermal Barrier Coatings,” J. Therm. Spray Technol. 26(6):1104–1114, 2017, doi:10.1007/s11666-017-0555-4.

94. Barroso, G.S., Krenkel, W., and Motz, G., “Low thermal conductivity coating system for application up to 1000°C by simple PDC processing with active and passive fillers,” J. Eur. Ceram. Soc. 35(12):3339–3348, 2015, doi:10.1016/j.jeurceramsoc.2015.02.006.

95. Zhang, Z., Li, Q., Maiti, S.C., Shen, X., et al., “Thermal properties of field-assisted-sintered SiCN–Y2O3 composites,” Int. J. Appl. Ceram. Technol. 20(2):1060–1070, 2023, doi:10.1111/ijac.14265.

96. Uczak de Goes, W., Somhorst, J., Markocsan, N., Gupta, M., et al., “Suspension Plasma-Sprayed Thermal Barrier Coatings for Light- Duty Diesel Engines,” J. Therm. Spray Technol., 2019, doi:10.1007/s11666-019-00923-8.

97. Weberbauer, F., Rauscher, M., Kulzer, A., Knopf, M., et al., “Allgemein gültige Verlustteilung für neue Brennverfahren,” MTZ - Mot. Zeitschrift 66(2):120–124, 2005, doi:10.1007/BF03227253.

98. Somhorst, J., Uczak de Goes, W., Oevermann, M., and Bovo, M., “Experimental Evaluation of Novel Thermal Barrier Coatings in a Single Cylinder Light Duty Diesel Engine,” SAE Technical Paper 2019-24–00, 2019, doi:10.4271/2019-24-0062.

99. Papaioannou, N., Leach, F., Davy, M., and Gilchrist, R., “The Effect of an Active Thermal Coating on Efficiency and Emissions from a High Speed Direct Injection Diesel Engine,” SAE Technical Papers 2020-April(April):1–13, 2020, doi:10.4271/2020-01-0807.

100. Shpilrain, E.E., “AIR (PROPERTIES OF),” *A-to-Z Guide to Thermodynamics, Heat and Mass Transfer, and Fluids Engineering*, Begellhouse, 2011, doi:10.1615/AtoZ.a.air_properties_of.

101. Kosaka, H., Wakisaka, Y., Nomura, Y., Hotta, Y., et al., “Concept of ‘Temperature Swing Heat Insulation’ in Combustion Chamber Walls, and Appropriate Thermo-Physical Properties for Heat Insulation Coat,” SAE Paper 2013-01–02:142–149, 2013, doi:10.4271/2013-01-0274.

102. Gainey, B., Gandolfo, J., Filipi, Z., and Lawler, B., “Thermodynamic analysis of heat transfer reduction in spark ignition using thermal barrier coatings,” Proc. Inst. Mech. Eng. Part D J. Automob. Eng., 2023, doi:10.1177/09544070231189545.

103. Filipi, Z., Hoffman, M., O’Donnell, R., Powell, T., et al., “Enhancing the efficiency benefit of thermal barrier coatings for homogeneous charge compression ignition engines through application of a low-k oxide,” Int. J. Engine Res. 22(6):1906–1923, 2021, doi:10.1177/1468087420918406.

104. Moser, S., O’Donnell, R., Hoffman, M., Jordan, E., et al., “Experimental Investigation of Low Cost, Low Thermal Conductivity Thermal Barrier Coating on HCCI Combustion, Efficiency, and Emissions,” SAE Technical Paper, 2020, doi:10.4271/2020-01-1140.

Symbols and acronyms

a	diffusivity
α	absorptivity
A	surface area
B	cylinder bore
c_v	volumetric specific heat
c_m	mass specific heat
δ_p	thermal penetration depth
e	effusivity
ε	emissivity
ϵ	surface roughness height
ϕ	porosity
h	mass specific enthalpy
h_c	heat transfer coefficient
H	enthalpy
k	thermal conductivity
κ	ratio of specific heats
L	characteristic length
μ	dynamic viscosity
Nu	Nusselt number
p	pressure
Pr	Prandtl number
$\dot{Q}$	heat flux
Q_n	net apparent heat release
ρ	density
R	gas constant
r_a	average surface roughness, ISO 4287
Re	Reynolds number
σ	Boltzmann constant
θ	crank angle
T	temperature
T_{cr}	crevice temperature
u	mass specific internal energy
U	bulk velocity
V	volume
V_{cr}	crevice volume
W	work

aRoHR	Apparent rate of heat release
aHR	Apparent heat release (accumulated)
CA	Crank angle
CCD	Combustion Chamber Deposit
CI	Confidence interval
CO	Carbon monoxide
CO_2	Carbon dioxide
CHR	Centroid of heat release rate
CR	Compression ratio
DOE	Design of experiments
EOP	Engine operating point
FMEP	Friction mean effective pressure
GdZr	Gadolinium-zirconate
HA	Hard anodized
HOSP	Hollow spheres
IMEP	Indicated mean effective pressure, complete cycle
IMEPH	Gross indicated mean effective pressure, closed cycle
IMEPL	Mean indicated pressure during gas exchange, open cycle
LHV	Lower heating value
MLR	Multiple linear regression
NO_x	Nitrogen oxides
PEO	Plasma electrolytic oxidation
RANS	Reynolds-Averaged Navier-Stokes turbulence formulation
ratExh	Ratio of enthalpy in the exhaust gas and energy content in the fuel
ratHT	Ratio of wall heat transfer and energy content in the fuel
ratWork	Ratio of gross indicated work and energy content in the fuel
SEM	Scanning electron microscope
SiRPA	Silica reinforced porous anodized aluminum
TBC	Thermal barrier coating
THC	Total hydrocarbons
YSZ	Yttria stabilized zirconia